INVESTIGATIONS OF THE COUNTER-INTUITIVELY SHORT LIFETIMES OF THE VISIBLE EMISSION FROM LASER-INDUCED PLASMAS FROM RDX

by

Daniel Ryan McMullan

A dissertation submitted to the Graduate Faculty of Auburn University in partial fulfillment of the requirements for the Degree of Doctor of Philosophy
Auburn, Alabama

May 2, 2020

[Laser induced plasmas, energetic materials, optical emission spectroscopy, time-resolved plasma plume imagery]

Rik Blumenthal, Chair, Associate Professor, Department of Chemistry
Wei Zhan, Associate Professor, Department of Chemistry
Evangelos Miliordos, Assistant Professor, Department of Chemistry
Jordan Harshman, Assistant Professor, Department of Chemistry
Byron Farnum, Assistant Professor, Department of Chemistry
Peter D. Johnson, Alumni Professor, Department of Mathematics and Statistics

Acknowledgments

I express my complete gratitude to my advisor, Dr. Rik Blumenthal. His mentorship, creativity, ingenuity, and direction are the reasons I was able to complete this work. He not only was a great example of a scientist, but taught me how to approach problems and work towards solutions, troubleshoot instrumentation issues, and rationalize and analyze anomalies in the data. Many thanks are also given to my committee members: Dr. Byron Farnum, Dr. Jordan Harshman, Dr. Evangelos Miliordos, and Dr. Wei Zhan for their comments and suggestions throughout my tenure as a student and in preparation of this manuscript. Thank you to my outside reader, Dr. Peter Johnson, for his participation in review of this work and examination. Thank you to all of the staff in the Chemistry Department for help on a daily basis. To my fellow graduate students, thank you for support with my work and the friendships I have made.

I would also like to thank my family for their love and support throughout this process, and perhaps most notably my dog Rudy, who always reminds me to relax and have fun, with a positive attitude.

Abstract

Through multiple studies on laser generated plasmas of materials, four phenomena have been curious and unexplainable regarding the non-energetic material polycarbonate (PC) and energetic material RDX (Cyclotrimethylenetrinitramine). First, the broad, blackbody emission of laser-induced PC plasmas decreases in intensity but does not shift in wavelength through the vast majority of the emission process.[1] Second, where the emission from the PC lasts for hundreds of microseconds, the emission from RDX is extremely short lived (ns). Third, laser induced ablation pits on RDX (ablation is the clean removal of material from a surface) are ten times as deep as they are with PC.[1,2] Fourth, the nature of the power density threshold for laser ignition that has been observed for RDX remained wholly unknown. To address the latter two issues, a model study was carried out to investigate whether the laser ignition of RDX at high laser fluence is simply the result of thermal ignition resulting from heating by a blackbody plasma raising the temperature of the RDX above the thermal threshold for reaction. Using a simple model of a plasma plume as a blackbody above the solid RDX surface, pit temperatures were estimated and the volume of RDX heated above the sublimation temperature and compared to the pit sizes observed in prior laser ablation experiments. The observation that the simple model, using only a few reasonable assumptions, produces laser ablation pits in RDX that are approximately ten times deeper than those observed on PC serves as strong evidence that the deeper pits are the result of black body plasma re-radiated onto the RDX surface. Further increasing the laser power in the model to a value comparable to those at the reported threshold for laser ignition results in temperatures of over 900K at the surface which would result in thermal ignition. The lack of a wavelength shift as the signal level drops seems to indicate that the plasma is emitting at a constant temperature; however, that makes no sense as the plasma is losing energy through emission of light, so it should expected to cool. To explain this observation, Casper hypothesized that the plasma in laser ablation is optically dense, meaning that only the surface is visible to the observer, and that the emission at constant wavelength, or constant temperature, is the result of a phase transition from a strongly emitting plasma to much less emissive neutral gas at the surface. Within this model, the decrease in intensity indicates a decrease in surface area of the plasma as the interface recedes radially inward, as the plasma radiatively cools. An improved experimental setup using a fast camera to image plumes directly

as well as spectrally using a diffraction grating spectrometer was built. The setup is identical to Casper's configuration, except that the slow camera and pulsed image intensifier, which could only collect one spectrum per laser pulse was replaced with a fast camera. In the new configuration, used for all experiments in this work, the fast camera was used to collect 20 images, each 100 μs apart in time, following each laser pulse. Collecting many more spectra, it became possible to construct an average RDX spectrum revealing that RDX plasmas are much hotter than PC plasmas, with a surface temperature estimated at 8725K +/- 50, compared to 2240K +/- 5 for PC. As a result, the rapid disappearance of the visible RDX emission is proposed to result from the much hotter surface of the RDX plasma radiating away its energy much faster than the lower temperature PC plasma. The results of this work are strong evidence in support of the proposition that these phenomena are the result of a plasma/gas phase transition.

Collection of hundreds of images of laser ablation plumes also revealed a new anomaly. When the same region of RDX coated PC is exposed to a series of laser shots, visible emission from the first shot is bright, then goes dark for the second and third shots, and returns to bright again for the subsequent shots. It is proposed that pure RDX which is cleanly ablated results in the bright image of the first images of the first and often the second shots. White layers that cannot be removed with solvent are observed on the PC around the laser irradiation pit following laser ablation. They are attributed to subsurface melting of the PC, into which RDX can diffuse. These RDX+PC mixtures are described as "snow-pack" in this work. By the second or third laser shot, the top layer of RDX has been removed, and the RDX+PC mixture is being ablated and the plasma appears dark. This is consistent with previous reports that RDX needs PC to initiate via laser irradiation under the conditions used in these experiments, and that without the PC component, the pure RDX plasma does not ignite. After the RDX and "snow-pack" have been fully removed, the images of the plasmas return to bright. The RDX and underlying "snow-pack" removal can take several laser shots for plasmas to return to bright, dependent on the thickness of the RDX film, and how much RDX diffused into the molten PC to create "snow-pack." It was also found that audio recordings on a smart phone indicate louder pops associated with the dark plasmas (energetic), which could provide an inexpensive way to investigate laser ignition further. Analysis of a histogram of plume photos indicates a distribution of pixel intensities that does not change in intensity or shift through time but just decreases in population. This observation indicates that the plasma emits at a constant temperature, and that proceeds by a reduction of the

number of hot pixels, rather than a drop in their intensity. Finally, out of curiosity, fast spectra were collected for the laser ablation of a few metals on double sided tape. Spectra of the metals on tape show signs of the plain tape, PC, and features not common to either, making blackbody fitting difficult. Only Iron could be fit to a blackbody, with a best fit temperature of 12,450K +/- 225, compared to an estimated 7920K +/-15 temperature for plain double sided tape.

REFERENCES

1. Casper IV, Walter F. ***A microsecond time-resolved spectroscopic study of laser induced plasmas and their interactions with solid materials.*** Ph.D. Dissertation, Auburn University, Auburn, AL, 2015.
2. J.L. Gottfried, ***Influence of exothermic chemical reactions on laser-induced shock waves***, Phys. Chem. Chem. Phys. 16, 21452 (2014)

Table of Contents

List of Tables

List of Figures

List of Abbreviations

AN	Ammonium Nitrate
CCD	Charge coupled device
II	Image Intensifier
IR	Infrared
LASER	Light Amplification by Stimulated Emission of Radiation
Nd:YAG	Neodymium-doped yttrium aluminum garnet
OES	Optical Emission Spectrometer
PC	Polycarbonate
PC/RDX	Polycarbonate coated RDX
RDX	Cyclotrimethylenetrinitramine or Research Department Formula X
UV	Ultraviolet
VIS	Visible

Chapter 1 Introduction

1.1 Background Literature

RDX has been studied for over a century. RDX was first discovered and patented by Georg Fredrich Henning in Germany in 1898.[1] The explosive was studied throughout the early 20th century [2, 3, 4] but was not utilized in war until World War II.[5] In the study of RDX and testing of RDX containing ordinance, there has been delicate balance between the safety and the performance of energetic materials. [6] Since 2009, there have been over 50 recorded instances of accidental explosions at munitions depots in 34 countries. [7] Work towards understanding the influence of aging on the performance and sensitivity of energetic materials is of the upmost importance in maintaining munitions stockpiles. [8] Beyond the inherent safety hazards of the full-scale detonating of explosives, there have been numerous reports of environmental contamination due to RDX in drinking water. [9] Additionally, the full-scale detonation of explosives is expensive. [10] As a result, the development of laboratory-scale techniques to characterize and develop energetic materials without full-scale detonation has received a lot of attention. [11, 12] It has been found that bench-top methods can be used to understand energetic material performance (detonation velocity and pressure) without full-scale detonations. Gottfried was able to linearly correlate the laser induced shock velocities acquired of an array of energetic materials using laboratory scale methods to the detonation velocities acquired with full-scale detonations. [13] Several advantages of micro-scale laser ablation experiments of energetic materials over full-scale detonations for materials characterization work and testing have been identified.

First, the micro-scale testing of energetic materials only requires mg amounts of material, compared to amounts of tens of grams needed for the direct measurement of the performance and sensitivity historically, and can be used to characterize energetics' performance prior to a more expensive scaled-up experiment. [8, 10, 17-20] Ignition of energetic materials with a laser can eliminate the need to incorporate traditional igniter materials, which can be unstable. [14] The technique described by Gottfried, LASEM (Laser induced air shock of energetic materials), is used to study the high-temperature chemical reactions of materials in the laser-induced plasma, that affect the expanding shock wave into the ambient surroundings.[16] Lasers have well defined pulse energy, wavelength, and duration that can be tuned to deliver precise energy to energetic materials and control the size and distribution of particles formed without detonation of the

explosive. [10, 15] Additionally, the use of lasers to initiate ignition of energetics could advance the field of energetic materials formulation and tuning research by facilitating more work on energetics without the need for full scale detonations as often. [10] Another advantage of laboratory scale methods of energetic material characterization using laser initiation is that there is very minimal sample preparation needed since the laser directly ablates the explosive and substrate material; there is no need for large quantities of material or packing of explosive powders or molds. [10] The study of the intermediate chemical reactions that occur in energetic material ignition have been demonstrated using laser initiation using only mg quantities, which eliminate the need for explosive containment apparatus, and increase the accessibility and feasibility of more research groups performing energetics work. [10] Laboratory scale laser induced plasma studies of energetic materials have facilitated simultaneous tracking of high-resolution, time resolved relative concentrations of atomic and molecular species. Benchtop energetics experiments using laser initiation facilitate the collection of data much faster than using full scale detonations. [11] The study of energetic material ignition using laser initiation of mg quantities of energetic material advance the timely development and study of energetics. This is due to the expense of producing large amounts of energetic material, and also safety and logistical limitations to the number of full-scale detonation events per year. The development of benchtop methods using laser initiation of mg amounts of energetic materials yields rapid data collection of multiple experiments without the expense or limitations associated with large scale detonations. [12]

In addition to the research and development of novel energetic materials, the benchtop methods of energetic material characterization have possible applications in standoff detection. Laser induced breakdown spectroscopy (LIBS) is an analytical technique involving the ablation of an explosive or residue to collect emission spectra for material identification without detonation. This method is an optical technique and enables the identification of chemical species at a distance and used for the detection and identification of explosives. [21-25]

Laboratory scale laser ablation experiments of energetics have also been proven useful in the performance assessment of composite energetic materials with metal additives, the characterization of novel energetic materials, the study of oxidized porous silicon samples for micro-thruster and on-chip applications, and in the identification of impurities in energetic materials as well as energetic material degradation. [16]

1.2 Direction of this work

The interaction of a UV laser with solid materials including polycarbonate (PC) and RDX is investigated to elucidate the mechanisms of several puzzling observations made in previous studies. First, the broad, blackbody emission of laser-induced PC plasmas decreases in intensity but does not shift in wavelength through the vast majority of the emission process.[26] Second, emission from PC lasts for hundreds of microseconds while emission from RDX is extremely short lived (ns). Third, laser induced ablation pits on RDX (ablation is the clean removal of material from a surface) are ten times as deep as they are with PC.[26, 27] Fourth, the previously unknown power density threshold for laser ignition has been observed for RDX. Additionally, the collection of hundreds of images of laser ablation plumes revealed two new anomalies: when the same region of RDX coated PC is exposed to a series of laser shots, visible emission from the first shot is bright, then goes dark for the second and third shots, and returns to bright again for the subsequent shots, and white layers were observed on PC films following laser ablation experiments of RDX films on PC.

When a UV laser of sufficient fluence (described below) strikes a solid surface such as PC, a plasma is produced as chemical bonds are broken and atoms and molecules are ionized by the laser pulse which lasts several nanoseconds. The high-pressure plasma plume then expands to its maximum size when the plume pressure drops to atmospheric pressure. [28] The plasma plume has been shown to emit at a single black-body temperature for several tens of microseconds. [26] During this process, the plume dissipates its energy into its surroundings by emission of light. Our simple model of this process begins with a plasma plume, assumed to be a sphere at a fixed height above the surface, that re-emits the full energy of the laser pulse back to the surface in the form of blackbody radiation.

1.3 Laser Ionization Mechanisms

Plasma is the fourth state of matter and is defined as an ionized gas composed of ions and free electrons. There are multiple mechanisms of laser adsorption that result in plasma formation (see Figure 1.1). The simplest mechanism is the formation of free, or continuum, electrons from direct adsorption by electrons in the ground state. This process, known as direct ionization, occurs by a first-order photoionization mechanism, meaning the rate of formation of free

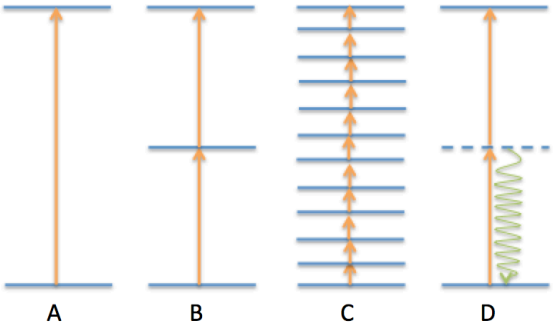

Figure 1.1: A: Direct Ionization, B: Resonant two-photon Ionization, C: Multiphoton Vibrational Ionization, D: Non-resonant two-photon Ionization

electrons is directly proportional to the laser fluence; see Figure 1.1A. Ionization by this mechanism requires laser radiation with a photon energy greater than the binding energy of the electrons, typically hard UV radiation. Plasmas can also be formed via promotion of electrons from the ground state to the continuum in multiple steps between allowed bound states; this photoionization mechanism is called resonant multi-photon ionization. It is also first order, as a combination of first order adsorption processes is still first order. A two-photon ionization, shown in Figure 1.1.B, typically requires UV/Visible radiation. Multiphoton ionization is the common mechanism for plasmas formed under IR irradiation, where ionization is achieved through multiple excitations along the vibrational energy levels manifold; see Figure 1.1C. Very importantly, multiphoton ionization requires a resonance between the energy levels of the material and the wavelength of the light. Plasmas can also be formed via the promotion of electrons from the ground state to the continuum through a short-lived (femtoseconds) virtual state, see Figure 1.1D. This mechanism is called non-resonant multi-photon ionization and is second order or higher, depending on the number of adsorptions necessary to span the energy difference between the ground state and the first allowed state or the continuum. Non-resonant multi-photon ionization requires a laser fluence to be sufficiently high so that a second incoming photon promotes the electron from the virtual state to the continuum before re-radiation returns the electron to the ground state, a process that takes only femtoseconds. In a second order process, the rate of formation of free electrons is directly proportional to the square of the laser fluence, resulting in a very sharp turn-on or threshold for the process as a function of laser fluence. At sufficient fluence for the second order process, it is important to note that non-resonant multiphoton ionization does not require a resonance between the energy levels of the material and the laser light. Direct ionization and resonant multi-photon ionization have much higher cross sections than non-resonant multi-photon ionization, which only occurs at high laser fluence, and below the threshold for non-resonant multi-photon laser ionization, irradiation

neither melts nor heats the irradiated material, as the radiation passes through the material without being absorbed. [29]

1.4 Laser Generated Plasmas

The mechanism of laser ionization for a specific material depends on the laser wavelength and the allowed states of the absorbing material. In IR laser irradiation, the wavelength of the light is frequently resonant with vibrational levels in the fingerprint region of the absorption spectrum of the material. Vibrational energy is what is typically thought of indicating temperature, and consequently, IR laser irradiation may be thought of as rapid elevation in temperature. Under increasing IR fluence, the material will successively first melt, then material will begin to be removed by evaporation, resulting in a melt pit. When the heating from the IR laser pulse is much faster than heat conduction to adjacent material, melting and evaporation will occur only in the irradiated area, forming a vertical-walled pit, characteristic of ablation. [30]

Visible and UV laser light is absorbed through direct electronic transitions between allowed states in metals and semi-conductors with band gaps less than the photon energy of the laser. Although UV photons have energies on the order of most atomic bonds, it often takes multiple photon adsorptions for an electron to be promoted all the way to the continuum. In metals and semi-conductors, when the incident photon has energy below the ionization threshold of the adsorbing material, ionization occurs through the first-order multiphoton ionization process, described above. [30]

The compounds used in most of the experiments herein, PC and RDX, are insulators or large band gap semiconductors. Both have band gaps larger than the 266 nm UV photon energies used in the experiments. Since a single photon does not have enough energy to directly promote an electron from the ground to an excited state, the laser light either passes through the material (PC is transparent) or is simply scattered by RDX, making it white. Insulators only ionize via non-resonant multi-photon UV ionization through virtual states via the second order process, as described above. Due to the sharp threshold of the second order process, these materials form vertical-walled ablation pit only under the center of the laser spot. [26, 27, 30, 31]

1.5 Plume formation and evolution

Whenever an ablation pit is formed on the surface of an insulating material, the ingredients of a plasma plume - ions, free electrons, and gas phase neutral species - are formed. As the laser fluence is increased beyond the ablation threshold, the density of the plasma above the surface also increases. Pairing of an ion and a free electron in the plasma creates a new potential mechanism for direct absorption of subsequent laser radiation, with a large dipole moment and a continuum of allowed states that results in strong absorption at all wavelengths, or a blackbody. At some point, the plasma may become optically thick, after which, the laser energy no longer goes into creating more plasma but instead results in heating of the plasma to higher temperatures. [29] In terms of laser ablation pit formation, once the plasma becomes optically dense, the pit should cease to become any deeper, as no further laser radiation reaches the surface.

Differences in laser fluences significantly impact where the laser energy is deposited. Near threshold fluence for laser ablation, a large fraction of the laser energy is used to ionize and form the plasma. As laser fluence is increased beyond the threshold for pit formation, an increasingly smaller fraction of the laser pulse energy is required for plasma formation, and an increasingly larger fraction of the photons heat the plasma. Consequently, a higher fluence results in higher plasma temperatures, and low fluence result in lower plasma temperatures and even lower degrees of ionization in the plasma. Laser fluence affects the duration of plasma emission, as hotter plasmas necessarily emit longer than initially cooler plasmas. Assuming that plasma emission ends at some minimum temperature required to maintain the highly ionized plasma environment, it is obvious that it will take longer for a hot plasma to lose sufficient energy to drop below this threshold of emission than an initially cooler plasma. In the experiments used herein, fluence is controlled with laser focus. When a laser pulse is focused to a larger spot, there is less fluence, meaning that more photons are used to create the plasma, with fewer contributions to heating the plasma. Focus also determines the irradiated area, and hence the total amount of material ablated. A highly focused beam results in a narrower ablation pit, whereas a less focused beam results in a broader ablation pit. [29, 30, 31, 32]

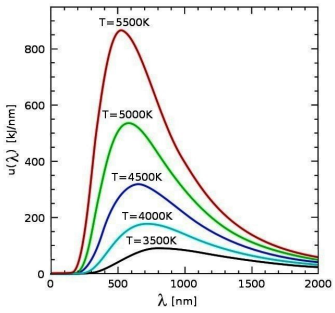

Figure 1.2: Blackbody emission at various temperatures

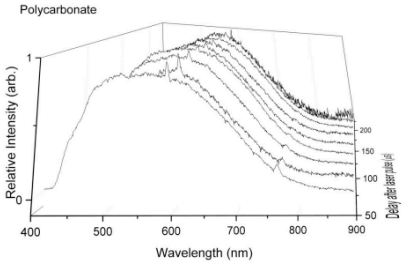

Figure 1.3: Normalized PC spectra (Casper)

1.6 Previous Work

Gottfried studied the influence of exothermic chemical reactions on laser-induced shockwaves of a variety of energetic and non-energetic materials using 6 ns, 900 mJ, 1064 nm laser pulses focused into 0.4 mm radius spots.[27] She observed that the shockwave velocities correlated well with the detonation velocities of the bulk materials. She attributed the higher shockwave velocities to the faster reactions that occur in energetic materials, which are the very reactions that have been used to categorize materials as energetic. It was also observed that non-energetic materials produced much more luminous and longer-lived plasmas than energetic materials. This later result was neither expected nor explained. While all materials exhibited plasma emission in the first frame of imagery (11 μs), however plasma emission for non-energetic materials continued to emit for hundreds of microseconds, while visible emission of RDX and all other energetics only lasted one frame. [27]

Casper performed fast optical emission spectroscopy experiments on laser (UV) induced plasma plumes of polycarbonate (PC), ammonium nitrate (AN), sucrose, and polyethylene (PE), using 6 ns, 50 mJ, 266nm laser pulses focused into 0.5 mm spots. [26] He initially expected to observe the cooling of the plasma plume as a shift of the maximum absorption wavelength to longer, less energetic wavelengths, as the intensity decreased, see Figure 1.2. However, when he normalized his spectra, no observable shift in the maximum absorption wavelength was observed, see Figure 1.3. All of the spectra after the first 40 μs could be least squares fit to Planck's blackbody equation using a 2275 K temperature for all spectra. It should be noted that all of the spectral shapes observed for a number of other non-energetic materials displayed a constant shape through time, but only the PC spectra could be fit to a pure blackbody. In the first

20-40 μs, shoulders at both shorter and longer wavelengths were observed for all non-energetic materials, see Figure 1.4. It was not determined what these shoulders indicated. [26]

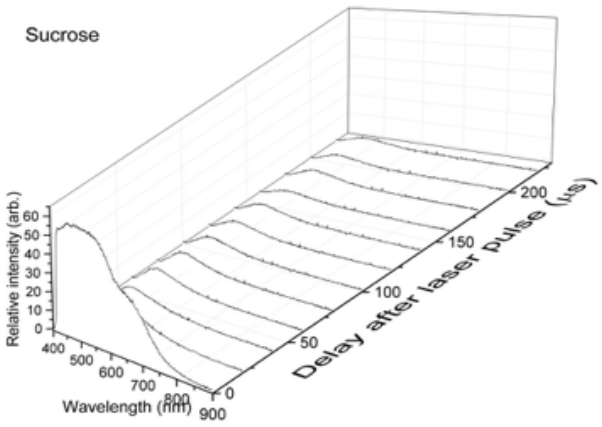

Figure 1.4: Shoulders present in first 20 μs

Casper also used an ultrafast photodiode to measure the lifetimes of these plasmas in the 400-700 nm (visible light) range, and found that PC and AN had the longest lifetimes, lasting ~200 μs. PE and sucrose emission intensity dropped after the first 20 μs, and RDX emission was minimal and decayed very rapidly, lasting only nanoseconds. As previously noted, Gottfried also observed the emission from non-energetic materials to last hundreds of microseconds and the emission from energetic compounds to be observed only during the first 11 μs frame following the laser pulse. Neither had an explanation for this. [26, 27]

To explain the unchanging shapes of Casper's fast emission spectra, a new model of laser ablation plasmas was proposed. In this model, the plasma is assumed to be optically dense, meaning that observable emission emanates from an outer plasma surface. The plasma surface is fixed at the temperature of a plasma to gas phase transition and the surface recedes inward though the volume of the initial plume as the plasma radiates away its energy. In an optically dense plasma, radiation from the hotter core is not visible because it is continually absorbed and re-emitted as the energy passes outward, resulting in, the only emission escaping the plume originating from the cooler surface. At the surface of the plasma, charged species are present which have with much larger transition dipole moments than neutral gaseous atoms. As a result, plasmas are much stronger emitters than neutral gases. This can be seen when examining a match flame; one only sees the light from the flame (plasma), but not the hot air (gas) surrounding it. Similarly, when observing the sun, only a ~5000 K blackbody surface emission is observed, despite the several million-degree core and the much cooler gas between the sun and the Earth.

Another experimentally observed difference between RDX (energetic material) and PC (non-energetic material) is their ablation pit sizes. Sun observed that the depth of the RDX

ablation pit were ten times as deep as PC pit depths.[33] She suggested that the difference in pit sizes could be attributed to RDX undergoing sublimation due to IR plasma emission, meaning that the greater depth of the RDX pit could be attributed to material removal via sublimation which is not expected with PC.

To investigate the aforementioned mechanisms of several puzzling observations with UV laser interaction with PC and RDX, a fast camera is incorporated into Casper's experimental setup to improve data collection by allowing the collection of 20 images for each laser pulse, and the acquisition of hundreds of images per experiment. The data collection method permitting time resolved image collection of individual plasma plumes following laser initiation revealed a new puzzling observation. When the same region of RDX coated PC is exposed to a series of laser shots, visible emission from the first shot is bright, then goes dark for the second and third shots, and returns to bright again for the subsequent shots. It is proposed that pure RDX which is cleanly ablated results in the bright image of the first image of the first shot. To investigate this theory as well as the effect that different amounts of RDX might have on the darkening of plasmas and the rate of return to brightness, experiments incorporating RDX films of varying film thicknesses were laser ablated and plume images collected.

1.7 REFERENCES

1. Henning, German Patent 104,280 (1899)
2. Herz, Swiss Patent 88,759 (1920); Chem. Zenlr., 92, IV, 926 (1921).
3. Hale, G. C.; THE NITRATION OF HEXAMETHYLENETETRAMINE. J. Am. Chem. Soc. 47, 2754-2763 (1925)
4. Bachmann, W. E.; Sheehan, J. C. A New Method of Preparing the High Explosive RDX. J. Am. Chem. Soc. 71, 5. 1842-1845. (1949)
5. https://www.britannica.com/technology/RDX
6. Wang, Y.; Jiang, W.; Song, D.; Liu, J.; Guo, X.; Liu, H.; Li, F., *Journal of thermal analysis and calorimetry* 2013, *111*, 85-92.
7. https://www.nato.int/docu/review/2011/arms-control/Danger-Stockpiles-Ammunition/EN/index.htm
8. Gottfried, Jennifer L.; Klapotke, Thomas.; Witkowski, Thomas G. Estimated Detonation Velocities for TKX-50, MAD-X1, BDNAPM, BTNPM, TKX-55, and DAAF using the Laser-Induced Air Shock From Energetic Materials Technique. Propellants, Explosives, Pyrotechnics. 42, 4. 353-359. April 2017
9. Lustgarten, Abrahm. The Bomb that Went Off Twice. ProPublica. December 18, 2017.
10. Gottfried, Jennifer L. Laser-Induced Plasma Chemistry for the Characterization of Energetic Materials. U.S. Army Research Laboratory, RDRL-WML-B Aberdeen Proving Ground, MD 21005.

11. Fajardo, M. E.; Fossum, E. C.; Molek, C. D.; Lewis, W. K.; Nep, R. M. *Benchtop Energetics Progress*; DTIC Document: 2011.
12. Fajardo, M. E.; Lewis Iii, W. K.; Ashley, V. L.; Nep, R. M.; Fossum, E. C.; Molek, C. D. *Benchtop Energetics: Research Progress, Concept Evaluation, and Apparatus Development*; DTIC Document: 2012.
13. Gottfried, Jennifer L. New laboratory-scale method for the determination of explosive performance from laser-induced shock waves. U.S. Army Research Laboratory Aberdeen Proving Ground, MD
14. Howard, S. L.; Beyer, R. A.; Reeves, P. Direct Laser Ignition of Gun Propellants: Simulator Tests of Modular Charges. U.S. Army Research Laboratory. Aberdeen Proving Ground, MD 21005-5066
15. Van Rooijen, M.; Lapebie, E.; Peugeot, F.; Opdebeck, F.; Gillard, P. Feasibility Study To Use A Laser System For An Insensitive Munition Deflagration Test. Presented at the 32nd International Annual Conference of ICT on Energetic Materials, held 3-6 July 2001, Karlsruhe, Federal Republic of Germany, (2001-5000), pp. 131-1.
16. Gottfried, Jennifer L. Laser-Induced Air Shock from Energetic Materials (LASEM) Method for Estimating Detonation Performance: Challenges, Successes and Limitations. U.S. Army Research Laboratory, RDRL-WML-B, Aberdeen Proving Grounds, MD 21005, USA
17. Gottfried, Jennifer L. Laser-induced plasma chemistry of the explosive RDX with various metallic nanoparticles. Applied Optics, 51, 7, B13-B21 (2012)
18. Roy, Sukesh; Jiang, Naibo; Stauffer, Hans U.; Schmidt, Jacob B.; Kulatilaka, Waruna D.; Meyer, Terrence R.; Bunker, Christopher E.; Gord, James R. Spatially and temporally resolved temperature and shock-speed measurements behind a laser-induced blast wave of energetic nanoparticles. *Journal of Applied Physics 113:18* (2013)
19. Delgado, Thomas.; Vadillo, Jose M.; Laserna, J. Javier. Primary and recombined emitting species in laser-induced plasmas of organic explosives in controlled atmospheres. *J. Anal. At. Spectrom., 2014,29, 1675-1685*
20. Kalam, S. Abdul; Murthy, N. Linga; Mathi, P.; Kommu, N.; Singh, Ajay K.; Rao S. Venugopal. Correlation of molecular, atomic emissions with detonation parameters in femtosecond and nanosecond LIBS plasma of high energy materials. J. Anal. At. Spectrom., 2017,32, 1535-1546
21. Gottfried, J. L.; Harmon, R. S.; Munson, C. A.; Winkel Jr, R. J.; Miziolek, A. W. *Detection of Energetic Materials and Explosive Residues With Laser-Induced Breakdown Spectroscopy: 1. Laboratory Measurements*; DTIC Document: 2007.
22. Sunku, S.; Gundawar, M. K.; Myakalwar, A. K.; Kiran, P. P.; Tewari, S. P.; Rao, S. V., *Spectrochimica Acta Part B: Atomic Spectroscopy* 2013, *79*, 31-38.
23. Gottfried, J. L.; De Lucia Jr, F. C.; Munson, C. A.; Miziolek, A. W., *Journal of Analytical Atomic Spectrometry* 2008, *23*, 205-216.
24. Lopez-Moreno, C.; Palanco, S.; Laserna, J. J.; DeLucia Jr, F.; Miziolek, A. W.; Rose, J.; Walters, R. A.; Whitehouse, A. I., *Journal of Analytical Atomic Spectrometry* 2006, *21*, 55-60.
25. Glumac, N., *Shock Waves* 2013, *23*, 131-138.
26. Casper IV, Walter F. *A microsecond time-resolved spectroscopic study of laser induced plasmas and their interactions with solid materials.* Ph.D. Dissertation, Auburn University, Auburn, AL, 2015.

27. Gottfried, J.L. *Influence of exothermic chemical reactions on laser-induced shock waves*, Phys. Chem. Chem. Phys. 16, 21452 (2014)
28. Bormotova, T.A.; Blumenthal, R. Ultraviolet laser ablation of polycarbonate and glass in air. Journal of Applied Physics, 2009, 105, 034910.
29. Ma, Q.; Motto-Ros, V.; Laye, F.; Yu, J.; Lei, W.; Bai, X.; Zheng, L.; Zeng, H., Journal of Applied Physics 2012, 111, 053301.
30. Johnson, S. L. Resonant-Infrared laser ablation of polymers: Mechanisms and applications. Vanderbilt University, Nashville, TN, 2008.
31. Wang, Q.; Jander, P.; Fricke-Begemann, C.; Noll, R., Spectrochimica Acta Part B: Atomic Spectroscopy 2008, 63, 1011-1015.
32. Greenfield, M. T.; McGrane, S. D.; Bolme, C. A.; Bjorgaard, J. A.; Nelson, T. R.; Tretiak, S.; Scharff, R. J., The Journal of Physical Chemistry A 2015, 119, 4846-4855.
33. Sun, H. Dissertation Auburn University 2011

Chapter 2 EXPERIMENTAL

2.1 Sample Translation

The movement of samples as well as the variable distance between the lens and sample were controlled with the use of a three axis computer-controlled positioning system on a 4'x4' optical breadboard table. The Parker-Dadaell motors and rails (Parker, 404-XR) were controlled with a Galil DMC-1800 motion controller. The resolution was 12 µm on the x and y axis (80 cm travel distance) and 8 µm on the z (30 cm travel distance), both with a 3 µm repeatability. The computer interface with the positioning system was handled through the Galil DMC "Smart Terminal" software which provided for integration of the motion to be synced to the q-switch output through a function generator with a wait for input command. The 140 mm focal length lens was positioned on the x axis of the motion control 125 mm from the sample surface in line with the laser beam. The 1" diameter polycarbonate films were attached with tape to a 3-D printed sample holder, which was then inserted into a glass tube mounted on the motion control stage and translated through the path of the stationary laser beam. The time the sample remains at a given position governs how many laser shots impact the sample at that position.

Typical experiments involve the translation of a freshly sprayed RDX or other material spot on the sample surface, see Sample Preparation below, with respect to stationary laser position along a serpentine pattern consisting of 14 rows of 9 spots, 1.25 mm apart. The sample remains at each position, referred to as the spot, sufficiently long enough to allow seven laser shots at each spot. In practice, images are acquired at 10,000 FPS following each laser shot, as the sample is translated every 1.4 seconds as the laser is fired every 0.2 seconds. The seven laser shots impingent on a given spot are labeled A-G with A designating the first laser shot on each spot, and G

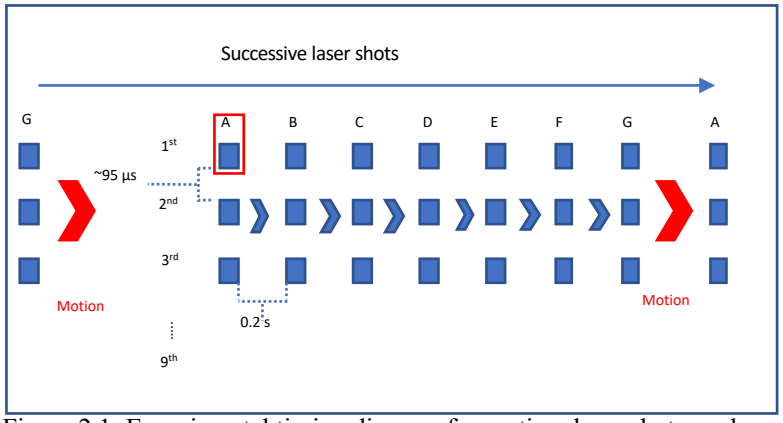

Figure 2.1: Experimental timing diagram for motion, laser shots, and image collection

designating the seventh laser shot on each spot. The timing for this process is presented in Figure 2.1 Twenty images are collected following each laser shot, one every 97 us. The timing is shown at the left of Figure 2.1 beginning with the G, or seventh laser shot at the previous spot. The three vertically stacked squares indicate three of the twenty images captured of the laser ablation for that laser shot. Moving to the right in Figure 2.1, the red arrow indicates translator motion to the next spot. As mentioned, the vertically stacked squares indicate image frame acquisition every 95 μs following each laser shot A-G. The blue arrows indicate the 0.2 second delay between each of the seven laser shots at each position. To summarize, following the last laser shot, G, at the current position, the translator moves, indicated by the red arrow, and the sequence starts again with first laser shot, A, at the next spot position. The Galil DMC program for the sample translation described above can be found in Appendix A.1.

The image files are named sequentially as they are collected. In a typical experiment, more than 2500 image files are collected. Post-acquisition, the image files are sorted into A to G top-level folders by laser shot and then again into subfolders (1^{st} image, 2^{nd} image, …) by the sequence of image acquisition after that laser shot. A typical data set consists images sorted into seven top-level folders named A-G, with A designating the plume of the first laser shot on each spot, and G designating the seventh laser shot on each spot. Within each lettered folder are subfolders named 1^{st} images, 2^{nd} Images etc. indicating the order of the images collected after the laser shot. In short, the subfolder 3^{rd} images found in the top-level D folder would contain all of the third images collected following the fourth laser shot from every spot, or sample position. A diagram of the serpentine pattern of motion is shown on the left of Figure 2.2. The ImageJ macro to sort the images as described above can be found in Appendix A.3. A montage of the first shot (A), 1^{st} images of polycarbonate plumes, arranged according to the serpentine pattern to reproduce to the physical pattern of laser shots on the PC sample surface, is shown in the middle of Figure 2. The montages of each laser shot (A-G) and sequential images (1^{st} – 9^{th}) are then assembled into a larger montage image, where the x direction corresponds to image number (1^{st}, 2^{nd}, etc.) through time, and the y direction corresponds to successive laser shots (A-G). A larger montage is shown at the right of Figure 2.2. The ImageJ macro to make these pattern montages as described above can be found in Appendix A.4. The missing spot on polycarbonate in the top right image in Figure 2.2 is related to the experimental timing. It is the result of translator motion being triggered on the Q-switch laser output. In the laser activation sequence, the Q-

switch must be on before the shutter can be opened, and lack of an electronic shutter open trigger signal upon which to begin translation. The result was that the motion began slightly before the shutter could be manually clicked opened using a mouse and hence, the motion that corresponded to what should have been the first one, two or occasionally three laser shots occurred before the shutter opened.

2.2 Timing of A Typical Experiment

All experiments were carried out using a Continuum Inlite III-10 laser system. The Inlite III-10 laser is a frequency quadrupled Nd:YAG produced a train of 6.5 ns laser pulses at 266 nm with 50 mJ of energy. The electronics of the laser provides TTL output signals timed with the operation of the flashlamps and the Q-switch. The laser pulse was focused to a spot size of 1.25 mm in diameter by adjusting the distance between the 140mm lens and the sample using the translator system at a sample to lens distance of 120mm. The laser was operated in a 10 Hz repetition rate with software divider of 2 resulting in laser pulses at 5 Hz. The q-switch was always set internally to fire at a 175 μs delay from the flash lamps. The q-switch output of the laser was sent through a Wavetek 50 MHz pulse/function generator model 166 to produce a sufficiently long pulse to trigger the other components of the experiment. Image collection and sample translation were both designed to be triggered by the Q-switch output of the laser. A

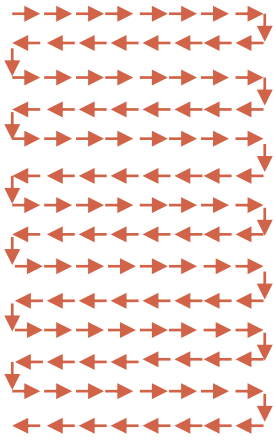

Serpentine motion pattern

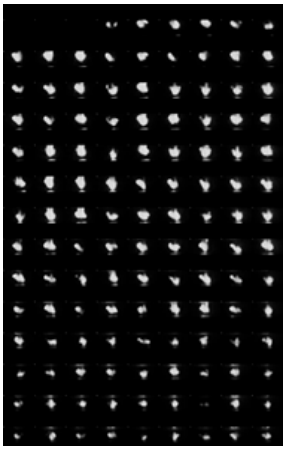

Montage of first shot (A) first images

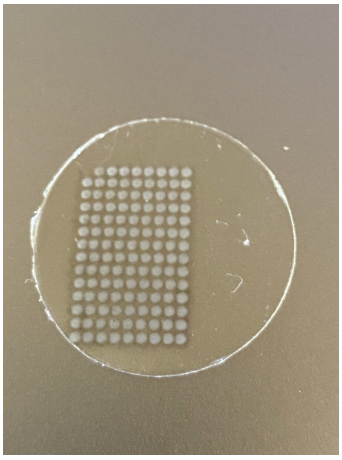

Shot pattern on Polycarbonate

Figure 2.2: Serpentine motion pattern (left), Montage of first shot plume images (middle), and shot pattern on polycarbonate (right)

buzzer also triggered by the Q-switch was added to provide an audible reference for the asynchronous collection of the sound files recorded on a smart phone using the VoiceRecorder app.

2.3 Sample Preparation

Polycarbonate (PC) thin films were purchased in 1 mil (256 μm) thickness sheets from McMaster-Carr; the protective film was removed from both sides. A nebulizing spray technique previously described[1] is used to spray RDX on these PC films, using a syringe pump (New Era, NE-300) with a 10 mL gas-tight syringe (Hamilton 1010), a solution of 5 mg/mL solution of RDX in acetonitrile that was pumped through a 32 GA SS-302 capillary at a rate of 1.5 mL/hour and surrounded by a flow of nitrogen that served as the carrier gas [1] [carrier gas pressure 20 psi flowing out a 1/16" ID steel tube]. Briefly, as the solution was slowly pumped through the capillary the small droplets of the solution emerging from the tip of the capillary were carried to the sample surface in the carrier gas. The droplets are dried as they are transported from the capillary to the surface by the dry N_2 carrier gas. The distance from the capillary tip to the surface of the wafer and the carrier gas flow rate have been previously shown to determine the size of the RDX crystals and the porosity of the thin film.[1] A 1.5 inch distance from sample to sprayer and flow rate of 15 psi was typically used for all experiments in this work. During deposition the sample was spun along the axis of the capillary at a constant rate of ~95 rpm on a motorized chuck. A PC mask with a 6 mm diameter hole punched in the middle was placed on top of the sample to define consistently sized/positioned RDX spots. A rough calculation, see equation 1, using a 5 minute spray time, the 1.5 mL/hour spray rate, a 5 mg/mL RDX solution, a density of RDX (1.82 g/cm^3) and a 6 mm diameter area defined by the mask result in an estimated film thickness of ~12 μm.

$$5\ minutes \times \frac{1.5\ mL}{60\ minutes} \times \frac{5\ mg}{mL} \times \frac{g}{1000\ mg} \times \frac{cm^3}{1.82\ g} = 0.000343\ cm^3$$

$$Volume\ Cylinder = \pi r^2 H \qquad (1)$$

$$0.000343\ cm^3 = \pi \times (0.3\ cm)^2 \times H$$

$$H = \frac{0.000343\ cm^3}{0.28274\ cm^2} = 1.213E^{-3}\ cm \times \frac{10{,}000\ \mu m}{cm} = 12.13\ \mu m$$

For some experiments, it was desirable to have RDX regions of different thicknesses on the same PC sample. To accomplish this, a rectangular mask was placed over half of the polycarbonate sample after a fixed period of spraying, typically 5 minutes. The sample, with half covered by a mask, was then sprayed for the same fixed period of time. At this point, the remaining exposed half of the sample was half covered with another rectangular mask, leaving only a quarter of the original polycarbonate surface exposed to spraying for a third and final fixed period of time. The resulting polycarbonate surface typically has one half that has been sprayed for 5 minutes, one quarter that has been sprayed for 10 minutes, and one quarter that has been sprayed for 15 minutes, see Figure 2.3.

Experiments involving the laser ablation of metals' powders were also conducted out of scientific curiosity of what affect the metals might have on spectral and plume characteristics. Films of Nickel, Iron, and Cobalt powders were prepared by covering double sided tape with fine powders of each metal. Metal samples on tape were then laser ablated and resulting spectra and plume images collected just as was done for typical RDX films on PC samples.

Laser ablation experiments of Ammonium Nitrate were also performed. The motivation behind these experiments was the presence of NO_x groups in Ammonium Nitrate and availability of this reagent in lab. NO_x groups are part of RDX, and it was of interest what role these groups might have in RDX ablation and plume behavior. Ammonium Nitrate experiments were performed in two methods. Ammonium Nitrate powder was dissolved in water and drop-cast on PC films and laser ablated identically to experiments of RDX films on PC were conducted. The

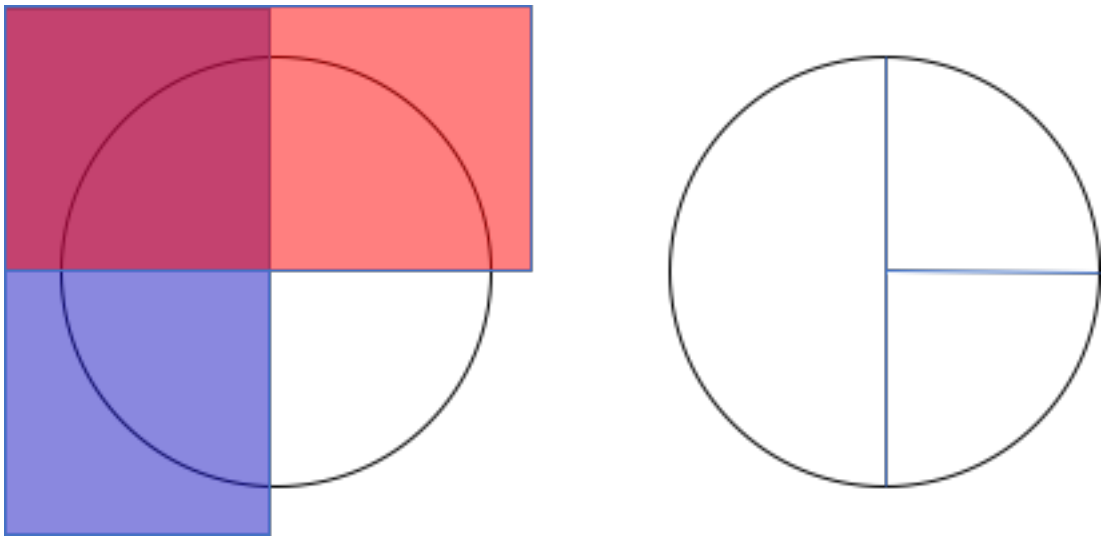

Figure 2.3: Variable spray pattern achieved with rectangular masks

second method of Ammonium Nitrate ablation was performed by backing in pellets of predominantly Ammonium Nitrate from the cold-pack found in first aid kits behind a PC film with a hole cut in the center. The Ammonium Nitrate pellets were then laser ablated through the hole in the PC film. Attempts at spraying Ammonium Nitrate dissolved in water was not an option due to corrosion of the metal capillary setup. Further, mixtures of Ammonium Nitrate in Acetonitrile could not be sprayed due to inability to dissolve the Ammonium Nitrate powder to a point that remaining particles would not clog the capillary.

2.4 Experimental Apparatus: The setup can be seen in Figure 2.4 below.

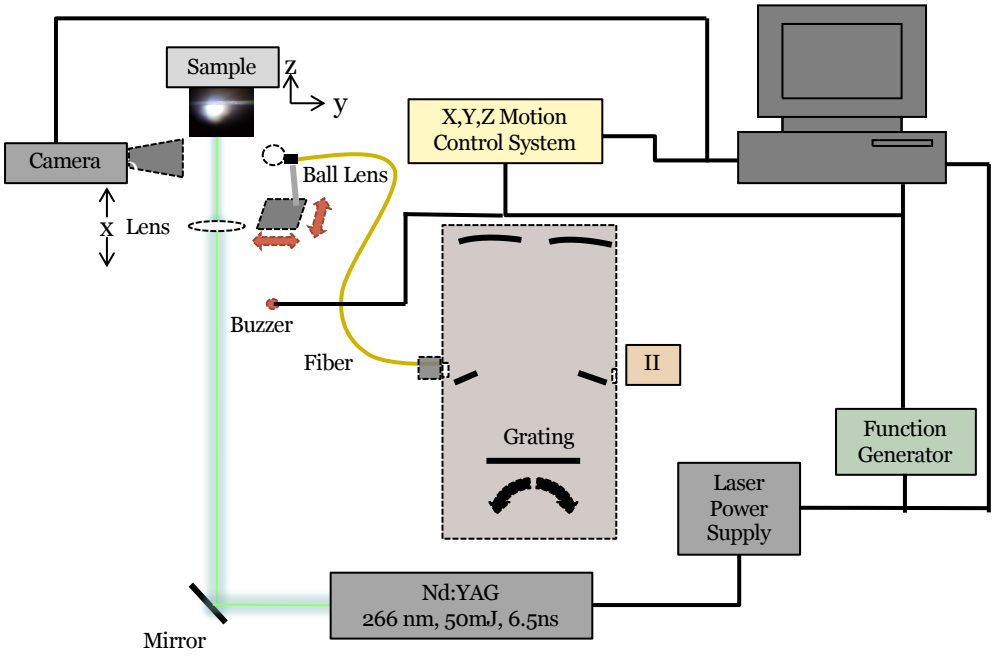

Figure 2.4: Schematic of experimental setup

2.5 Spectra Image Collection

Light from laser induced plasmas was delivered to the spectrometer through a ball lens (Edmund Optics, 32-748), which was focused onto the input end of a Ø1000 µm, 0.48 NA, 1 m long fiber (ThorLabs, M71L01). The output end of the fiber is positioned by an XY translator in front of the entrance slit (108 µm) of the spectrometer. The diffraction grating (PG&G 4160) was set to a grating of 150 grooves per millimeter with a blaze of 450 nm, to allow a ~400-1000 nm range of emission to be continuously output through the exit slit**.**

The diffraction grating based spectrometer (PG&G 4160) distributes the 460-820 nm region of the optical spectrum onto the part of a Varo image intensifier (Model# 510-9323-301) that is imaged by the fast camera (Miktronics MC 1311). The overall experimental set-up is identical to system utilized by Casper, except that a constant amplification is used in the Image Intensifier and images of the rear of the Image Intensifier are collected with the fast camera, described in more detail below. [2] In Casper's configuration, using a slow camera and pulsing on the image intensifier, only one spectrum, at a specific delay following the laser q-switch trigger, could be obtained per laser pulse. In the new configuration using the fast camera, twenty images, each 95 μs apart in time were collected for each laser pulse, as follows. A Helios HEL2MDBCL controller board and custom software built using Matrox Imaging Software Mil-Lite are used to collect the digital images. The operation of the camera is triggered with the same buffered q-switch signal as the translators and the buzzer. To optimize speed, the twenty buffered images are saved to bmp image files in the time between triggered camera operation. The frames per second (which determines the time between buffer images), black level, and analog and digital gain are set in the MC Control Tool fast camera control program, prior to the experiment. Image J was extensively used to analyze the plasma, spectra and microscope images. The Microsoft Visual Basic routine to operate the camera and collect 20 images following each laser shot can be found in Appendix 11.6.

The size of images is related to maximum camera frame per second speed. Higher frame speeds can be achieved with smaller frame sizes. Images of 100 x 50 pixels were used throughout the vast majority of this work, but some spectral images were obtained using 200 x 50 pixel image size to collect a wider range of the spectrum. This size was chosen as a compromise between speed and the appearance of a very small number of all white images that occur as errors when speed is set too high. These can occasionally be seen in the full montage images. The optimal speed was found to be 10,000 FPS or one frame every ~100 microseconds.

2.6 Data Analysis Routine to Estimate Plume Temperatures from Spectra

Blackbody temperature curves were fit to plume spectra of laser ablation experiments. The blackbody curves were fit to experimental spectra using the Microsoft Excel Solver tool to minimize the error between the blackbody curve and the spectral data by changing vertical offset, a scaling factor, and temperature, as seen in Figure 2.5. The plume temperature was taken as the temperature that provided the best fit to experiment. Confidence intervals were estimated according to a Poisson distribution. First a Microsoft Excel macro was run to vary the plume temperature from 0.5 to 1.5 times the best fit temperature and copy these temperatures and difference squared to the spreadsheet. These temperatures vs difference squared values were plotted and the minimum in differences squared identified. The square root of the minimum difference squared value is used to back calculate the temperature that produced that amount of error to estimate confidence intervals. This method is based on the assumption that the square root of the minimum difference squared provides a reasonable estimate for the Poisson distribution. [3]

Blackbody Equation

$$I = \left(\frac{8\pi hc}{\lambda^5}\right) * \left(\frac{1}{e^{\frac{hc}{\lambda KT}} - 1}\right) \qquad (2)$$

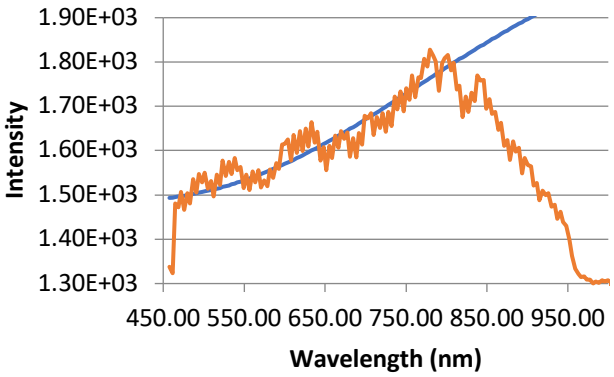

Figure 2.5: PC spectra fit to Blackbody

2.7 Plume Image Collection

The complete experimental setup for plume image acquisition is also shown in Figure 2.6, blue camera. The laser is set at 90 degrees from the sample surface as to prevent any plasma radiation from reflecting back into the laser cavity. The beam is then turned 90 degrees towards the sample by the 266 nm specific mirror (Melles Griot Y4-2037-0) positioned in front of the laser head at a 45 degree angle. The laser light then passes through the 120 mm focal length lens located on the X translator as described above, and onto the sample surface along the x axis. The y and z axis of the translator control the sample movement left to right and up and down, respectively. The fast camera is positioned perpendicularly above the sample holder, creating a

viewing plane that extended outward from the surface of the sample along perpendicular to the surface to image plumes as they expand from the surface.

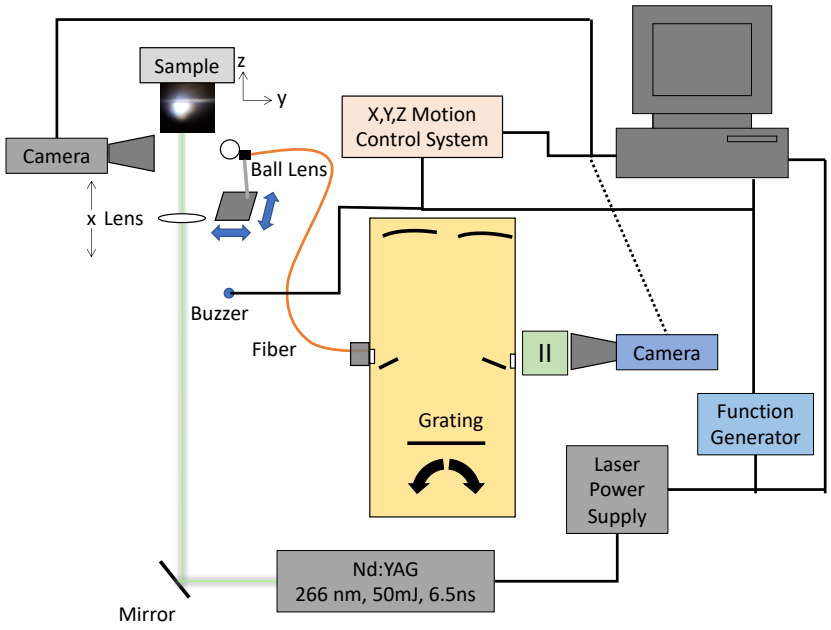

Figure 2.6: Experimental schematic: for plume images camera is aimed at the sample, for spectral images the camera is aimed at the Image Intensifier

2.8 Spectral Analysis Routine for Variably Sprayed Experiments

The plume photos from each variable spray time for each shot (A-G) were compiled in separate stacks in ImageJ. Each stack of plume photos for the variable sprayed region for each shot A-G were summed and histograms of each plotted. The histogram of each was then exported to Microsoft excel as the counts of pixels at each intensity. The number of bright pixels in each shot/variably sprayed region were defined as pixels with intensities from 185-255. The number of pixels was normalized by the number of shots in each sprayed region. For example, there were 19 laser shots in the A-shot/15 minute sprayed region, so, the number of pixels extracted from the histogram were divided by 19 (the 19 frames used to construct the histogram) to achieve the number of pixels per single frame. Normalizing the histogram data enabled comparison of different shots/spray times that contained different numbers of shots, and hence a different number of frames contributing to each histogram. The normalized histogram data was also used to compile the number of bright pixels per frame in each shot and sprayed region by summing the number of pixels of intensities 185-255. This value of bright pixels per frame was compiled for shots A-G in each region of the variable spray time experiments. The number of

bright pixels per frame of each shot and sprayed region were then averaged across all timed experiments of the same spray-time regiments, and compiled in tables and plots, organized by shots A-G.

Spectral images were calibrated, using the known emission lines of He from a gas discharge tube, to map out the locations of these spectral lines (388 nm, 447 nm, 501 nm, 587 nm, 667 nm, 706 nm) to pixel values on spectral images using the equation below.

Formula to calibrate wavelengths in Spectral Images

$$\text{Wavelength (nm)} = 335.7 + 3.6556 * \text{pixel} \quad (3)$$

2.9 Sound Images

Audio data was recorded using the VoiceRecorder app on an iphone. The mp3 file was then exported to Sonic Visualizer for analysis. A sound image montage was then constructed from coloring boxes, corresponding to the individual images of the montages, with the ratios of the relative magnitude of the laser pop to the reference buzzer sound following the same serpentine pattern as the sample translation.

2.10 Microscope Images

Microscope images were acquired using a 10x magnification.

2.11 References

1. Orland, A.; Blumenthal, R., *Nebulizing Spray Technique for Deposition of Propellant Thin Films*, *Journal of Propulsion and Power* 2005, *21*, 571-573.
2. Casper IV, Walter F. *A microsecond time-resolved spectroscopic study of laser induced plasmas and their interactions with solid materials.* Ph.D. Dissertation, Auburn University, Auburn, AL, 2015.
3. https://stattrek.com/regression/slope-confidence-interval.aspx

Chapter 3 Is the observed threshold for laser ignition of RDX an optical or thermal process?

3.1 ABSTRACT

A curious phenomenon has been observed in the laser ablation of non-energetic material polycarbonate (PC) and energetic material RDX (Research Department Formula X: Cyclotrimethylenetrinitramine/$C_3H_6N_6O_6$). The laser induced ablation pits were ten times as deep for RDX as they were with PC, and in our experiments RDX is clearly not ignited, but instead ablated, while others reported a threshold for laser ignition at ~250 mJ. The observation of the laser pits on RDX being deeper than those observed on PC has been proposed to be the result of sublimation due to plasma emission heating the RDX at the surface. Through a simple model of the plasma plume as a blackbody above a solid RDX surface, the possibility that ignition is the result of heating of sublimed vapor above the threshold for thermal reaction at high laser fluence has been investigated. The model, which included only the black-body temperature of the plasma plume surface and the height of the center of the plume above the surface was fit to observed pit sizes at 50 mJ per pulse irradiation. It is shown that at higher laser power (~250 mJ/ pulse), the temperature of the surface or subliming molecules become high enough for spontaneous thermal ignition of RDX.

3.2 INTRODUCTION

The interaction of a UV laser with the solid material RDX is modeled to investigate the mechanism of RDX ignition under high laser fluence. When a UV laser of sufficient fluence (described below) strikes a solid surface such as PC, a plasma is produced as chemical bonds are broken and atoms and molecules are ionized by the laser pulse, lasting several nanoseconds. The high-pressure plasma plume then expands until the plume pressure drops to atmospheric pressure. [1] From its maximum size, the plasma plume has been shown to emit at a single black-body temperature for several tens of microseconds. [2] During this process, the plume dissipates its energy into its surroundings by emission of light. After fitting the model to the observed rate of sublimation under irradiation conditions shown to produce pits ten times larger than those in PC, the effects of increasing the laser power to the reported threshold for laser ignition is investigated to determine the maximum temperature of heating by re-radiation in the IR range.

3.3 Model of Laser Ablation Pit Formation

A model to investigate whether laser ignition might be a thermal process has been proposed. In this model, the experimental observations about pit sizes were used to calibrate the model. Before assuming that the RDX laser ablation pits observed under 50 mJ UV laser irradiation in a 1.5 mm spot arise from the sublimation of molecular RDX, the first logical question would be what fraction of the experimental laser energy would be required to form them. This can be easily calculated from the standard enthalpy of sublimation of RDX, the density of solid RDX, and the volume of the pits as follows:

$$E_{pit\ formation} = \Delta H_{sub}\ x\ \frac{\rho}{MM}\ x\ V_{pit} \quad (1)$$

where $E_{pit\ formation}$ is the energy necessary for a sublimation pit, ΔH_{sub} is the molar heat of sublimation for RDX (112.5 kJ/mol), ρ is the density of RDX (1.804g/cm^3), MM is the molecular mass of RDX (222.1 g/mol), and V_{pit} is the typical experimental volume of a pit (4.71 x 10^{-6} cm^3; 500 μm radius and 6 μm depth), resulting in a total energy required to form such a pit of ~4 mJ. This energy is significantly less energy than that provided by the 50 mJ laser. The estimate E_{pit} for the ionization of initial plasmas similar to the sublimation but using the 0.6 um depth and the bond enthalpy for a 0.6 um pit depth is estimated at 0.00287018 mJ.

The actual experiment begins with a 6 ns, 50 mJ, ND-YAG 266 nm laser pulse focused into a 1.5 mm spot. The laser pulse is initially absorbed by the surface material, in a second order adsorption (non-resonant multi-photon ionization), resulting in the ionization and eventual bond breaking that creates the plasma. After this fraction of the laser light has been absorbed by the RDX, an optically dense plasma is formed and any remaining laser light is adsorbed by the plasma via a first order process, resulting in direct heating of the plasma. Once formed in this nanosecond long process, the plasma expands into the ambient gas environment until the plume pressure drops to atmospheric pressure, a process that takes a few microseconds. During this expansion process, the plasma plume loses energy both as it does work on the ambient gas and as it emits light. From this point forward, the plume will cool to room temperature through subsequent emission and thermal conduction into the environment, the later taking hundreds of microseconds, and hence ignored herein.

Our simple model begins after plume expansion and simulates the behavior of the solid below as the plume cools to room temperature. The plasma is assumed to be a sphere that emits its full energy as blackbody radiation. The sphere is placed at a variable fixed height above the

surface and is assumed to emit at a fixed temperature consistent with the observations of Casper.[2] Taking into account the cylindrical symmetry of a sphere over a solid surface, the surface below the plasma is divided into concentric rings extending into the surface of the RDX. The energy absorbed by each ring is then calculated as the product of laser pulse energy, the fraction of light impingent on the ring, and the fraction of that light absorbed by RDX, as follows:

$$E_{adsorbed} = E_{emitted}\ x\ fraction_{impingent\ on\ ring}\ x\ fraction_{light\ adsorbed\ by\ RDX} \quad (2)$$

where $E_{adsorbed}$ is the total energy adsorbed by the ring, $E_{emitted}$ is the total energy emitted by the plume as it cools to room temperature, $fraction_{impingent\ on\ ring}$ is the fraction of the energy emitted that would be impingent on the ring and $fraction_{light\ adsorbed\ by\ RDX}$ is the fraction of the blackbody spectrum that would be adsorbed by the RDX molecules of the ring. To determine the amount of energy that is impingent on each ring, one must first calculate the fraction of the light that is emitted from the plasma plume into the solid angle that is defined by the ring. For rings on the surface, the fraction emitted from the plasma plume is the fraction of the light impingent on the ring. For rings below the surface, the fraction of light impingent on the ring is reduced by light adsorption from the material present above the ring. From Beer's Law, one can calculate the intensity of light as it penetrates a material. Using an ATR transmittance spectrum for RDX,[5] the amount of light absorbed by a ring given its position was calculated. Using the heat capacity of RDX, the final temperature of the ring was calculated from the energy absorbed by the ring. Lastly, rings whose final temperature were calculated to be above the sublimation temperature were assumed to be sublimed and define the resulting pit.

The fraction of light emitted into the solid angle, defined by the ring, was calculated as the fraction of surface area of a sphere contained between two cones originating at the center of the sphere and extending to the inner and outer upper edges of the ring. Consequently, the fraction of the light emitted impingent on the ring is calculated as:

$$Fraction = -\frac{1}{2}\left[1 - cos\left(tan^{-1}\left\{\frac{r-\frac{s}{2}}{h+d}\right\}\right)\right] + \frac{1}{2}\left[1 - cos\left(tan^{-1}\left\{\frac{r+\frac{s}{2}}{h+d}\right\}\right)\right] \quad (3)$$

where r - s/2 is the inner radius of the ring, r + s/2 is the outer radius of the ring radius, h is the height of the center of the plasma sphere above the surface and d is the depth of the top of the ring below the surface of the RDX. The fraction of the light absorbed by the ring was calculated from the digitized ATR transmission as a function of wavelength, assuming black-body emission

at a constant temperature and a penetration depth of the evanescent wave into the RDX of 1/e times the wavelength as follows:

$$Fraction = \left(\sum_{\lambda} \left[100 - \left(Tr(\lambda)^{\left(\frac{L}{\frac{1}{e}\lambda} \right)} \right) 100 \right] x \left[\frac{2\pi hc^2}{\lambda^5 \left(e^{\frac{hc}{\lambda kT}} - 1 \right)} \right] \right) \Bigg/ \sum_{\lambda} \left[\frac{2\pi hc^2}{\lambda^5 \left(e^{\frac{hc}{\lambda kT}} - 1 \right)} \right] \quad (4)$$

where Tr(λ) is the transmittance at a given wavelength (λ), L is the distance the light must travel through the RDX on its way to the ring, h is Planck's Constant, c is the speed of light, k is Boltzmann's constant and T is the temperature of the black-body emitter. It should be noted that the fraction must be calculated across all relevant wavelengths and summed to get the total fraction of light adsorbed. The energy adsorbed by each ring was then calculated as in equation 2. From the energy adsorbed by the ring, the final temperature of the ring was calculated form the heat capacity of RDX (251.17 J/K·mol) as follows:

$$T_{final} = \frac{E_{ads}}{C_p V_{ring}} + T_{initial} \quad (5)$$

where E_{ads} is the total energy adsorbed by the ring, C_p is the heat capacity of RDX, V_{ring} is the volume of the ring and T initial is the temperature of the ring before the laser pulse. Finally, the volume of RDX removed, or the size of the resulting pit, was determined as the sum of all rings that achieve a final temperature above the sublimation temperature of RDX calculated as:

$$T_{sub} = \frac{\Delta H_{sub}}{C_p} \quad (6)$$

where T_{sub} is the sublimation temperature of RDX, ΔH_{sub} is the heat of sublimation of RDX (112.5 kJ/mol) and Cp is the heat capacity of RDX. Plugging in the experimental values for RDX, one gets a rough estimate of the sublimation temperature of 447K.

3.4 Results and Discussion

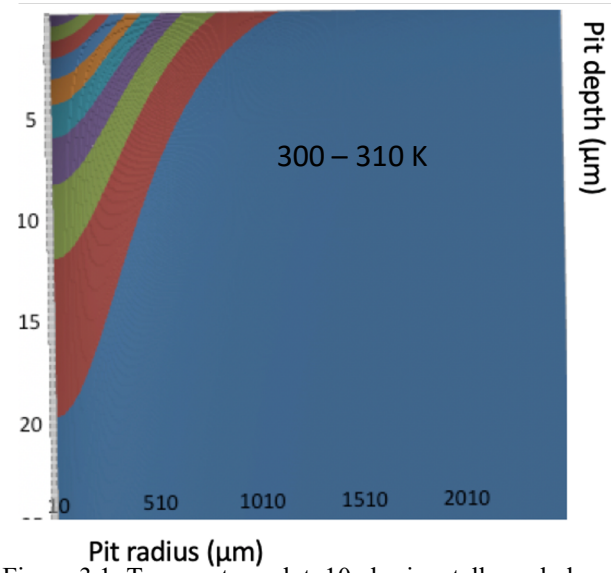

Figure 3.1: Temperature plot, 10x horizontally scaled, the blue region is 300-310 K, and each incremental color inward represents an incremental increase by 10 degrees

The model described above was used to generate temperature profiles of the solid RDX below the plasma, see Figure 3.1, using only two variable parameters: the emission temperature of the surface of the optically dense plasma and the height of the plasma above the surface. A third singular variable parameter, the sublimation temperature of the rings, was introduced to convert the temperature profiles into pit sizes for comparison with the 50 mJ UV laser ablation studies experimental data of Sun.[3]

Figure 3.1 is a plot of calculated ring temperatures with incremental colors indicating increasing temperature gradients in 10 K; the largest blue region is 300 – 310 K, with the next red region being 310 – 320 K. It is important to note that because the way the plot is scaled, the pit is actually ten times as wide as it appears to be in Figure 3.1, and is much wider (hundreds µm) of than it is deep (~1-20 µm).

The most critical parameter in fitting the data to the experimental results was the temperature of the plasma surface which re-radiates the laser power adsorbed by the plasmas, as

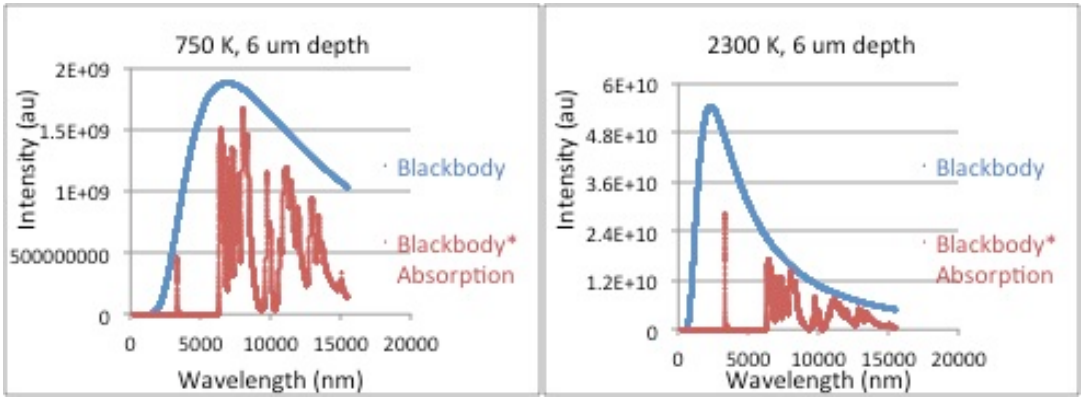

Figure 3.2: RDX absorbs more of the radiation at lower plasma temperatures

described above, to the surface. Based on the polycarbonate emission spectra of Casper, the initial guess for a plasma emission temperature was set to 2300K. The overlap of 2300K blackbody emission and the adsorption of light by a 6 um thick slab of RDX, based on the experimental ATR adsorption spectrum, is shown in Figure 3.2, left. Assuming blackbody emission at 2300K, the areas under the absorption curve divided by the integrated are under the blackbody curve results in a fraction of the energy absorbed that is only 5% the total emitted energy. Assuming all 50 mJ of the laser light to have been adsorbed by the plasma, the resulting 2.5 mJ adsorbed would be less than our previous estimate of ~4 mJ necessary to produce the observed pit sizes. This would seem to be evidence that material removal cannot just be sublimation as described by our model. However, the 2300K observed by Casper was observed for a polycarbonate plume not an RDX plume. Given that the true emission spectrum of a laser generated RDX plasma is not known, the possibility of lower plasma surface temperatures was then explored. The overlaps of 750K and 2300K blackbody emission with the adsorption of RDX are shown in figures 4.2. They result in 17.3% (750 K) and 1.639% (2300 K) of the emitted light, both of which would at first approximation appear to result in sufficient energy absorption to produce the experimentally observed pits.

As a result, full calculations of temperature profiles of the solid RDX below plasma radiating a total of 50 mJ of energy as a function of the height of the plasma were carried out at all four plasma surface temperatures (500K, 600K, 750K, 2300K) with 0.1 μm thick rings with

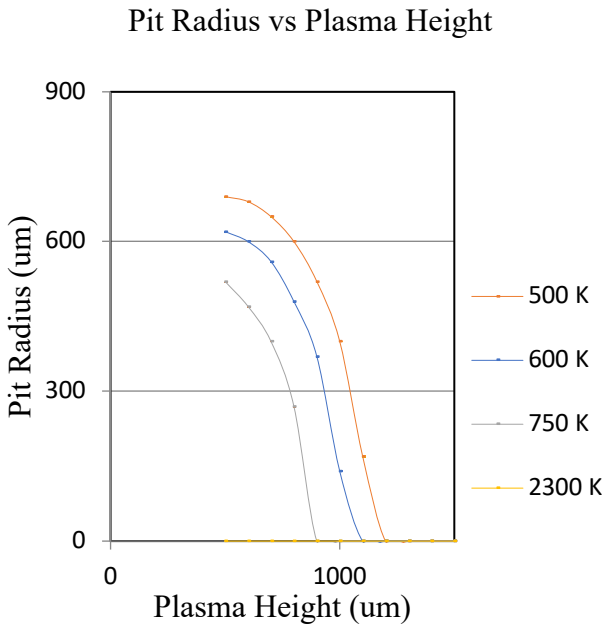

Figure 3.3: Lower temperature plasmas have wider pits

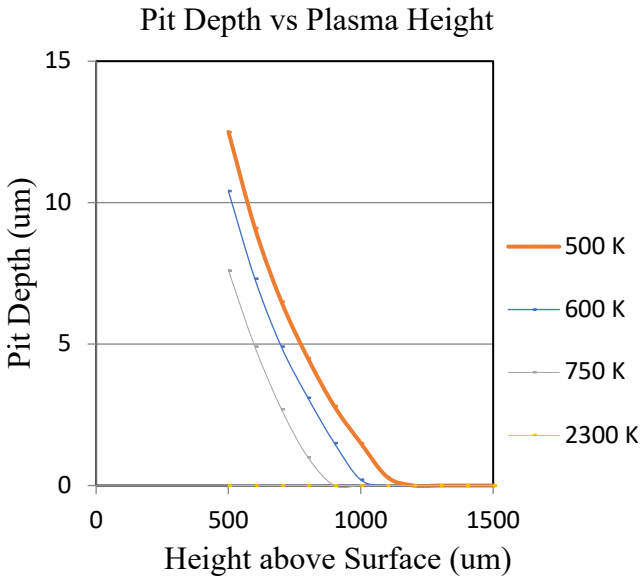

Figure 3.4: Lower temperature plasmas have deeper pits

radii spaced every 10 μm. Pit sizes were then determined to be composed of all rings for which a final temperature was above the roughly estimated sublimation temperature for RDX, ~450 K. Using 450 K as the pit defining temperature, yielded pits that were significantly smaller than those reported in the literature. As a consequence, a lower 400 K was tested as the threshold for sublimation. With 400 K as the pit defining temperature, model pits were brought into agreement with literature values of Sun using the same laser conditions.[2] The depths and widths of the resulting pits as a function of plume height above the surface at several possible surface emission temperatures are shown in Figures 3.3 and 3.4. It can readily be seen that 2300K plasma surface temperature cannot produce pits of the experimentally observed depth, but all of the lower temperatures could. The best fit to the experimentally observed 6 μm deep, 500 μm radius pits, was found by identifying the height of the plasma above the surface that results from a specific surface emission temperature, see Figure 3.3, and then reading the depth of the pit at that same height above the surface from the data in Figure 3.4. The resulting best fits to Sun's experimental RDX laser ablation pits, [13] measured with a profilometer to have a radius of 500 μm and depth of 6 μm, is between 600K at 0.6 mm above the surface and 750K and 0.5 mm above the surface.

To evaluate the reasonableness of the fit parameters, one can compare the heights above the surface to fast camera images of polycarbonate and RDX plumes, which are indistinguishable in the experiments, see chapter 5.-Using the same camera settings as used in the plume imaging, a ruler was placed where the plumes occur to determine the physical size of a pixel (10 pixels = 1 mm), and it was determined that plasma plumes occur an average of 0.75 - 1.50 mm above the surface of the polycarbonate film, see Figure 3.5.

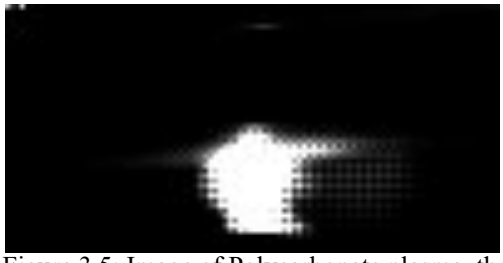

Figure 3.5: Image of Polycarbonate plasma, the bright spherically mass is the plasma plume, and the bright line extending to the right is the reflection of the plume on the planar polycarbonate surface

The diameters of the plasma plumes were determined in the same manner, and typically are 1.00 - 1.50 mm. The height of the center of the plume (0.6-0.7) that best fit experimental pit size is in reasonable agreement with the experimental imaging.

Calculations were then carried out for a 250 mJ laser pulse energy. In Figure 3.6 it can be seen that plasma temperatures at 50 mJ reach temperatures high enough for sublimation, and that at 250 mJ temperatures are sufficiently high to thermally ignite the surface RDX.

3.5 Conclusion

The formation of laser ablation pits in RDX as originating from the sublimation of RDX below the plasma plume as the plasma thermally radiates away its energy has been modeled. Correlating this model with experimental observations of pit depth and radius, it has been found that the RDX plume radiates at a surface temperature between 600-700 K from a height of 0.5-0.7 mm above the surface, which is in good agreement with experimental imaging , and that material removal requires a maximum temperature of 400K.

Carrying out the same calculation for a 250 mJ laser pulse, it has been found that RDX reaches temperatures in excess of 900K, sufficient for thermal ignition of the RDX itself, see Figure 3.6. Hence, laser ignition of RDX under these high fluences is an indirect result of laser exposure and more correctly correlated with thermal ignition.

Finally, considering the fact that Gottfried did not observe strong emission from RDX after the first frame of imagery, it would be consistent with the conclusion that the emission (fixed temperature emission of plasma) is at ~600k, which emits in the infrared and would not be likely to observed by her instrument (invisible to her instrument). The same would be true for the similar observations of Casper. [4]

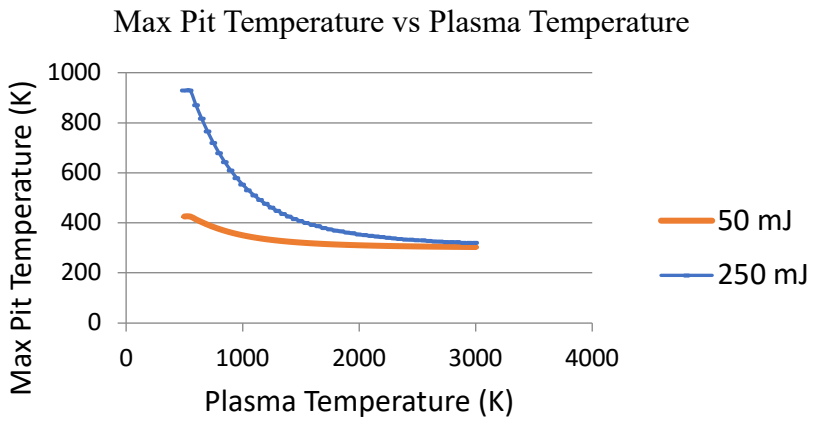

Figure 3.6: 50 mJ can sublime, 250 mJ is hot enough for ignition

3.6 REFERENCES

1. Bormotova, T.A.; Blumenthal, R. Ultraviolet laser ablation of polycarbonate and glass in air. Journal of Applied Physics, 105, 034910 (2009)
2. Casper IV, Walter F. *A microsecond time-resolved spectroscopic study of laser induced plasmas and their interactions with solid materials.* Ph.D. Dissertation, Auburn University, Auburn, AL, 2015.
3. Sun, H. Dissertation Auburn University 2011

4. J.L. Gottfried, *Influence of exothermic chemical reactions on laser-induced shock waves*, Phys. Chem. Chem. Phys. 16, 21452 (2014)
5. http://www.chromacademy.com/lms/sco533/images/P15-Evanescent-wave-1.jpg

Chapter 4 Investigations Of The Counter-Intuitively Short Lifetimes Of The Visible Emission From Laser-Induced Plasmas From RDX

This chapter is identical to a paper previously published for JANNAF (Joint Army, Navy, NASA, Air Force), with the exception of the removal of the abstract and introduction sections.

4.1 Plume Images

PC disks and PC disks with thin films of RDX sprayed on them were laser irradiated, and the resulting plumes were imaged directly with the fast camera as the disks were translated. A data set of all the single laser shots was then sorted by the laser shot (A-G, with A designating the plume of the first laser shot on each spot and G designating the last) and also by image (1st indicating the first image in the buffer, etc.) and then assembled into a montage image, where the x direction corresponds to successive images through time, and the y direction refers to successive laser shots on the same spot of the sample. For example, the top left frame is all the 1st images collected of the A (first) laser shot for a PC sample. Below it are all the 1st Images collected from the B (second) laser shot. To its right, are all of the 2nd Images collected of the A laser shot.

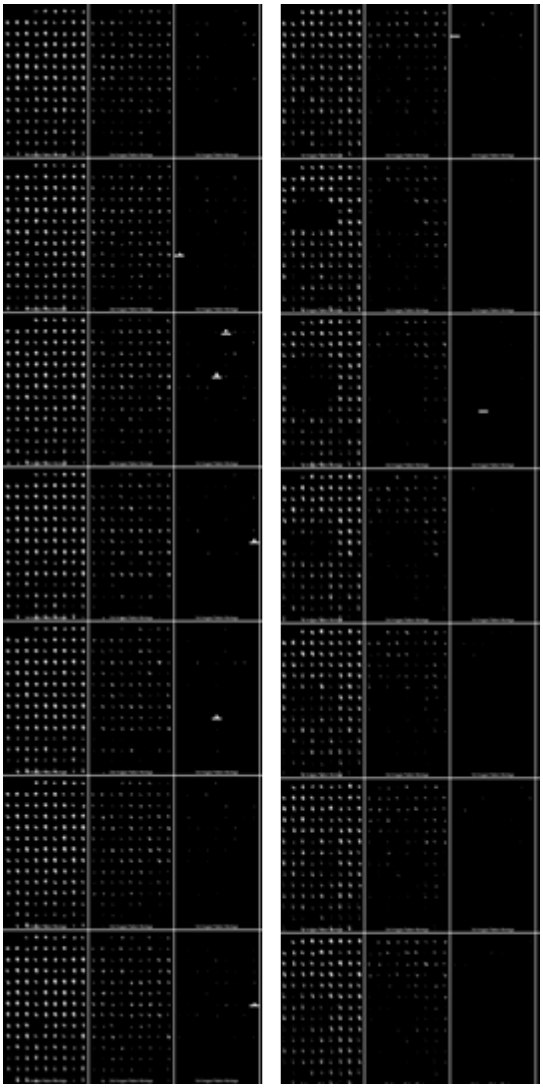

Figure 4.1: Photo Montages of laser irradiated PC (left) and RDX on PC (right)

When pure PC is laser irradiated, the 1st images of all of the laser shots (A-G) at each sample spot are almost equally bright, as seen in the very similar frames running vertically down the PC image in Figure 4.1. For PC films upon which RDX films of at least five minutes of spray time have been deposited, something very different is observed. On the right side of Figure 4.1, one can see that the 1st images of the A

laser shot resembles the rectangular pattern seen in all shots for PC, but in subsequent laser shots, B, C, D, E and F a dark region appears that corresponds exactly to the location where the RDX film had been sprayed. This dark hole in the rectangular pattern of plumes can be readily seen in the 1st and 2nd images collected. Finally, in the later laser shots, the hole appears to fade back to the original bright rectangles. Further, with longer spraying times, and thicker films, the dark region is observed to not appear until laser shot C and for the thickest films not until laser shot D.

It is suggested that for the sample shown in Figure 4.1, the first laser shot ablated only a little more than the top half of the RDX, resulting in a bright plume. However, upon the next shot, due to the first laser shot thinning of the RDX film, the B laser shot removes both the RDX and underlying PC, resulting in a dark image. The proposed process is depicted in Figure 4.2. Basically, it is suggested that the region where RDX has been deposited goes dark only when the laser pulse produces a plume that includes both RDX and PC. This assertion is at a minimum consistent with previously been reported results that, under the laser conditions used in this and prior work, laser ignition of RDX is only achieved when the plume contains PC in the plasma, and we think they appear dark because combustion products are not visibly emissive and/or energetic plasma plumes decay much faster than non-energetics, and are typically not imaged on this timescale.[1, 2] Simply put, depending on RDX film thickness, the

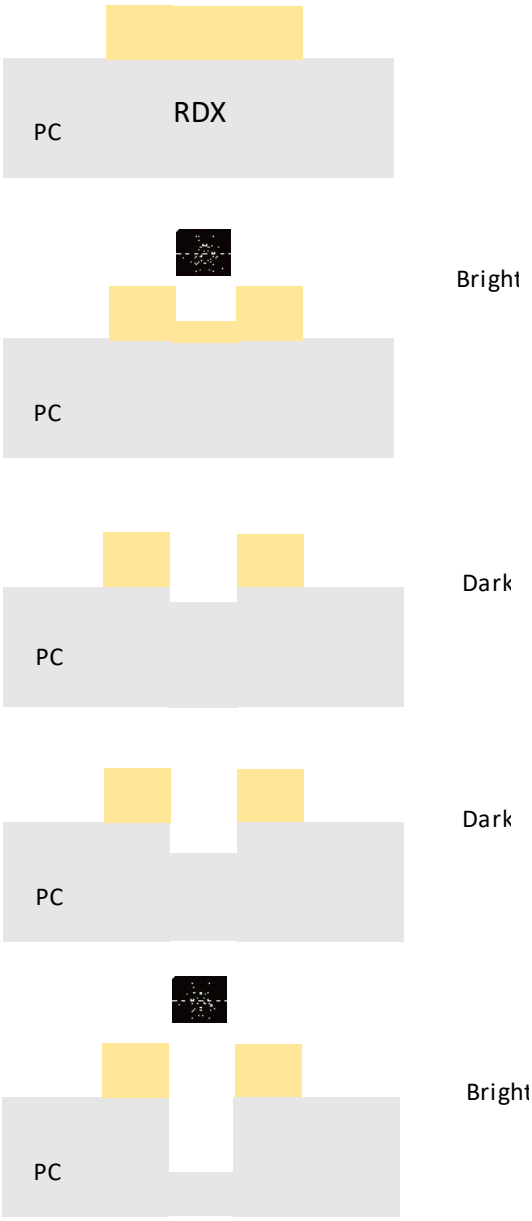

Figure 4.2: Schematic diagram of material removal on successive laser pulse (top to bottom)

first one or two laser shots ablate pure RDX creating bright plumes until the RDX film is thinned to the point when the next laser shot interacts with both PC and RDX, igniting the RDX (dark). Finally, as the RDX is removed by subsequent shots, the frames return to the bright rectangular images as only the underlying PC is exposed to laser shots. The explanation of why it takes multiple laser shots after the dark "ignition" is presented below in the discussion of the optical microscope images of the films before and after laser irradiation.

Under the model above, the laser shot (A-G) where the dark circles should appear in the rectangular images should depend linearly on time of RDX spraying. The longer spray times would require more laser shots to ablate RDX to the point where the laser can interact with both RDX and PC resulting in ignition. This has generally been observed to be the case. The dark region appears in later shots for longer spray times, but this relationship has not been completely consistent. We suspect that this could be related to flow fluctuations through the capillary, which is used repeatedly, possibly as RDX precipitates at within the capillary or at the tip.

PC plume images have also been analyzed for the number of pixels with a specific intensity as a function of intensity. Plots of this sort of data are referred to as histograms of the data. Histograms of the 1st, 2nd, 3rd and 4th images of a single laser plume on PC are shown in Figure 4.3. What is obvious from the plots is that through time, while the number of bright pixels decreases, the absolute brightness of the fewer bright pixels does not. In other words, at later times, a smaller population of the same distribution of bright pixels still exists. If the plasma were in fact a cooling blackbody, one would expect to see the brightness at each physical position to exponentially decrease through time, and that would be seen as a continuous shift of distribution to lower brightness through the four images. We believe

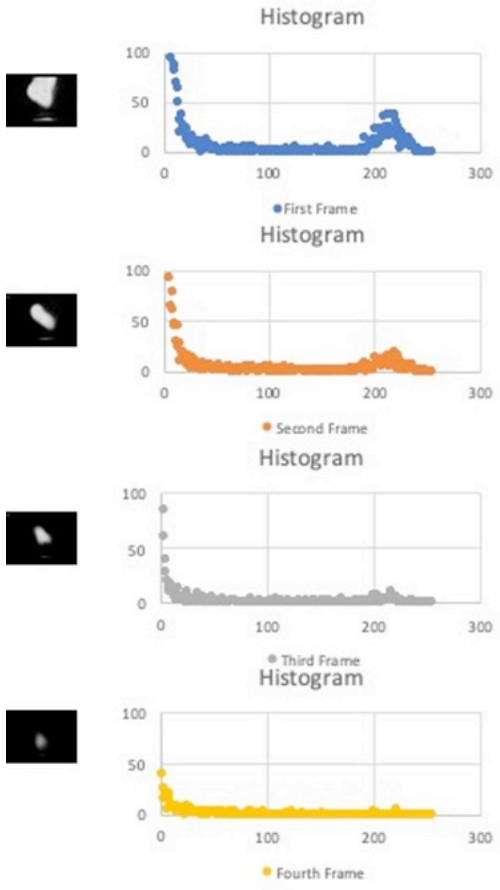

Figure 4.3: PC plume Images and Histograms for 1st, 2nd, 3rd and 4th Images

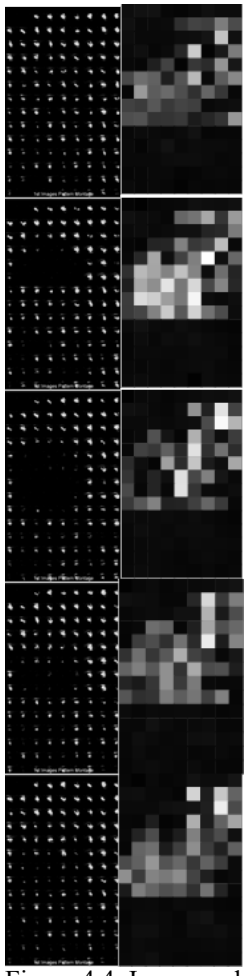

Figure 4.4: Image and sound montages for the same experiment

that this is further evidence that the emission of these plumes is the emission from a constant temperature surface of an optically dense plasma with a receding volume, where the temperature of the surface reflects the temperature of a phase transition between the plasma and hot gas states. In other words, the plasma volume recedes as the energy loss by emission from the surface results in an insufficient temperature to maintain the plasma state. So, as the plasma recedes, there is less surface to emit, resulting in a smaller population of equally bright pixels.

4.2 Sound Images

During the RDX experiments described above, it was observed that some of the pops were louder than others in a recurring pattern, and as a consequence it became standard practice to collect audio recordings simultaneously to collecting the images of the plumes. Analysis of audio recordings of experiments indicated a recurring pattern of louder pops every seven laser shots. The addition of a buzzer provided an audio marker of sample motion in the recordings. Assuming that the ignition of RDX produces a distinguishably louder pop than the laser ablation of PC, "sound images" were assembled to compare with the plume images. The ratio of the magnitude of the sound of each laser shot to the buzzer sound at each spot was used to generate a color for each box corresponding to laser shot in a montage assembled the same way that was done with the plume images, with brighter colors corresponding to a greater relative amplitude of laser pop to buzzer beep than darker colors. Figure 4.4 is the plots of the sequence of sound images to the right of the corresponding plume images of the same experiment. A correlation appears to exist between the dark regions of the plume images, previously asserted to indicate ignition, and the bright regions of the sound image.

4.3 SPECTRAL IMAGES

After repositioning the camera to view the Image Intensifier, twenty images, containing the spectrum of each plume every 100 μs, were collected for each laser shot and sorted in a manner identical to that employed in the plume imaging experiments. Montages of these spectral

images were constructed. They revealed the same emergence of a dark region where a thick RDX film had been sprayed after one or two laser shots as was observed in the plume images. Spectra were obtained from the spectra images by subtracting a background, the sum of the 9th images taken 900 μs after the laser shot, before summing the image vertically. Spectra images of Hydrogen, Helium, and Krypton gas discharge tubes where collected and used to calibrate the relationship between wavelength and horizontal pixel number, which turned out to be linear. Temperatures of the respective plumes were then obtained by fitting the experimental spectrum to that of a standard blackbody, over the range 550-820 um wavelength range. The spectra have not been corrected for lenses etc. and have only been fit to a Blackbody for crude temperature estimates. A spectrum for "pure" RDX plumes could theoretically be obtained by summing the spectra of A (or A and B) laser shots of only those spots where the dark region would appear in laser shot B (or laser shot C). The process was repeated for the 1st, 2nd and 3rd images. For reference, the spectrum for "pure" PC plumes was obtained by summing the spectra of all laser shots at spots prior to the sample translation moving over the first sample spot that went dark in the B or C laser shots. Preliminary measurements of temperatures of "pure" RDX and PC plumes proved them to be indistinguishable, with a temperature between 4600 and 4700K, which lasted through all three images, over 300 μs. This observation is also consistent with the model of laser-initiated plasma plume emission, where the emission comes from a constant temperature surface of an optically dense plasma that is shrinking in volume over time, where the surface is defined by the boundary between the plasma (emitting) and hot gas (non-emitting) phase.

4.4 MICROSCOPE IMAGES

RDX films were analyzed with a 10x microscope for any changes in morphology occurring after laser irradiation. Figure 4.5 (left) is a top down image of the surface of a RDX film on PC that was not laser irradiated. The film is not uniform, there are some abnormalities and some black dust is observed on the film. Figure 4.5 (right) is an image of the same RDX film after a typical laser irradiation experiment. A pattern of ovals, spaced as would be expected for the laser irradiation spots, are observed with white regions between them separated by dark rings. These ovals are believed to be the regions of the film that were directly irradiated.

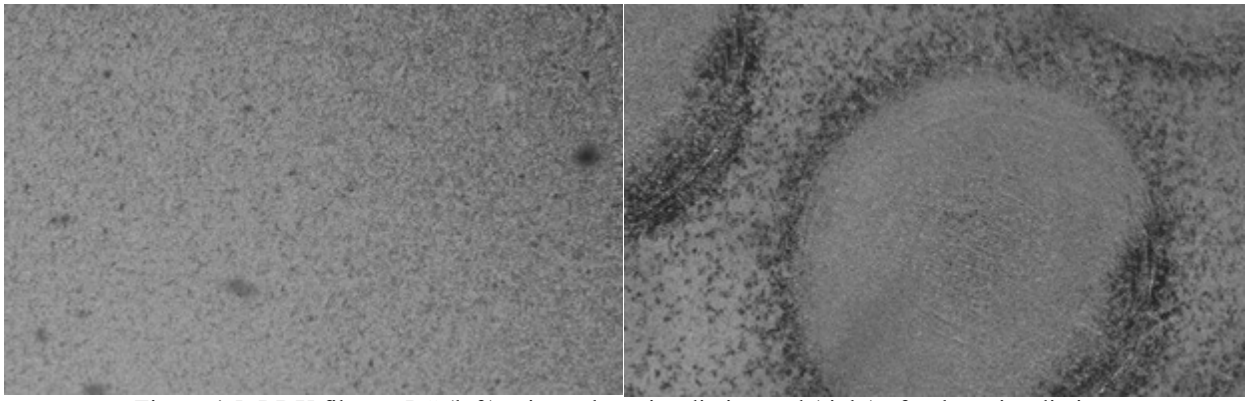

Figure 4.5: RDX film on PC (left) prior to laser irradiation and (right) after laser irradiation

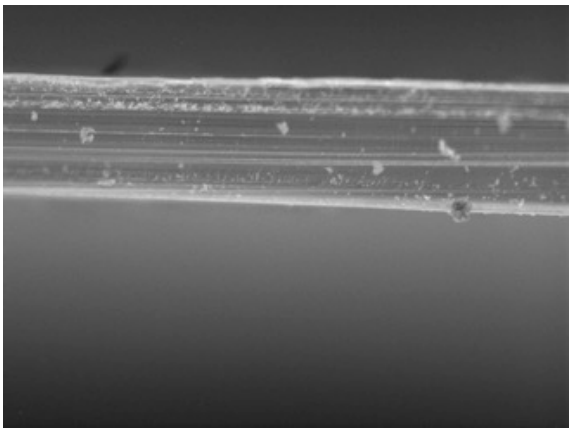

Figure 4.6: Cross-section image of RDX on PC

Figure 4.6 displays a cross sectional image of a RDX film on PC that had not been irradiated. A thin white layer, the RDX film, is seen on the top of the 256 μm thick PC. Calibrating distance in pixels from the known thickness of the PC, it is found that the RDX film in this image is ~13 μm thick, in good agreement with the estimate for the 5 minute spraying time.

Figure 4.7 is a cross-sectional side view of an RDX on PC sample irradiated seven times as in the previous imaging experiments taken across a region of an oval, or where the film was directly irradiated. All measurements of thickness are made using the calibration from the 256 μm thickness of the non-irradiated PC film, in Figure 4.7. In the irradiated area there is extensive

fracturing or melt regions to a depth of 142 µm that are not present with pure PC. At point A, the depth of unperturbed PC, the lowest potion of the material, goes from 114 µm at point A to 134 µm at point D. The total thickness of the sample is 225 µm at B and 236 µm at C. The other important feature of this image is that moving from left to right, the upper layer of the sample appears to go from clear to cloudy. Based on the thickness trend of the unperturbed PC, it is concluded that this cross section is leading to the center of an oval irradiation feature.

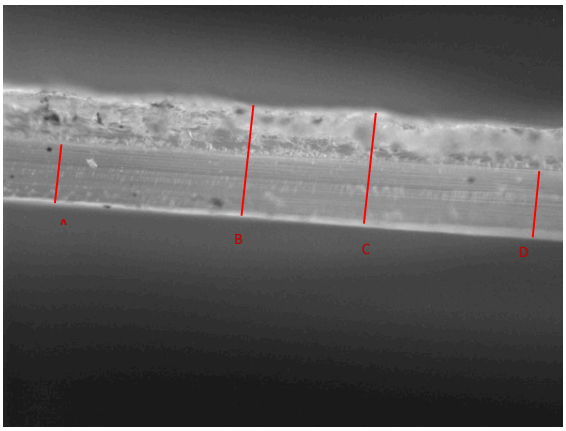

Figure 4.7: Cross-sectional view of irradiated RDX on PC in the oval feature

Figure 4.8 is a microscope image of a different cross-sectional region of the same irradiated sample shown in Figure 4.7. The white region on the top of the film is referred to as the "snow-pack" region, and is 34 µm in depth. The white region appears to be heavy/thick melt located at the periphery of the crater. There is fracturing or further melt below the "snow-pack," with a thickness of 75 µm. The unperturbed PC region is 135 µm thick. This thickness is consistent with point D, also likely at the periphery of the crater. The "snow melt" region cannot be wiped off nor can it be dissolved with water, so it is not simply RDX. It is either highly fractured PC, or more likely, a region of the sample where the PC temporary melted allowing the RDX to be incorporated into the PC before it re-solidified.

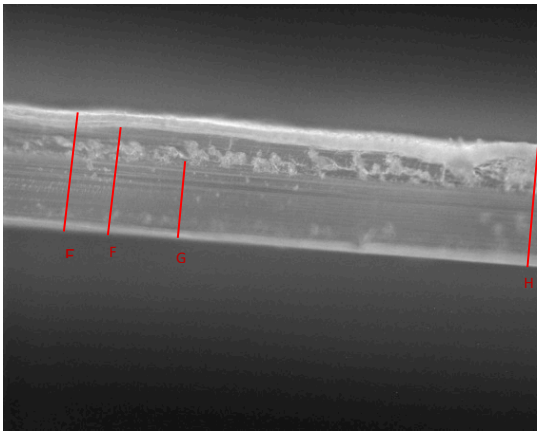

Figure 4.8: Cross-sectional view of RDX on PC, post laser irradiation at another position

More of the "snow-pack" features are evident in Figure 4.9; this position is likely also at the periphery of the crater. The total thickness is at point K including the "snow-pack" is 242 μm. The snow-pack is 61 μm at point M is thicker than at point F. The unperturbed PC is 143 μm in thickness, thicker than in either of the previous images, suggesting this image must be at the periphery of a crater since the unperturbed PC is thicker.

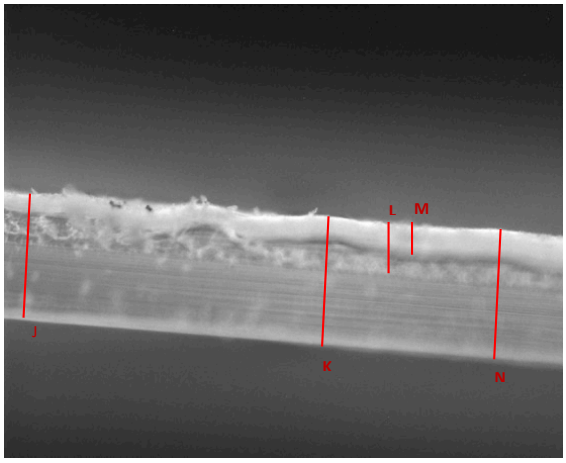

Figure 4.9: Cross-sectional view of irradiated RDX on PC between oval features

Finally, it is this "snow-pack" found between directly laser irradiated regions that explains why more than one laser shot may appear dark and why it frequently takes more than one laser shot for the plumes to return to the brightness of pure PC. If, as suspected, the "snow-pack" is PC that melted under re-irradiation by the laser plumes near it, made white by RDX dissolving into it before it re-solidifies, it is not hard to imagine that a similar process could also occur at the bottom of thick RDX films as bright "pure" RDX plumes are formed at the top of the RDX film. The multiple dark images of laser shots may be the result of ablation/ignition of a thin "snow-pack" formed below the film. Ignition or dark images would then be expected to continue until the underlying the "snow-pack" is completely removed.

4.5 CONCLUSIONS

We have observed several interesting phenomena in the UV laser irradiation of RDX films on PC. UV laser irradiation of thick RDX films produces bright plumes resulting from the first, second, or even third laser shot depending on film thickness; these plumes are currently indistinguishable from those observed for PC. Subsequent laser shots on the regions of the PC covered with the circular RDX films sprayed on PC appear dark in the plume spectra and in the plume images and brighter in the sound images. Following the appearance of the dark circles in the rectangular pattern in the montages of individual laser shot images, there is a return to bright plumes after 2-3 laser shots. The presence of the first bright plumes from the RDX region is interpreted as indicating that the RDX films are thicker than the amount removed by a single

laser shot and the "pure" RDX plume is bright. Subsequent laser shots remove more than the remaining RDX thickness (and therefore remove some of the underlying PC to mix with the RDX) are the ones that appear dark. We hypothesize that this lack of a bright plasma in this scenario corresponds to ignition in mixed RDX and PC plasma, similar to what was observed for thin PC films on RDX.[4] It takes several laser shots for the plumes to return bright from dark. This is because "snow-pack" features may form below the RDX film, and the "snow-pack", which is believed to be RDX that has dissolved into melted PC also make mixed RDX and PC plumes when irradiated. Then once all RDX and snowpack features have been removed, subsequent laser irradiation returns the plume images to those of PC after the RDX film has been removed. Observations of PC plumes at ~100, 200, 300, and 400 μs indicate that the surface of the emitting plume is nominally at the same temperature as the size of the plume recedes.

Analysis of the intensity of the sound emanating from the laser irradiation of RDX coated PC films can be used to produce "sound images" that replicate light-dark differences of the RDX region in the fast camera images, suggesting that the fast camera, though useful, may not be necessary. This preliminary work characterizing RDX via the analysis of spectra and plume images of laser induced plasmas demonstrates the feasibility of laboratory scale experiments rather than full-scale detonations to study energetics.

4.6 REFERENCES

1. Casper IV, Walter F. *A microsecond time-resolved spectroscopic study of laser induced plasmas and their interactions with solid materials.* Ph.D. Dissertation, Auburn University, Auburn, AL, 2015.
2. J.L. Gottfried, *Influence of exothermic chemical reactions on laser-induced shock waves*, Phys. Chem. Chem. Phys. 16, 21452 (2014)

Chapter 5 Plume and Spectra Image Montage Investigations of Multiple Laser Shots on thin RDX Films

In chapter 4, the process of the formation of and structure of a "snow-pack" region was proposed. To further investigate this "snowpack" and its effects on plumes, experiments were carried out on thinner films.

5.1 Spectral Image Montages

5.1.1 15 minute RDX on PC

Figure 5.1 is a photograph of a PC film sprayed for 15 minutes with RDX. Figure 5.2 is a montage of plume spectral images for that 15 minute RDX spray on PC. Spectral image montages were produced in a similar manner to previously described plume image montages. The individual plume spectral images are arranged to reproduce the physical arrangement of shots on the substrate surface. Because the spectral images are wider than they are tall, black background is placed between each row of shots so that the rectangularly shaped spectral images can be arranged in the same square pattern of shots on the PC surface. Note that this is a much shorter spray time used in chapter 4 experiments (they were at least 30 minutes). There is a dark region visible in the first and second frames of shots A-E, at the location the RDX was sprayed. This is consistent with previous findings that the region sprayed by RDX generally does not display bright plumes. In experiments with longer spray times, 30 minutes or longer, the first image is typically bright, with the dark region where the RDX was sprayed appearing in subsequent images. This observation was interpreted as the result of the first laser shot on a thick layer of RDX producing a bright plume similar to that observed for laser shot on PC. The fact that the first laser shot of this experiment is dark in the RDX region could imply that with the shorter spray time, i.e. a thinner film, the first laser shot (shot A) is able to interact with both PC and RDX, resulting in the dark spectral images from the RDX region. This is consistent with the assertion that plumes go dark when only when the laser pulse produces a plume composed of

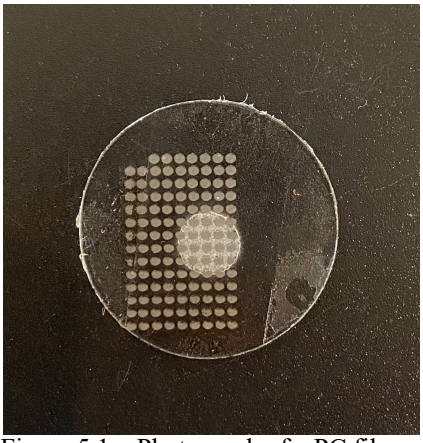

Figure 5.1 – Photograph of a PC film sprayed for 15 minutes after laser exposure.

both PC and RDX. In this montage, the dark region persists through the second laser shot (B) and all the way to the fifth laser shot (E). By the 6th and 7th laser shots (F and G), the RDX region

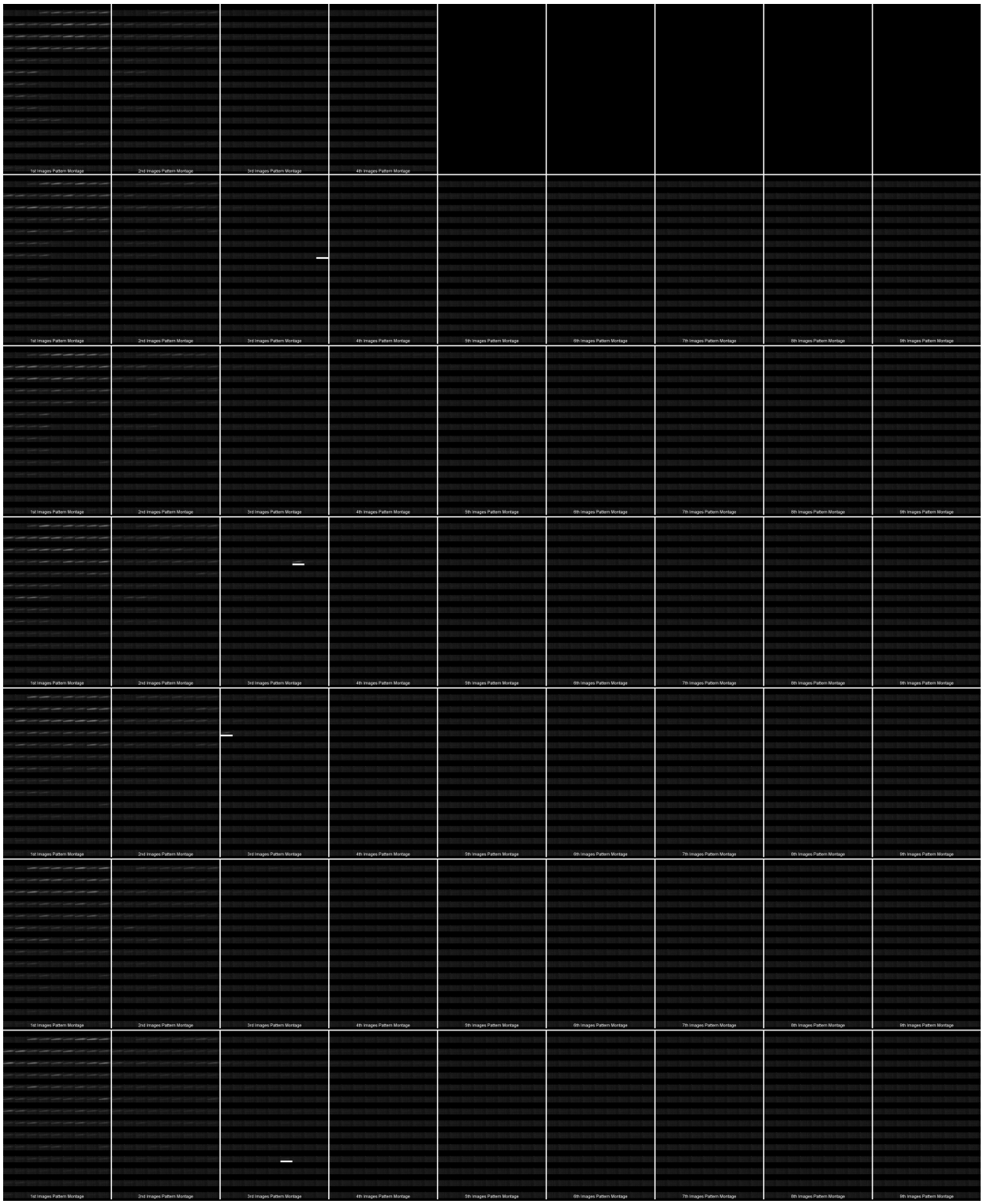

Figure 5.2 – Spectral Montage of the same 15 min RDX on PC (multiplied 3x in ImageJ) as seen in Fig. 5.1

returns to bright plume images, likely indicating the complete removal of RDX and, hence, laser ablation of the underlying pure PC.

Figure 5.3 is a photograph of another PC sample sprayed for 15 minutes with RDX, as an example of the variability of the appearance of the dark regions where the RDX was sprayed in these experiments. The Spectral Image Montage of the same experiment is displayed in Figure 5.4. It should be noted that A and B shots in the first image start out bright across all spots. The dark region appears in shot C and persists until shot E. The bright spectra then returns in shots F and G.

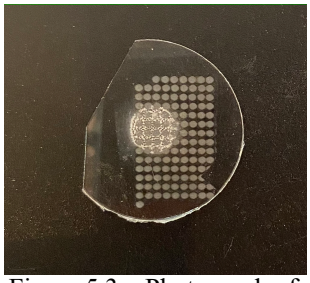

Figure 5.3 – Photograph of another PC film sprayed for 15 minutes after laser exposure.

5.1.2 15 min RDX on glass

RDX was sprayed on glass slides and then laser ablated to investigate whether the appearance and disappearance of the dark region, where the RDX was sprayed, in intermediate laser shots might be related to the interaction of the laser with both PC and RDX. Figure 5.5 displays the full spectral montage images of a 15 minute RDX spray on glass that has been background subtracted (-25) and then multiplied 3x (using ImageJ) for visual enhancement. Since most of the full montage is virtually identical, the first two frames of images of the first and second laser shots (A & B) are shown in Figure 5.6. The spectral images of plumes produced by the laser exposure on glass are much less intense than those on PC. There is a faint dark region where the RDX was sprayed in the first shot only. This is inconsistent with the assumption that the dark regions are due to the interaction of the laser pulse with both PC and RDX. Since the dark spot is smaller than the RDX spot itself, it is unclear if the dark spot on the glass is due to the RDX, or simply the obscuring of the underlying glass by the RDX, or perhaps some other physical phenomena. Because the effect of interest is so subtle, a similar figure of an experiment carried out under the same conditions is shown in Figure 5.7. The dark region can again be seen in the first and second images of shot A only. The spectral images of plumes transition back to bright through the second shot (B), and by the third shot (C), the spectral images of plumes in the RDX region are indistinguishable from the plumes on the glass region. It is significant to note that the plumes formed from laser shots on glass that was not coated with RDX are much brighter than the plumes in the first shot of the RDX-covered region on glass. In addition to this difference in spectral intensity.

The observations of 15 minute films were consistent with previous findings using thicker films (30+ minute sprays). RDX on PC experiments had dark regions visible in the first and second frames of shots A-E, at the location where the RDX was sprayed. In contrast to the longer sprays of 30+ minutes, with the 15 minute sprays, the first shot image has a dark region rather than appearing bright. This is attributed to the thinner film thickness which permits the

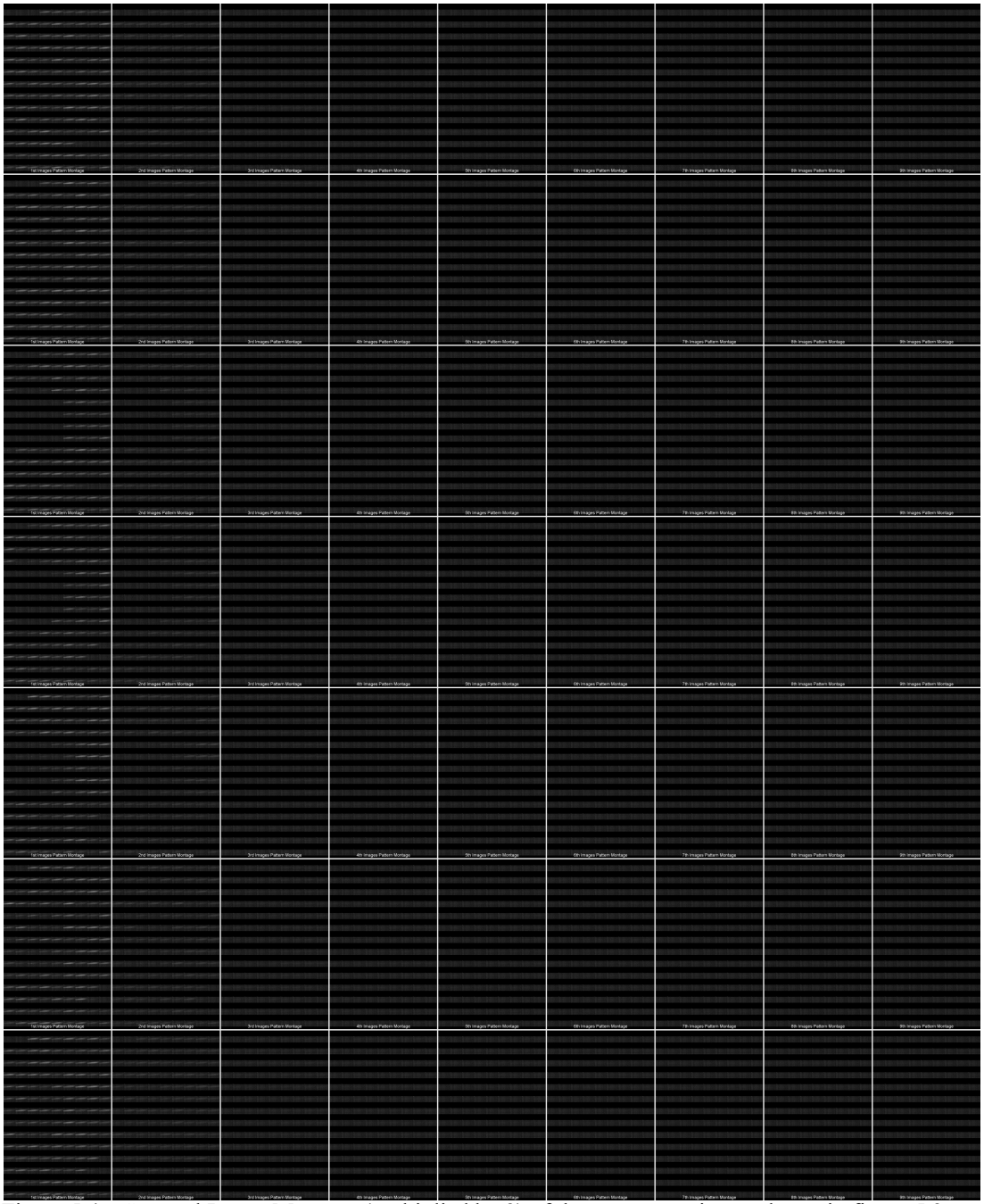

Figure 5.4 – Spectral Image Montage (multiplied by 2) of the same experiment shown in figure 5.3

interaction of both RDX and PC in the first shot, creating the “snowpack,” and resulting in the lack of a bright plume, whereas bright plumes were seen in the first shot images of longer spray times.

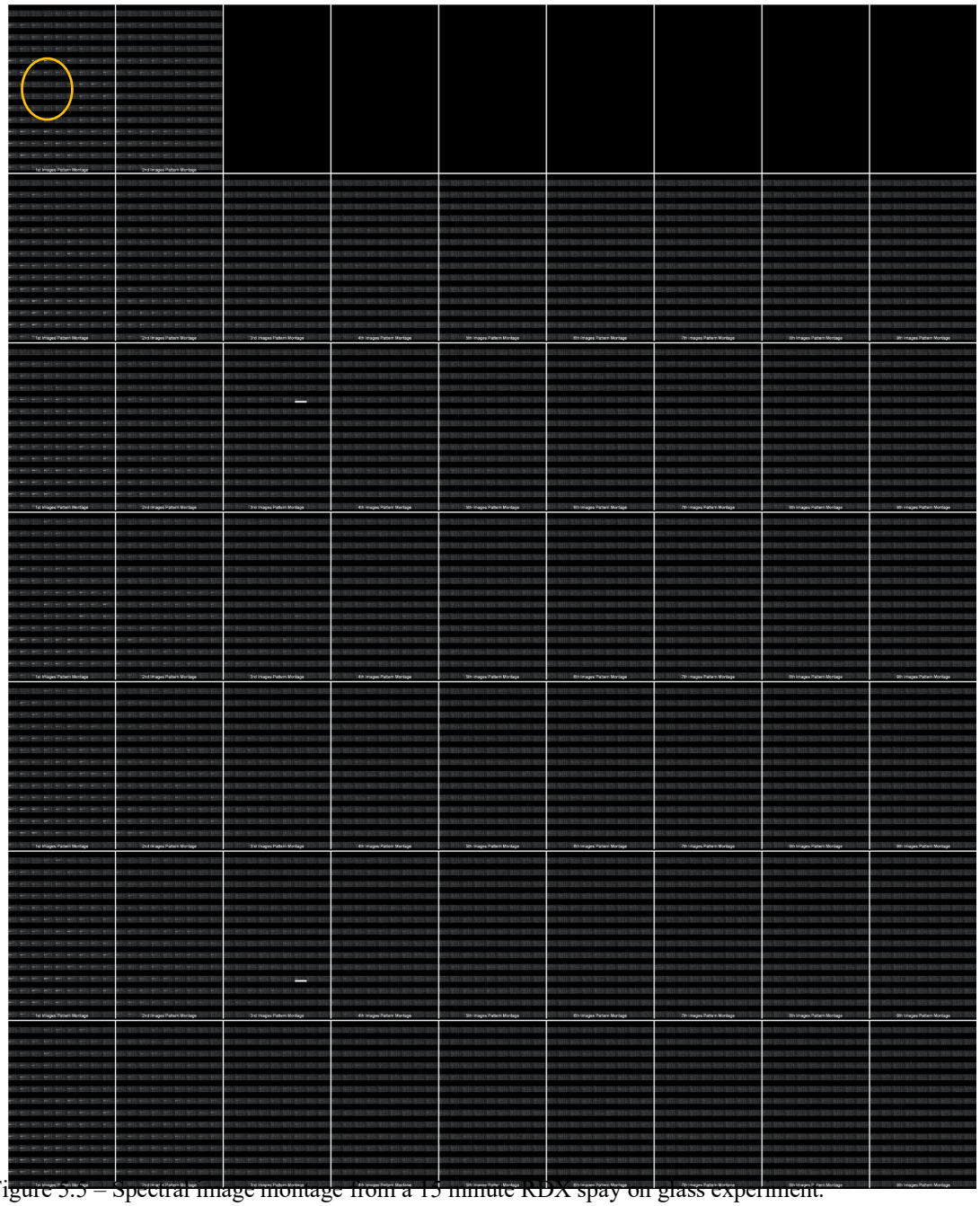

Figure 5.3 – Spectral image montage from a 15 minute RDX spay on grass experiment.

Figure 5.6 the 1st and 2nd images of shots A and B from the same RDX on glass experiment shown in fig. 5.6.

Figure 5.7 the 1st and 2nd images of shots A and B from a duplicate RDX on glass experiment.

5.2 Plume Image Montages of single films with RDX films of variable thicknesses

5.2.1 Introduction

In chapter 4, the process of the formation of and structure of a "snow-pack" region was proposed. To investigate the "snowpack" and its effects on the observed plumes, experiments needed to be carried out on thinner and thinner RDX films. To minimize the variability between the spray conditions of different experiments, it was decided to prepare films of different thicknesses on the same PC sample by masking different regions of the sample during spraying, see Chapter 2 for full details. The "snow-pack" is a white film observed in microscope images of RDX exposed to laser irradiation that is presumed to be a mixed layer of RDX and PC formed by melting during the laser pulse and re-freezing shortly after. It is proposed that the first laser shot melts part of the RDX/PC interface which mixes RDX into the underlying PC forming the

observed “snow-pack.” It is proposed that the thicker the layer of RDX, the more “snow-pack” is formed as more RDX melts and diffuses into the PC. Since the removal of this “snow-pack” is presumed to be RDX diffused into PC, the removal of this “snow-pack” would not be presumed to occur at the typical rate of RDX removal. It is important to recall that laser ablation on RDX removes 10x the depth of material than on PC. In the last chapter it was shown that this “snow-pack” requires multiple shots.

5.2.2 Variable 15/30/45 minute RDX on PC

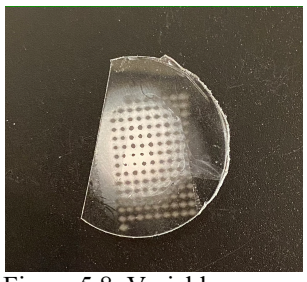
Figure 5.8: Variably sprayed RDX on PC 15/30/45 minutes

Figure 5.8 is the photograph of a PC film sprayed in different regions with RDX for 15, 30, and 45 minutes and then exposed to laser ablation. Figure 5.9 displays the plume image montage from the same experiment. In the first image of shot A, there is a small region of darkness, indicative of the region the RDX is located. In the first image of shot B, the dark region covers a larger fraction of the RDX sprayed region. This is interpreted as the result of a higher portion of the RDX spot being thinned by the first shot to the point that the second laser shot interacts with both RDX and underlying PC, resulting in more widespread dark plumes. In the first image of shot C, the dark region has increased more from shot B. In shots D, E, and F, the dark region seems to be diminishing and bright plumes return. This is interpreted as the removal of a fraction of the “snow-pack” with each successive laser shot, the return of bright plumes as the material being ablated becomes more pure PC. A detailed analysis of the distribution of brightness of the plumes as a function of RDX film thickness is described below in table 5.1.

Figure 5.10 are the first image montages of the A, C, and G shots with an overlay indicating regions sprayed for different amounts of time. All three film thicknesses sprayed in this experiment (15, 30, and 45 minutes) exhibit the characteristic visible plumes in the first shot A, a lesser population of visible plumes in the C shot, and then an increase in visible plumes after shot C, with many visible plumes in shot G. Table 5.1 includes the average percentage of visible plumes from four experiments in each region of the RDX film with the percentages of the experiment from Figures 5.8-5.10 in parenthesis. Focusing on the A shot where there has been no opportunity for RDX to mix into the underlying molten PC, the thinnest RDX film results in the

fewest number of visible plumes (50%) compared to 77% visible plumes in the 30 minute region and 81% visible plumes in the 45 minute region. The variation in visible plumes observed here demonstrates the variability observed in the experimental results. Although the exact fractions may vary, the trend observed in the single experiment is consistent with what is seen upon multiple duplications in the average values.

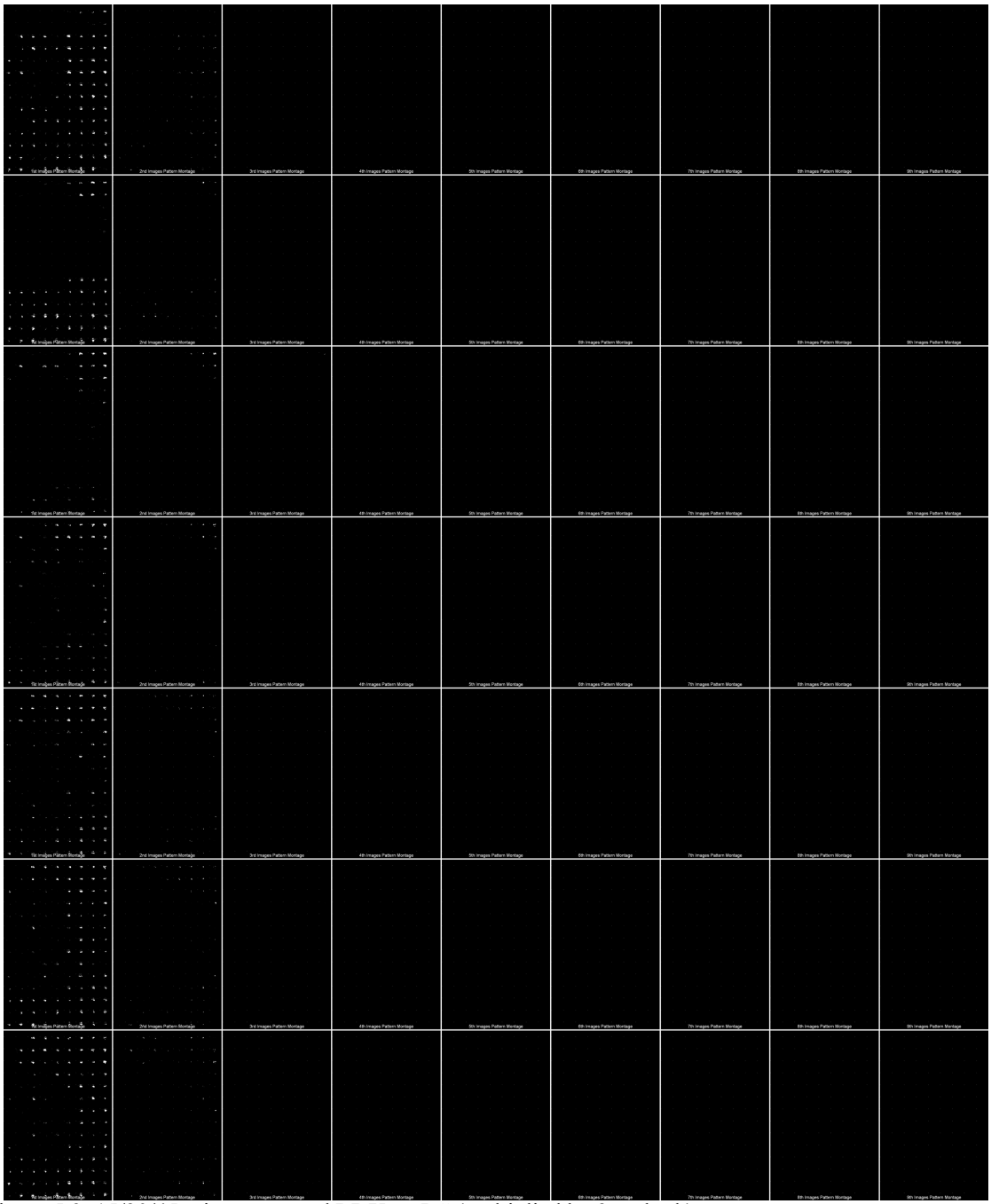

Figure 5.9: 15/30/45 minute sprayed RDX on PC (multiplied by 3x – both)

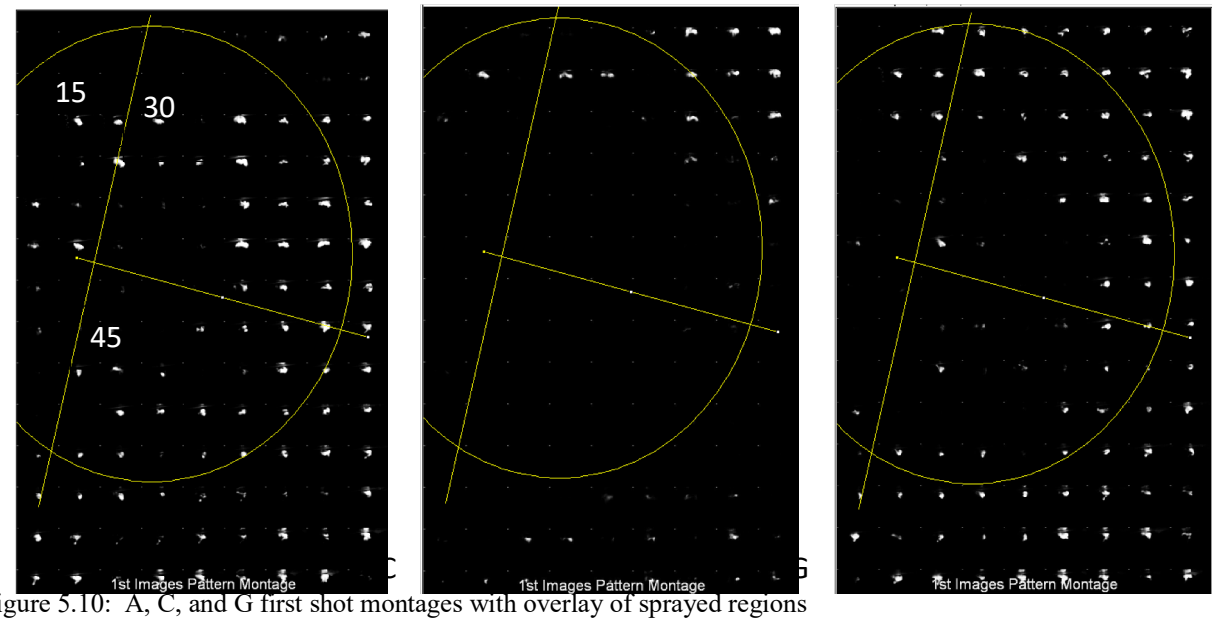

Figure 5.10: A, C, and G first shot montages with overlay of sprayed regions

The regions of thicker films have, on average more visible plumes because the first shots on the thicker films typically interact only with "pure" RDX as these RDX films are thicker than the amount removed by a single laser shot, whereas the thinner films display on average fewer visible plumes, indicative of laser interaction with both RDX and PC. Subsequent laser shots on thick RDX films remove more than the remaining RDX thickness and appear dark. In this scenario, it is believed that some of the underlying PC is also removed and melted, resulting in the mixing of RDX down into the PC surface. It is hypothesized that this lack of a visible plasma corresponds to ignition in mixed RDX and PC plasma, similar to what was observed for thin PC films on RDX. It takes several laser shots for the plumes to return visible from dark. Previous work performed by Orland indicated that sprayed RDX films lack uniformity and are uneven. It was observed that RDX films become continuous and that thicker films do not see any increase in coverage uniformity but instead have more dense crystals, until total coverage is achieved. [1] Hence, the morphology of the spray deposited film is an important consideration when interpreting the irreproducibility of experiments, as it is suspected that initial laser shots cause a

	15 min	30 min	45 min
A Shot	44% (50%)	63% (77%)	62% (81%)
C Shot	31% (15%)	51% (33%)	31% (7%)
G Shot	68% (50%)	75% (80%)	67% (63)

Table 5.1: Average percentage of visible plumes in each region with percentages from the example experiment in parenthesis

portion of the RDX to melt down into the molten PC below, forming the "snow-pack" features. Because the RDX film is uneven and polycrystalline, there is the potential that molten RDX and PC could mix to a depth deeper than the capacity for material ablation in a single laser shot (which is 10x as deep in RDX than it is in PC), resulting in multiple laser shots with a lack of visible plumes. Then once all RDX and snowpack features have been removed, subsequent laser irradiation returns the plume images to those of PC (bright) as the RDX film has been removed, see Figure 5.10. By shot C, there are significantly fewer visible plumes across all film thicknesses, and by shot G the number of bright plumes across all thicknesses increases, indicating likely RDX removal and ablation of underlying PC resulting in bright plumes. The 45 minute sprayed region never recovers the amount of bright plumes as 30 minute sprayed region did, likely indicative that RDX has been mixed further into the film, requiring more shots to remove.

Figure 5.11 is a plot of the bright pixels per laser shot (first images only) in each variably sprayed region by shot (A-G) averaged across all experiments sprayed for 15/30/45 minutes. This analysis is different than counting the visible plumes as done in Figure 5.10. For details on how this analysis was performed see chapter 2, section "Spectral Analysis Routine for Variably Sprayed Experiments". Table 5.2 includes these same average pixels per laser shot (first images only) values for each shot/sprayed region as well as the values in parenthesis for the specific experiment pictured in Figure 5.8. There is a noticeable variability when comparing different

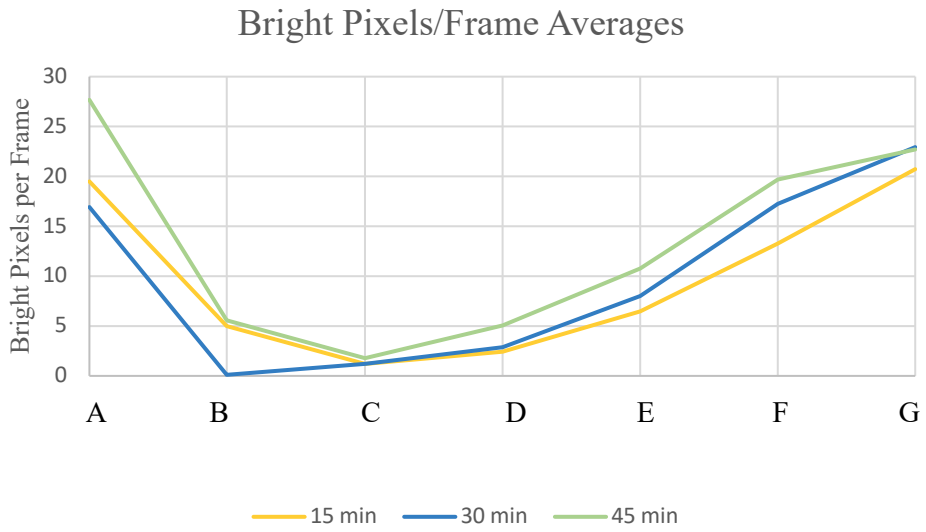

Figure 5.11: Bright pixels per shot as a function of spray time

15/30/45 RDX spray time experiments to each other. The general trend of bright, dark, bright is upheld across experiments, however there are some differences in bright pixels per frame between the average and the specific experiment referenced in parantheses, notably the A, F, and G shots in the 30 minute region. The data for the plot was obtained as follows. The laser spots within each variably sprayed region were identified from the sample image Figure 5.8. Figure 5.12 is the shot map from this experiment with sprayed regions highlighted. The first images of each laser spot within the region of interest are selected and summed. The summed image is histogrammed to allow the counting of all bright pixels as those with an intensity of 185 or greater. Figure 5.13 is the representative histogram of the summed shot images of the 15 minute sprayed region. This analysis was done separately for each shot A-G, using the built-in ImageJ macros and the custom macros included in Appendix A.

Examing the plot in Figure 5.11, one sees brighter plumes in the first laser shot, followed by a decrease and ending in a slow increase. This behavior is consistent with the previously

AVERAGES							
	A Shot	B shot	C Shot	D shot	E shot	F shot	G Shot
	1	2	3	4	5	6	7
15 min	16.8 (29.3)	1.8 (5.2)	1.7 (3.8)	2.4 (4.1)	7.9 (14.7)	7.0 (10.1)	12.3 (24.1)
30 min	30.2 (68.7)	0.0 (0.1)	1.3 (3.7)	4.7 (10.6)	8.2 (20.4)	16.2 (37.8)	17.3 (43.6)
45 min	31.7 (39.4)	7.5 (22.6	0.8 (0)	5.8 (0.4)	11.6 (4.3)	20.8 (13.8)	18.2 (13.7)

Table 5.2: Average Bright Pixels per Frame of 15/30/45 minute experiments with values from experiment from Figure 5.8-5.10 in parenthesis

proposed theory of the first laser shot (A) producing bright plumes, because it ablates only pure RDX from the top of the sprayed film. Intermediate shots appear dark. As described above, the first laser shot may result in the melting of the underlying PC and mixing of the crystalline RDX into the molten PC below to form the "snow-pack" structure observed in optical microscopy. Consistent with the previous hypotheses, the supression of bright plumes in subsequent laser shots (B-D) results from the ablation of "snow-pack," which is a combination of RDX and PC. It takes several shots to remove the molten PC/RDX mixture. The slow rise in the number of bright pixels in the latter laser shots E-G are the result of thinning of the "snow-pack" and plasmas formed from increasing fractions of PC. A slope representative of the rate of a return to bright from dark, is estimated from the increase in bright pixels per laser shot from the darkest laser

shot (C) to the last shot (G) in the 15 minute sprayed region. In 4 laser shots the bright pixels per shot increases from about 1.2 to 20.7 in 4 laser shots (c to G). The rate of return to bright from dark is about 4.88 bright pixels/shot for the 15 minute sprayed regions. The rates of bright pixel recovery for the 30 and 45 minute sprayed regions are 4.56 and 5.22 Pixels per frame, respectively.These are slow rates of return to bright when compared to the shorter sprayed regions which have thinner films. It is hypothesized that the slow return to bright from dark is due to a thicker

0	7	14	21	28	35	42	49	56	15 minutes
119	112	105	98	91	84	77	70	63	30 minutes
126	133	140	147	154	161	168	175	182	45 minutes
245	238	231	224	217	210	203	196	189	
252	259	266	273	280	287	294	301	308	
371	364	357	350	343	336	329	322	315	
378	385	392	399	406	413	420	427	434	
497	490	483	476	469	462	455	448	441	
504	511	518	525	532	539	546	553	560	
623	616	609	602	595	588	581	574	567	
630	637	644	651	658	665	672	679	686	
749	742	735	728	721	714	707	700	693	
756	763	770	777	784	791	798	805	812	
875	868	861	854	847	840	833	826	819	

Figure 5.12: A spot map showing the image number of the first image collected of the A shots with color coding of the spray time in that region

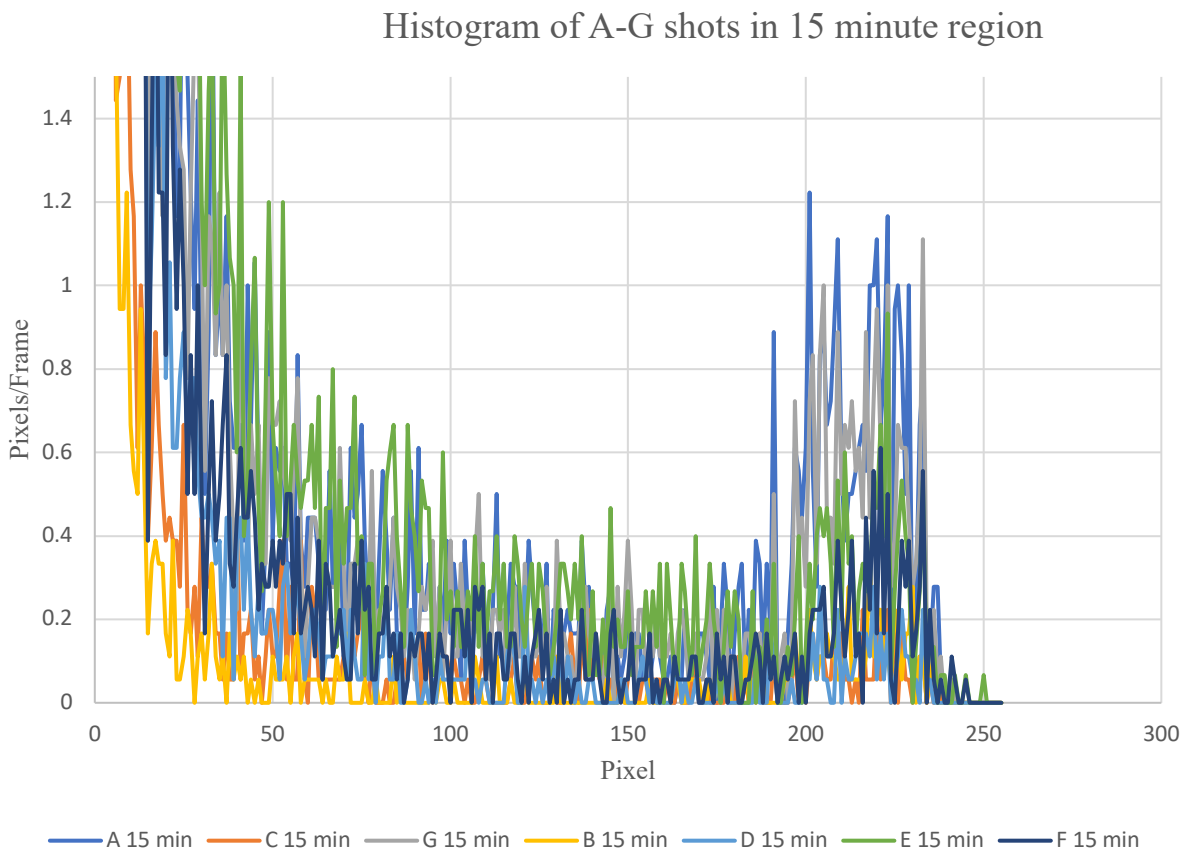

Figure 5.13: Histogram of 15 minute summed plume images from experiment in Figure 5.8

"snow-pack" formed when the thicker RDX films in the 15/30/45 minute regions mixed with PC, requiring more laser shots to entirely remove than with a thinner "snow-pack."

Figure 5.13 are the 15 minute region A-G shot histograms normalized by shot number. In shots A and G there is no significant change in the shape of the pixel distribution between shots, and all of them have a flat-topped or constant number of pixels over most of the range of the plot. This obvervation is in contrast to pointy nature of 3/6/9 that will be discussed later. Comparison of shots A, C, and G support the theory of the first laser shot (A) producing bright, visible plumes, intermediate shot (C) not producing as many bright plumes, and the seventh shot (G) producing bright plumes. This theory is supported across all sprayed regions (15, 30, and 45 minutes) of this experiment as the shot-A trace (blue) and shot-G trace (gray) indicate much higher numbers of pixels per frame than the shot-C trace (orange).

Previous investigations of RDX sprayed films show that at very low coverage the films are individual crystals of RDX covering only a fraction of the surface. As the spray time

(coverage) is increased, the films become more continuous and at highest coverages they become thick continuous films. [1] It is then important to investigate RDX thicknesses before a film becomes continuous, 1/2/3, 2/4/6, 3/6/9, and 5/10/15 minutes are included using the same film masking procedure to generate regions of different thicknesses on the same sample. The next set of film thicknesses to be considered are 5 minute, 10 minute, 15 minute (5/10/15) samples.

5.2.3 Variable 5/10/15 Minute RDX Films on PC

Figure 5.14 is the photograph of a PC film sprayed for 5, 10, and 15 minutes with RDX and then exposed to laser ablation. Figure 5.15 displays the plume image montage of the same experiment. As observed in previous experiments of longer spray times, the first shot (A) has many visible plumes, with the number of visible plumes decreasing in following shots B and C, followed by an increase in visible plumes in shots D, E, F, and G. This supports the general trend of early shots (shot A) ablating only RDX, resulting in a visible plume, intermediate shots (shot C) ablating both RDX and PC, resulting in few numbers of visible plumes and the dark region on the plume montage image as the "snow-pack" is ablated. Finally the latter shots (shot G) ablate PC left behind after the RDX and "snow-pack" have been removed, resulting in a return to visible plumes. A more detailed analysis of the variably spray timed regions by shot is to follow.

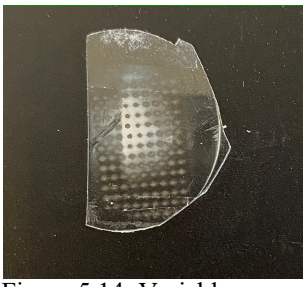
Figure 5.14: Variably sprayed RDX on PC 5/10/15 minutes

Figure 5.16 displays the A, C, and G shot first image montages with an overlay indicating the regions sprayed for 5, 10, and 15 minutes. The progression from bright plumes, darkness, and a return to bright plumes is evident in the A, C, and G shot montages with the overlay of spray times. The average of percentages of visible plumes produced in each variably sprayed region of the 5/10/15 minute experiments can be seen in Table 5.3 with the percentages from Experiment 12/16/19 16.32.54 5/10/15 in parenthesis. There is wide degree of variability in the thinner sprayed regions of these experiments. The average percentage of visible plumes drops from shot A to shot C in the 15 minute sprayed region but the 5 and 10 minute sprayed regions do not

clearly decrease for both the 5 and 10 minute sprayed regions. The thinner regions of RDX coverage have had high degrees of variability, as will be discussed later. On average and in the featured example experiment there is an increase in the percentage of visible plumes from shots

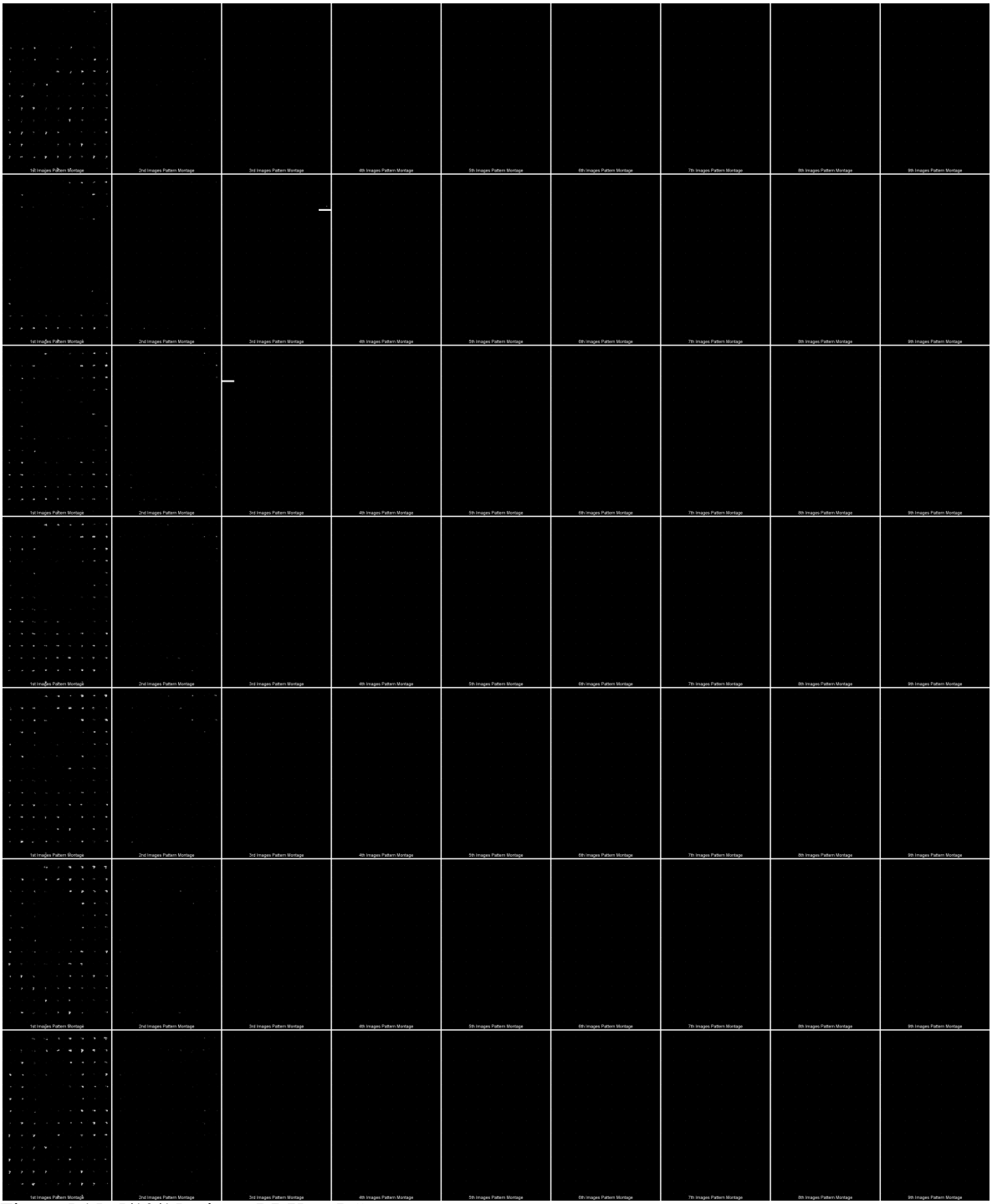

Figure 5.15: 5/10/15 minute RDX on PC

C to G. The 15 minute sprayed regions are consistent with the theory that first laser shots on predominantly pure RDX produce visible plumes, intermediate shots (C) interact with RDX and the molten RDX/PC "snow-pack" mixture and do not produce visible plumes, followed by

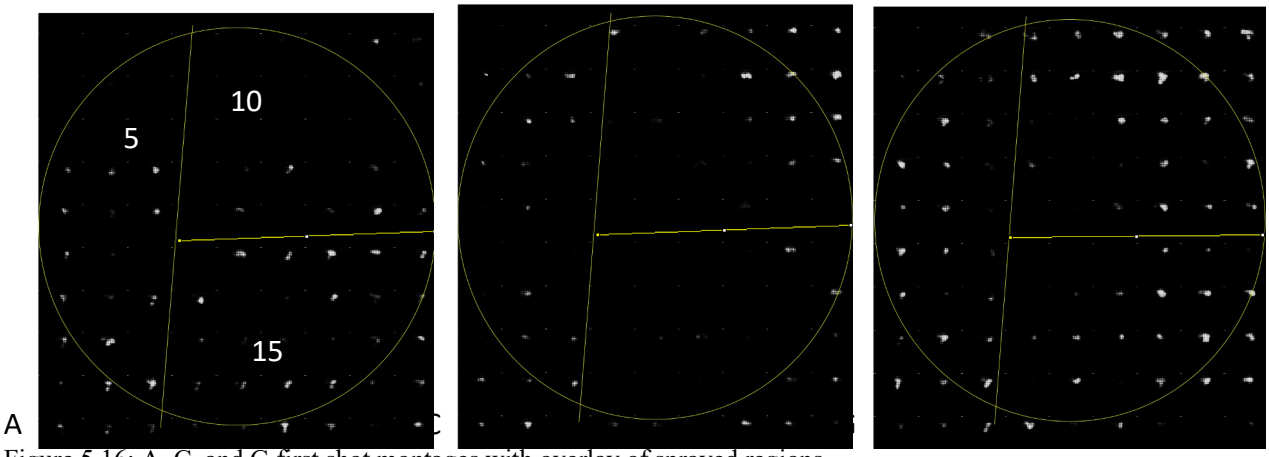

Figure 5.16: A, C, and G first shot montages with overlay of sprayed regions

visible plumes on successive laser shots as the underlying PC is ablated.

	5 min	10 min	15 min
A Shot	41% (67%)	43% (27%)	60% (86%)
C Shot	49% (52%)	38% (54%)	22% (29%)
G Shot	74% (90%)	78% (85%)	73% (71%)

Table 5.3: Average percentage of visible plumes in each region with percentages from the example experiment in parenthesis

Figure 5.17 is a plot of the bright pixels per laser shot (first images only) in each variably sprayed region by shot (A-G) of the 5/10/15 minute sprayed experiment. Table 5.4 includes the average values for pixels per laser shot (first images only) in the 5/10/15 minute sprayed experiments with the specific values for pixels per laser shot in the example 5/10/15 experiment included in parenthesis. The hypothesis of early shots producing bright plumes, intermediate shots going dark, and later shots producing bright plumes is generally supported in the 5/10/15 minute sprayed experiments. Examination of Figure 5.17 indicates moderately bright plumes in the first laser shot (A), followed by a decrease in brightness in the second shot (B) and third shot C in all sprayed regions. The 5 minute sprayed region has the lowest amount of bright pixels per shot and has a minimum in the B shot, while the 10 and 15 minute sprays have a minimum in the C shot. This observation indicates that the first shot ablates mostly pure RDX, leaving behind the

	A Shot	B shot	C Shot	D shot	E shot	F shot	G Shot
	1	2	3	4	5	6	7
5 min	11.44 (18.25)	2.23 (2.90)	10.52 (8.67)	19.78 (13.81)	20.95 (27)	25.99 (16.57)	26.64(44.38)
10 min	11.59 (7.92)	24.24 (6.24)	4.48 (15.80)	13.95 (33.24)	22.57 (46.84)	27.87 (52.76)	34.91 (66.52)
15 min	27.40 (34.48)	8.88 (0)	3.96 (3.33)	5.35 (3.57)	12.80 (11.90)	19.45 (17.33)	36.39 (42.48)

Table 5.4: Average Bright Pixels per Frame of 5/10/15 minute experiments with values from experiment from Figure 5.14-5.16 in parenthesis

motel RDX/PC mixture below in the "snow-pack" formation. The 5 minute spray has the least amount of "snow-pack" and begins to recover brightness beyond shot C, while the 10 and 15 minute regions have minimums at shot C, indicating slightly more of the "snow-pack" formation, and recover brightness beyond shot C. With each laser shot C and beyond, there is generally an increase in brightness with each successive shot. This is indicative of the progressive removal of the "snow-pack" formation as each shot ablates more of this mixture and produces more bright pixels in the plume images. The early recovery of brightness in the 5 minute sprayed region shot

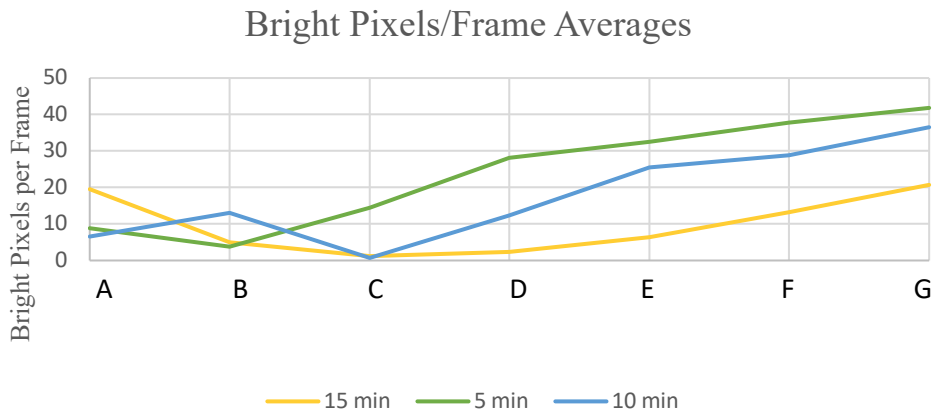

Figure 5.17: Bright pixels per shot as a function of spray time

B, indicates a thin RDX coverage because it did not take but one laser shot to begin recover brightness and ablate the "snow-pack." The slope calculated for the rate of return from dark to bright in the 5 minute sprayed region of this experiment is 7.6 bright pixels/shot. The slope calculated for the rate of return form dark to bright in the 10 and 15 minute sprayed regions are 8.95 and 4.88 bright pixels/shot, respectively. These rates are faster than what was observed in the 15/30/45 minute experiments. The faster rate is attributed to a thinner "snow-pack" layer with 5/10/15 sprays as compared to 15/30/45 minutes due to a thinner coverage of RDX

available to mix with PC, which is ablated faster, resulting in the faster rate of bright pixel recovery.

Figure 5.18 are the 5 minute region A-G shot histograms normalized by shot number. From shots A to G there is no significant change in shape regarding pixel distribution within this experiment's shots, except that there is an increase in the number of bright pixels per shot in shot G when compared to shot A. The shape of this distribution is slightly sharper than what was observed in the 15 minute sprayed region of the 15/30/45 minute experiment previously mentioned.

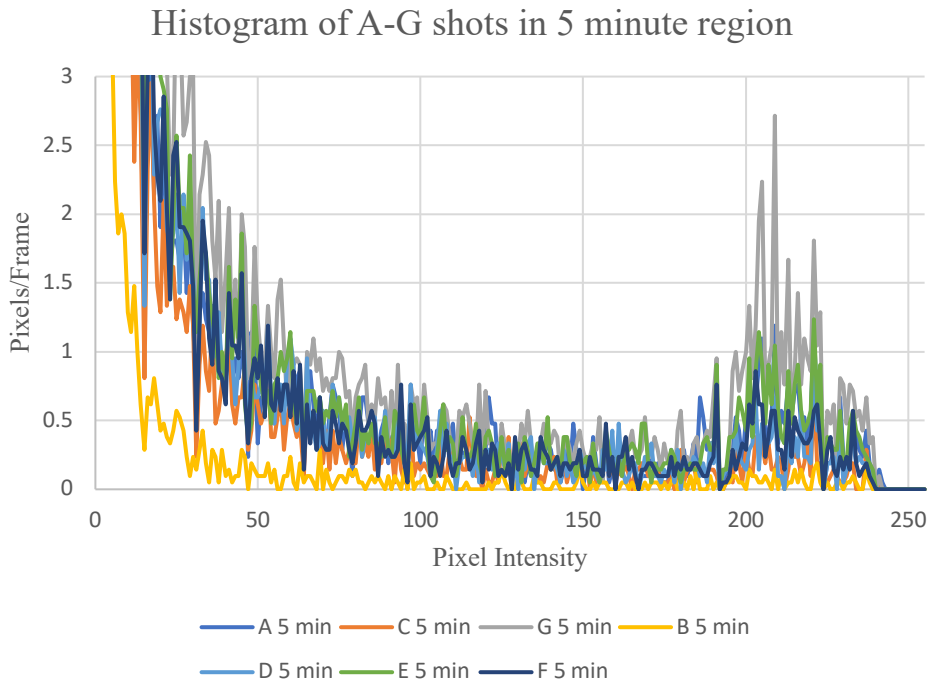

Figure 5.18: 5 min Plume Histogram of experiment from Figure 5.14-5.16

5.2.4 Variable 3/6/9 Minute RDX on PC

Figure 5.19 is the photograph of a PC film sprayed in different regions with RDX for 3, 6, and 9 minutes and then exposed to laser ablation. Figure 5.20 is the plume image montage from the same experiment. In the first frame of shot A, there is a large population of visible plumes. In the first frame of shots B and C, a dark region is observed where the RDX is located. Beyond shot C the dark region associated with plumes of both RDX and PC decreases in each shot, and by shot G there is a large population of visible plumes. These observations are consistent with previous experiments, where initial laser shots produce visible plumes from the top layer of the RDX film. Intermediate shots ablate the RDX and PC mixture that is the result of RDX thinning and subsequent mixing of RDX down into the PC below forming the "snow-pack," resulting in a low population of visible plumes. Beyond shot C, the population of visible plumes increases with each shot, until shot G there is a large population of visible plumes as the RDX has been largely removed and underlying PC ablated.

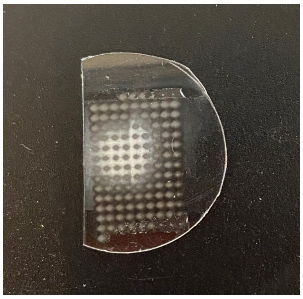

Figure 5.19: Variably sprayed RDX on PC 3/6/9 minutes

In Figure 5.21 the first image montages of shots A, C, and G are displayed with an overlay indicating regions sprayed for different amounts of time. Table 5.5 is the average percentage of visible plumes in each 3, 6, and 9 minute sprayed region of laser shots A, C, and G for all 3/6/9 minute experiments performed. In parenthesis is the percentage of visible plumes for the experiment in Figure 5.19. On average the A shots have low percentages of visible plumes for 3, 6 and 9 minute RDX sprayed regions. The average population of visible plumes increases from shot A to shot C, and then increases again more significantly from shot C to shot G. These observations differ somewhat from what was observed for experiments involving thicker films. With thicker films, there was a higher population of visible plumes in shot This specific 3/6/9 minute experiment is somewhat of an outlier compared to other 3/6/9 minute experiments as it has a very high percentage of visible plumes across all spray times in shot A. On average, the A shot for the 3/6/9 minute sprayed regions have few bright plumes (30% - 45%). This difference in visible plume population when compared to thicker films is attributed to films in these experiments being thin enough that the first laser shot is able to penetrate RDX and interact with

the PC below, resulting in a low population of visible plumes. With this in mind, the increase in

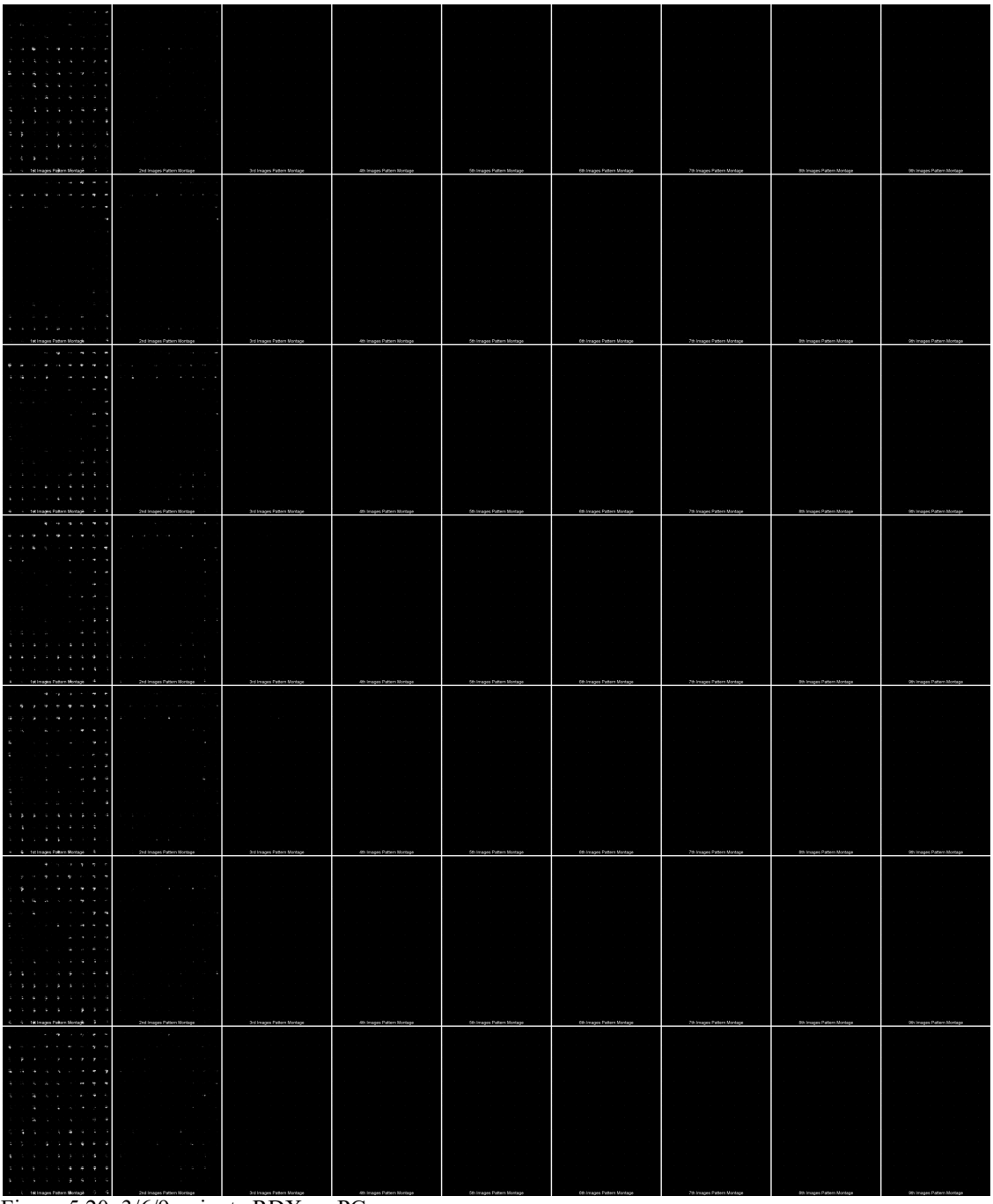

Figure 5.20: 3/6/9 minute RDX on PC

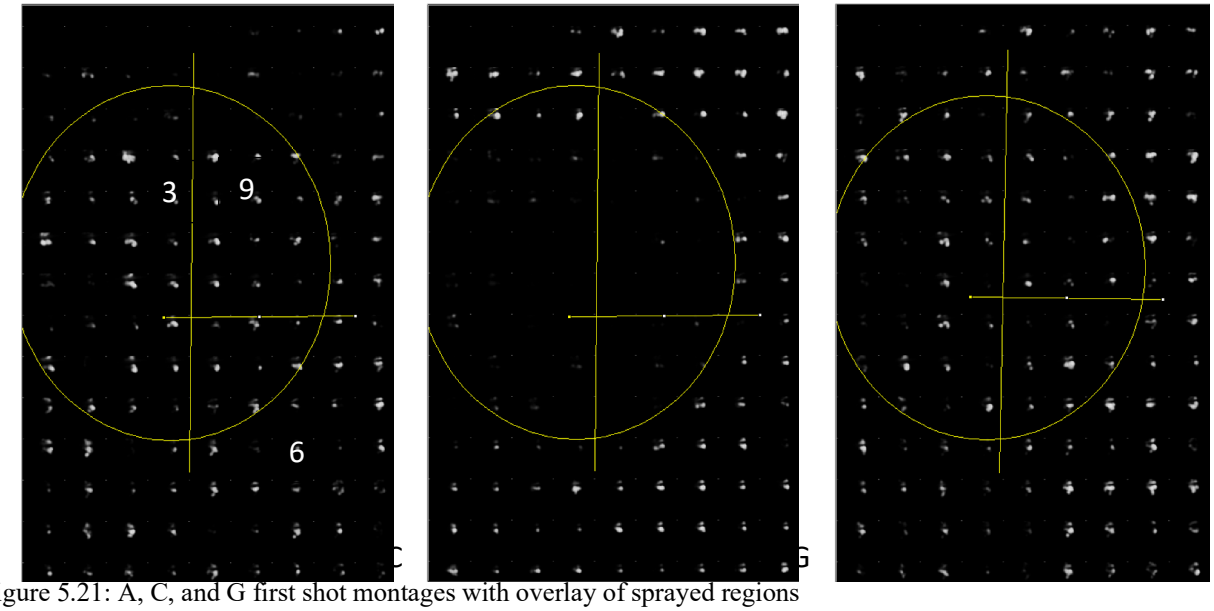

Figure 5.21: A, C, and G first shot montages with overlay of sprayed regions

population of visible plumes from shots A to C, and then again from shots C to G is rationalized as the gradual removal of RDX and the underlying "snow-pack" features, and formation of more bright plumes of only the underlying PC.

	3 min	6 min	9 min
A Shot	38% (97%)	45% (100%)	30% (86%)
C Shot	76% (53%)	54% (38%)	42% (29%)
G Shot	96% (93%)	94% (88%)	95% (100%)

Table 5.5: Average percentage of visible plumes in each region with percentages from the example experiment in parenthesis

Figure 5.22 is a plot of the bright pixels per laser shot (first images only) in each variably sprayed region by shot (A-G) averaged across all experiments sprayed for 3/6/9 minutes. Table 5.6 includes these same average pixels per laser shot (first images only) values for each shot/sprayed region as well as the values in parenthesis for the specific experiment pictured above. There are some bright plumes in shot A, followed by a drop in bright plumes in shot B, and then an increase in bright plumes beyond shot B to shot G. This indicates that the thin RDX coverage in the 3/6/9 minute regions is likely removed in the first shot and a small amount of the "snow-pack" formation is formed which is gradually removed in shots B and beyond, evident in the return to brightness. Analysis of the plot of bright pixels per frame in figure 5.22 indicates a fast rate of return to bright plumes following the dip in brightness associated with the ablation of RDX and underlying "snow-pack." The rate of return to brightness is calculated at 6.22 pixels per frame in the 3 minute region, 6.54 pixels per frame in the 6 minute region, and 8.82 pixels per frame in the 9 minute sprayed region. These rates are

faster than rates for the 15/30/45 minute spray times, which seems logical considering the RDX coverage is thinner, meaning the RDX and "snow-pack" features can be ablated to a higher degree than in thicker RDX films.

The histogram of the 3 minute sprayed region of experiment in Figures 5.19-5.21 is

averages (>184)	A Shot	B shot	C Shot	D shot	E shot	F shot	G Shot
0	1	2	3	4	5	6	7
3 min	17.81 (65.59)	12.75 (7.88)	27.77 (16.03)	38.11 (13.06)	47.74 (21.75)	57.88 (31.78)	47.69 (47.63)
6 min	15.07 (56.5)	3.16 (0)	15.53 (0)	28.00 (1.38)	34.96 (17.38)	45.62 (54.5)	54.32 (55.38)
9 min	16.04 (63)	6.72 (1.8)	12.51 (11.27)	32.79 (38.07)	54.23 (48.4)	50.95 (53.13)	58.69 (51.73)

Table 5.6: Average Bright Pixels per Frame of 3/6/9 minute experiments with values from experiment from Figure 5.19-5.21 in parenthesis

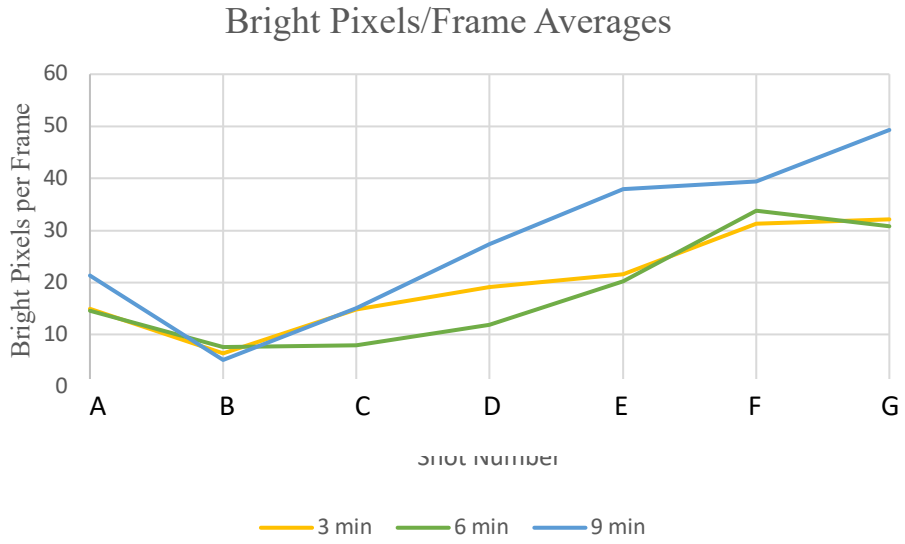

Figure 5.22: Bright pixels per shot as a function of spray time

above in Figure 5.23. The population distribution of bright pixels in this experiment has a different shape than those in the longer spray time experiments, and has a triangular shape in the bright region (185-255), as opposed to the flatter shape in the 15/30/45 minute regions.

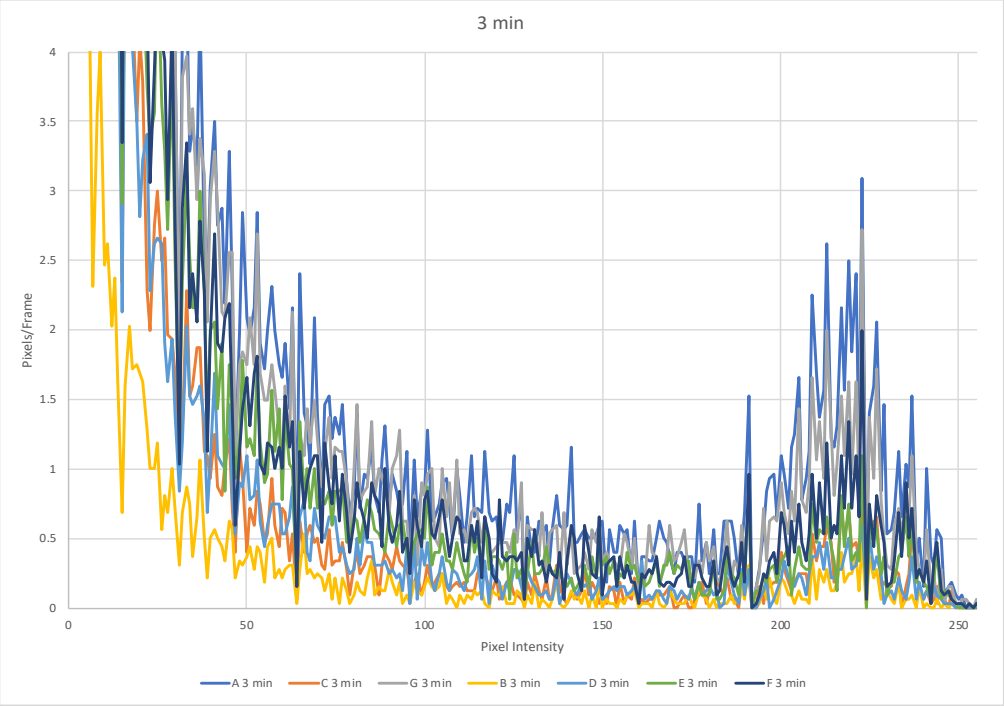

Figure 5.23: 3 min Plume Histogram of experiment from Figure 5.19-5.21

5.2.5 Variable 2/4/6 Minutes RDX on PC

Figure 5.24 is the photograph of a PC film sprayed in different regions with RDX for 2, 4, and 6 minutes and then exposed to laser ablation. Figure 5.25 displays the plume montage from the same experiment. In the plume image montage there is a dark region evident in the first frame of shot A, which gradually decreases in area through successive laser shots as the population of visible plumes increases with each laser shot. This observation is consistent with the theory of thinner films producing less visible plumes. It has been suggested that when thin RDX films on PC are exposed to laser irradiation, the first laser shot is often able to interact with both RDX and the underlying PC resulting in the lack of a visible plume. As each successive laser shot interacts with the film, more RDX and the underlying "snow-pack" feature is removed, and there is an increase in the population of visible plumes. With the thin coverage of RDX in these experiments, it might be expected that the lack of visible plumes would last only one laser shot, since the laser is able to penetrate the RDX and reach the underlying PC. However, it is important to remember that RDX films are not uniform, but are crystalline, and also that this RDX likely mixes with the molten PC below on the first

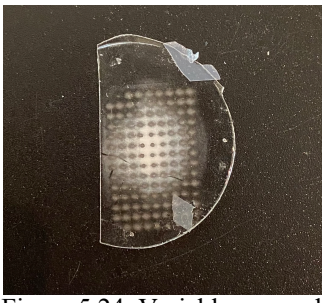
Figure 5.24: Variably sprayed RDX on PC 2/4/6 minutes

laser shot. This PC/RDX mixture, referred to as the "snow-pack" persists for several laser shots as the laser removes 1/10th the depth of PC as it does for pure RDX. By the seventh laser shot G, there is a large population of visible plumes across 2/4/6 minute RDX sprayed regions.

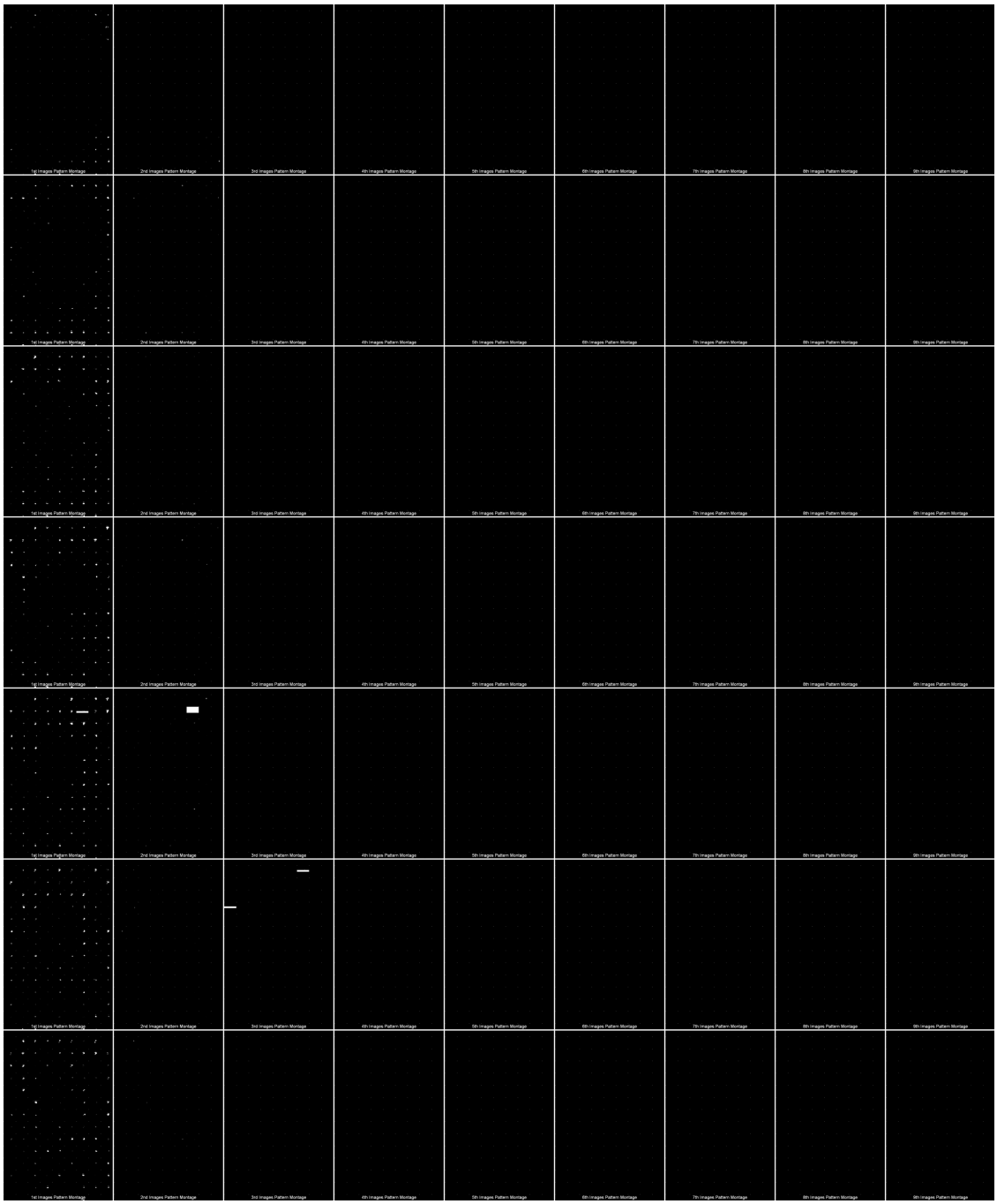

Figure 5.25: 2/4/6 minute RDX on PC (multiplied 10x in ImageJ)

Figure 5.26 are the A, C, and G shot first image montages with an overlay indicating regions sprayed with RDX for 2, 4, and 6 minutes . In general, the trend expected for thin films is confirmed: few visible plumes in the A shot, followed by an increase in the population of visible plumes in shot C and beyond to shot G. Table 5.7 displays the average percentage of

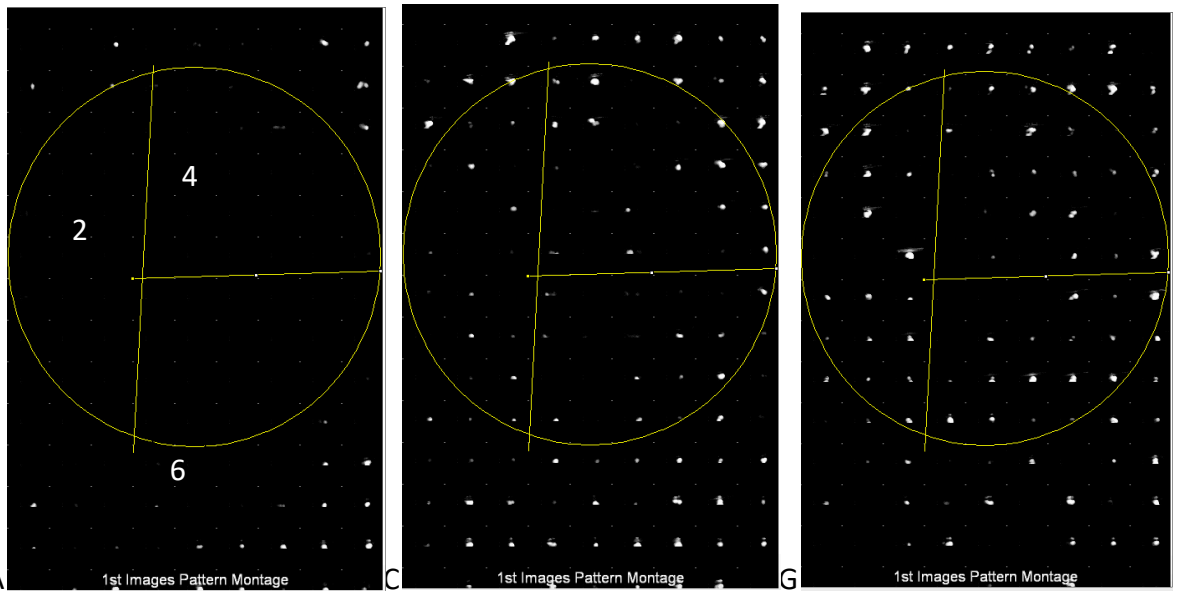

Figure 5.26: A, C, and G first shot montages with overlay of sprayed regions

visible plumes in each sprayed region by shot A, C, and G of the 2/4/6 minute experiments. In parenthesis are the percentage of visible plumes in the featured example. Compared to the 3/6/9 minute RDX sprayed experiments, the 2/4/6 minute experiments have a slightly lower percentage of visible plumes in shot A, which is consistent with what is expected for thinner films.

Figure 5.27 is a plot of the bright pixels per laser shot (first images only) in each variably sprayed region by shot (A-G) averaged across all experiments sprayed for 2/4/6 minutes. Table 5.8 includes these same average pixels per laser shot (first images only) values for each shot/sprayed region as well as the values in parenthesis for the specific experiment pictured above. There are a few bright plumes in shot A, followed by a drop in bright plumes in shots B and C, and then an increase in

	2 min	4 min	6 min
A Shot	35% (14%)	33% (0%)	31% (20%)
C Shot	57% (71%)	54% (80%)	66% (80%)
G Shot	89% (81%)	89% (80%)	89% (76%)

Table 5.7: Average percentage of visible plumes in each region with percentages from the example experiment from Figure 5.24 in parenthesis

bright plumes beyond shot C to shot G. The 2 and 4 minute regions start to recover brightness following shot C, while the 6 minute sprayed region begins to recover brightness following shot

averages (>184)	A Shot	B shot	C Shot	D shot	E shot	F shot	G Shot
	1	2	3	4	5	6	7
2 min	15.37 (24.43)	12.37 (2.9)	6.91 (8.67)	23.33 (13.81)	24.22 (27)	15.60 (16.57)	31.06 (44.38)
4 min	32.10 (7.92)	13.84 (6.24)	8.96 (15.8)	19.60 (33.24)	39.16 (46.84)	30.89 (52.76)	39.44 (66.52)
6 min	21.16 (34.48)	13.00 (0)	11.73 (3.33)	11.19 (3.57)	16.82 (11.9)	27.59 (17.33)	36.68 (42.48)

Table 5.8: Average Bright Pixels per Frame of 2/4/6 minute experiments with values from experiment from Figure 5.24-5.26 in parenthesis

D. It is inferred that the reason the 6 minute region stays dark longer, and returns to brightness on a later shot than the 2 and 4 minute regions is due to a slightly thicker RDX coverage and the resulting "snow-pack" formed takes an additional laser shot to remove. There is a considerable amount of variation in the experiments of shorter spray times with thinner RDX coverages which will be further exemplified with the 1/2/3 minute sprayed experiments.

Analysis of the plot of bright pixels per frame in figure 5.27 indicates a fast rate of return to bright plumes following the dip in brightness associated with the ablation of RDX and

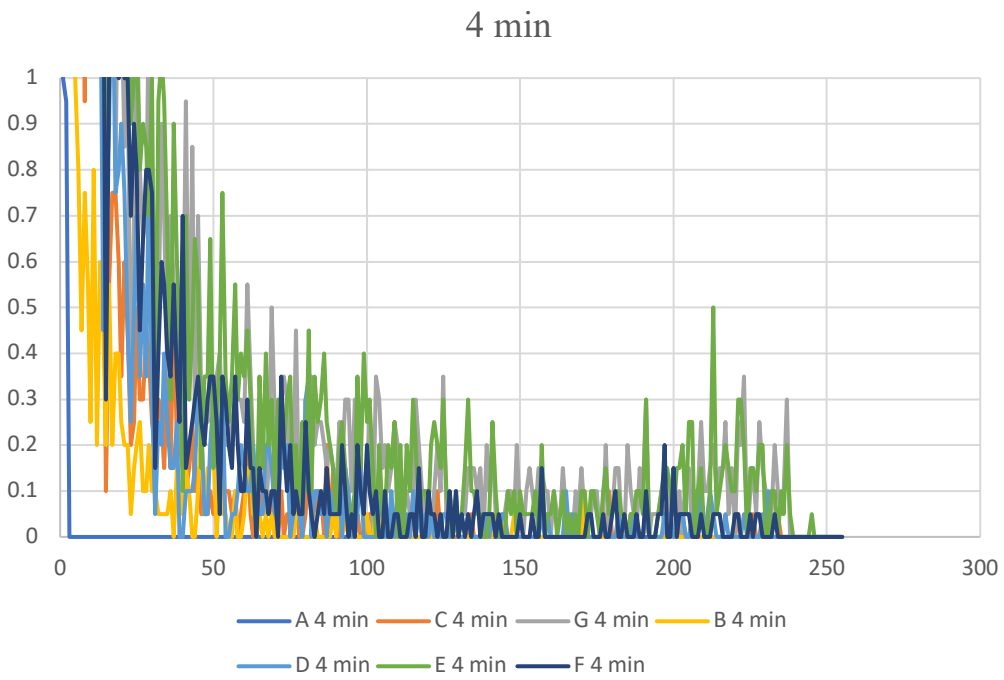

Figure 5.28: 4 min Histogram from 2/4/6 Experiment in Figure 5.24-5.26

underlying “snow-pack.” The rate of return to brightness is calculated at 3.76 pixels per frame in the 2 minute sprayed region, 10.9 pixels per frame in the 4 minute region, and 6.54 pixels per

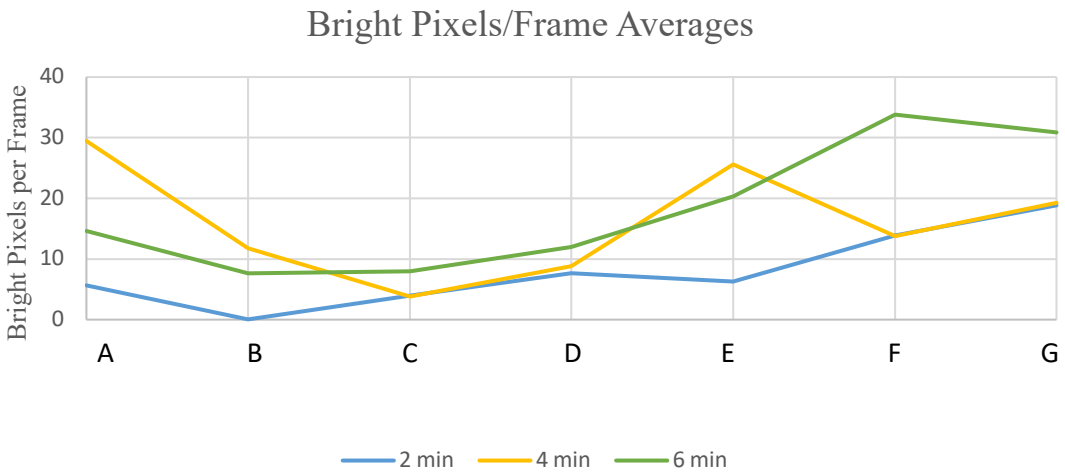

Figure 5.27: Bright pixels per shot as a function of spray time

frame in the 6 minute sprayed region. These rates are highly variable, particularly for the 2 and 4 minute sprayed regions. This is a ttributed to the high variability associated with the crystalline nature of RDX thin films at short spray times. The faster rate for 2/4/6 minute sprayed regions when compared to 15/30/45 minute sprayed regions is attributed to the thinner RDX coverage and thinner “snow-pack” which can be ablated to a higher degree with thinner films than with thick films. It is inconsistent, however, that the 2/4/6 minute rate is slower than the 3/6/9 minute rate, and this might be due to the high degree of variability observed in the experiments of shorter spray times and thus thinner RDX films. It is important to recall the crystalline, non-uniform nature of thin RDX films, previously mentioned.

The histogram of the 4 minute sprayed region of experiment is shown in Figures 5.24-5.26. The population distribution of bright pixels in this experiment has a different shape than those in the longer spray time experiments, and has a sharp shape in the bright region (185-255), as opposed to the flatter shape in the 15/30/45 minute regions.

Figure 5.29: Variably sprayed RDX on PC 1/2/3 minutes

5.2.6 Variable 1/2/3 Minutes RDX on PC

Figure 5.29 is the photograph of a PC film sprayed in different regions with RDX for 1, 2, and 3 minutes and then exposed to laser ablation. The scratches on the film

surface occurred after the experiment, and are not effects of laser ablation. Figure 5.30 is the plume image montage from the same experiment. In the first frame of images of shot A, there are some visible plumes accompanied by dark regions where no plumes are visible. Beyond shot A, the population of visible plumes increases with each successive shot. The films in this experiment are the thinnest and thus it is expected that the lack of visible plumes is most prevalent in the first shot. The first incident laser shot is able to interact with both RDX and the underlying PC, resulting in very few visible plumes. Each following laser shot removes more RDX as well as any "snow-pack" that formed and more visible plumes appear. This transition does not occur in a single laser shot because of the RDX and PC mixing phenomena suggested previously. The RDX is likely able to mix down into the PC at a depth that is deeper than can be removed in a single laser shot.

Figure 5.31 displays the A, C, and G shot first image montages with an overlay indicating regions sprayed with RDX for 1, 2, and 3 minutes. The dark region evident in the first image of shot A clearly decreases in size through shots C and G. The average percentage visible plumes in each sprayed region of 1/2/3 minute RDX sprayed experiments are in Table 5.9. The percentage of visible plumes in this featured experiment are included in parenthesis. The 1 minute sprayed region of the A shot has significantly fewer visible plumes than the 2 and 3 minute sprayed regions. This observation is consistent with what would be expected of the region of thinner RDX coverage. Following the first shot A, there are mostly visible plumes on all shots in later shots C and G, consistent with the removal of RDX and ablation of underlying PC.

Figure 5.32 is a plot of the bright pixels per laser shot (first images only) in each variably sprayed region by shot (A-G) of the 1/2/3 minute sprayed experiment. Table 5.10 includes the average values for pixels per laser shot (first images only) in the 1/2/3 minute sprayed experiments with the specific values for pixels per laser shot in the example 1/2/3 included in parenthesis. The considerable ~~and~~ irreproducible variation with thin RDX films is evident in the 1/2/3 minute sprayed experiments. There is no trend or pattern observed with regard to early, intermediate and late shots as observed for thicker RDX films of spray times 2/4/6 minutes and longer . It is hypothesized that the short 1/2/3 minute spray time experiments are highly variable due to the crystalline nature of thin films of RDX, mentioned previously. The lack of uniformity and crystalline nature of thin RDX films means that there is little observable distinction between films of 1, 2, and 3 minute spray times. The 3 minute film is dark in the early

shots and then increases in brightness beyond shot C, however there is no such pattern observed with the 1 and 2 minute sprays. The recovery rate for the 1 minute sprayed regions are 4.89 pixels per frame, 3.76 pixels for frame for the 2 minute sprayed regions, and 6.22 pixels per

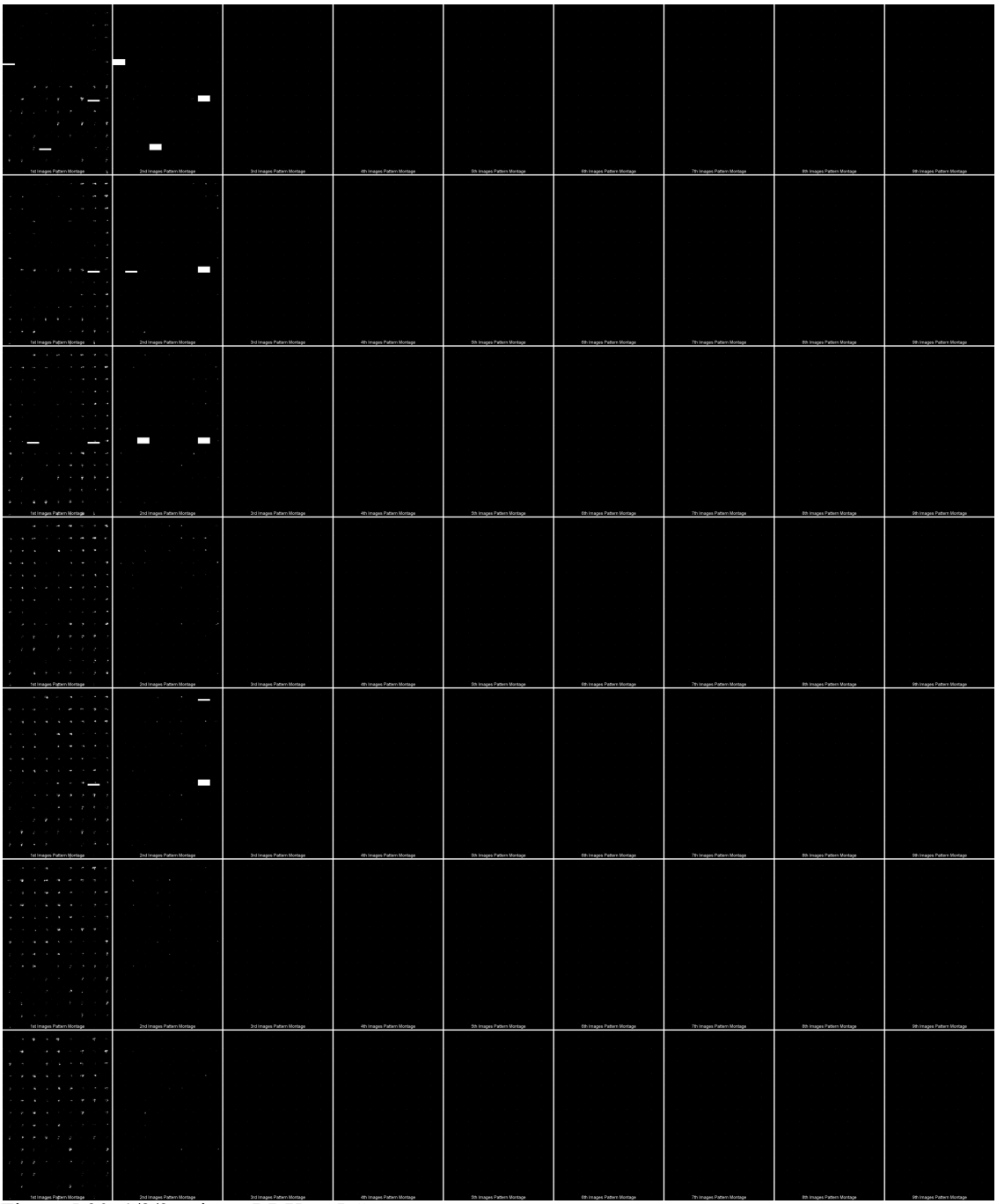

Figure 5.30: 1/2/3 minute RDX on PC

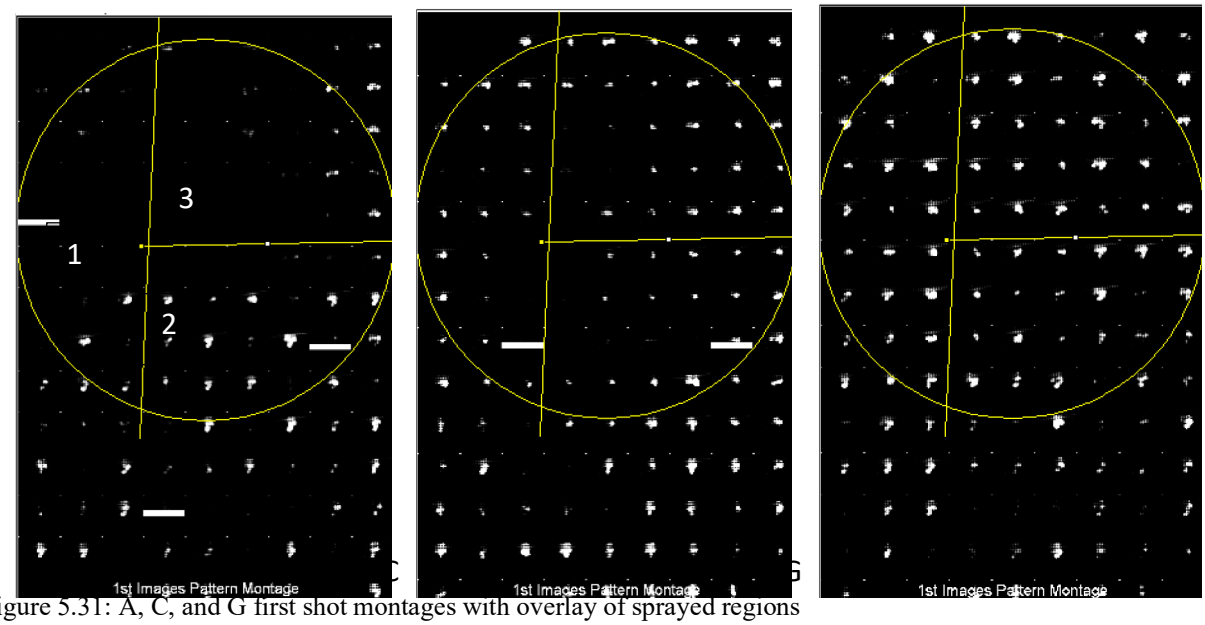

A C G

Figure 5.31: A, C, and G first shot montages with overlay of sprayed regions 1/2/3

	1 min	2 min	3 min
A Shot	52% (40%)	82% (76%)	65% (42%)
C Shot	78% (80%)	74% (81%)	68% (88%)
G Shot	89% (90%)	97% (100%)	83% (100%)

Table 5.9: Average percentage of visible plumes in each region with percentages from the example experiment from Figure 5.29 in parenthesis

frame in the 3 minute sprayed regions. The high variability is evident in these rates as the 2 minute rate is uncharacteristically slow compared to the rates of other thin films.

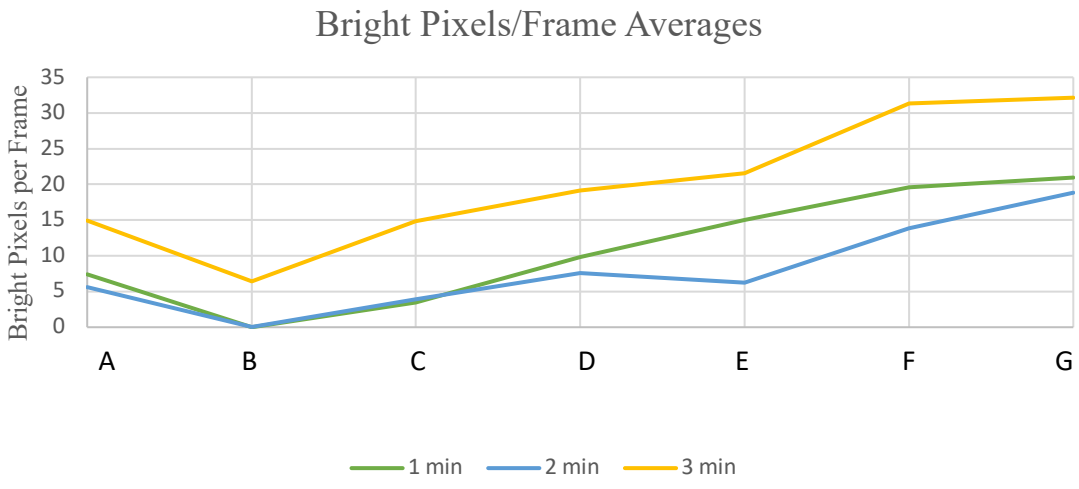

Figure 5.32: Bright pixels per shot as a function of spray time

averages (>184)	A Shot	B shot	C Shot	D shot	E shot	F shot	G Shot
	1	2	3	4	5	6	7
1 min	44.14 (79.15)	5.98 (11.95)	41.79 (82.7)	30.21 (43.05)	23.63 (33.5)	37.23 (48.2)	38.96 (57.05)
2 min	51.77 (94.14)	39.29 (78.57)	51.16 (88.71)	29.11 (30.43)	64.04 (108.48)	37.13 (48)	24.06 (30.19)
3 min	14.63 (2.44)	5.60 (10.68)	15.72 (24.68)	39.55 (60.8)	39.67 (67.04)	37.71 (56.48)	30.96 (49.04)

Table 5.10: Average Bright Pixels per Frame of 1/2/3 minute experiments with values from experiment from Figure 5.29-5.31 in parenthesis

Figure 5.33 is the Histogram of the same example 1/2/3 minute sprayed experiment pictured above. The pixel distribution from the plume histogram in these experiments is sharp and triangular similar to the other shorter spray time experiments, rather than flat like the 15/30/45 minute experiments' pixel distribution.

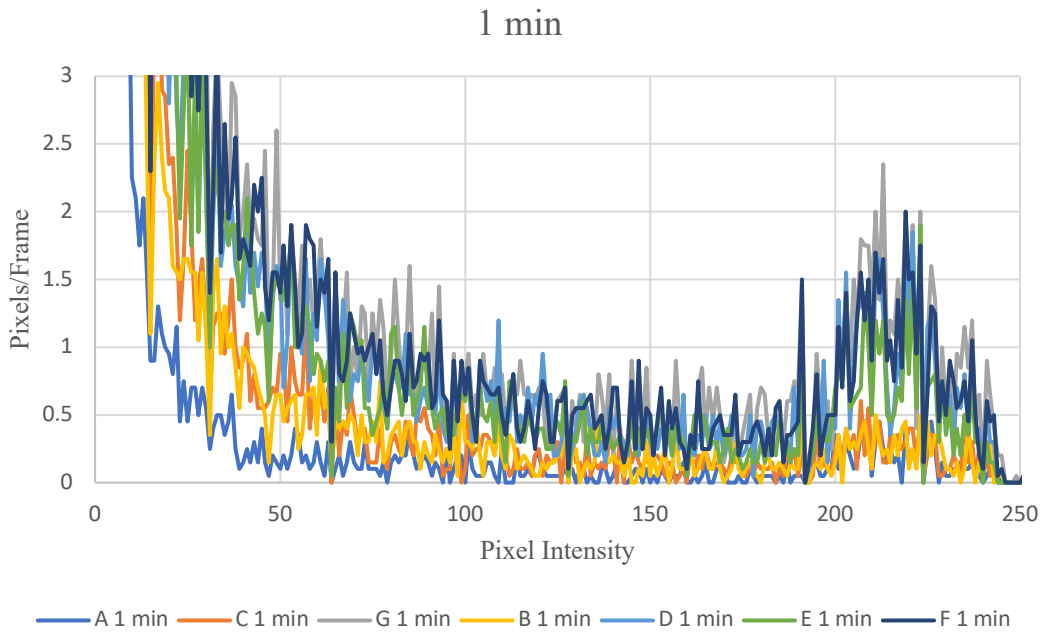

Figure 5.33: 4 min Histogram from 1/2/3 Experiment in Figure 5.29-5.31

5.3 Ammonium Nitrate Spectral Images

Laser ablation experiments of ammonium nitrate were performed to investigate the role NO_2 groups might have with respect to RDX plume lifetimes and temperatures, and to reproduce the unique spectra of AN observed by Casper. There are three NO_2 groups on RDX molecules. Ammonium Nitrate solution was sprayed on PC and no spectra were observed. It was suspected that there was not enough ammonium nitrate to generate a plume, so ammonium nitrate pellets

were placed behind a PC film with a small hole cut in it. Figure 5.34 is a photograph of the PC film with a hole, after it had been removed following the experiment. Figure 5.35 is the spectral image montage of the Ammonium Nitrate (AN) ablation experiment for which the PC film is shown above.

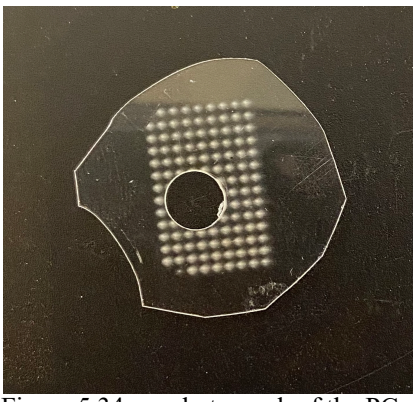

Figure 5.34 – a photograph of the PC film used to constrain the AN pellets for study

Another set of AN experiments were performed. In these experiments AN was dissolved in water to the point of saturation, and then drop-cast

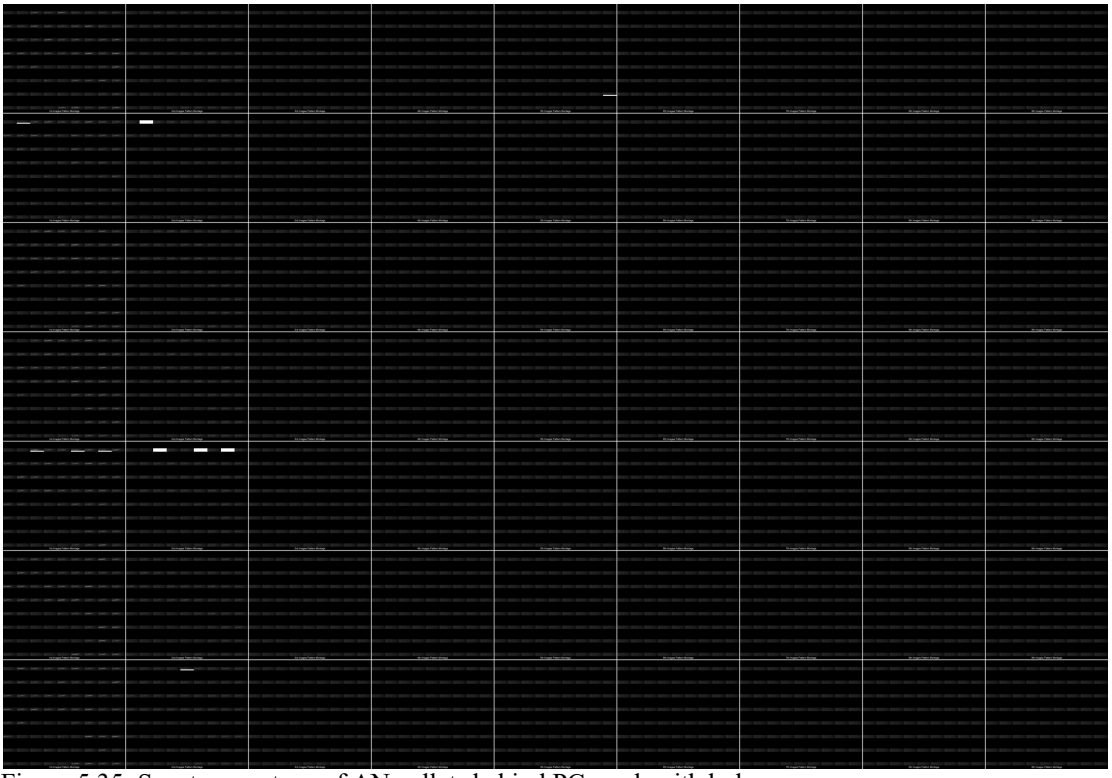

Figure 5.35: Spectra montage of AN pellets behind PC mask with hole

on a PC film. This AN film on PC photographed following laser ablation is in Figure 5.36. The summed spectra from the A shot spectral images of AN on PC compared to PC are shown in Figure 5.37. The spectra have been smoothed using a 5-2-1 signal averaging, discussed in more detail in chapter 8. The summed spectrum of AN has a clearly different shape and intensity than the PC. The major feature of the AN spectra is a broad peak located at higher energy, shorter wavelength, than the PC spectra. This observation is in agreement with Casper's spectra of ammonium nitrate films. [2]

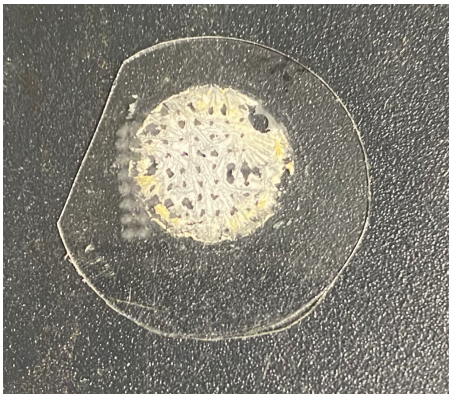

Figure 5.36: Drop-cast AN on PC following laser ablation

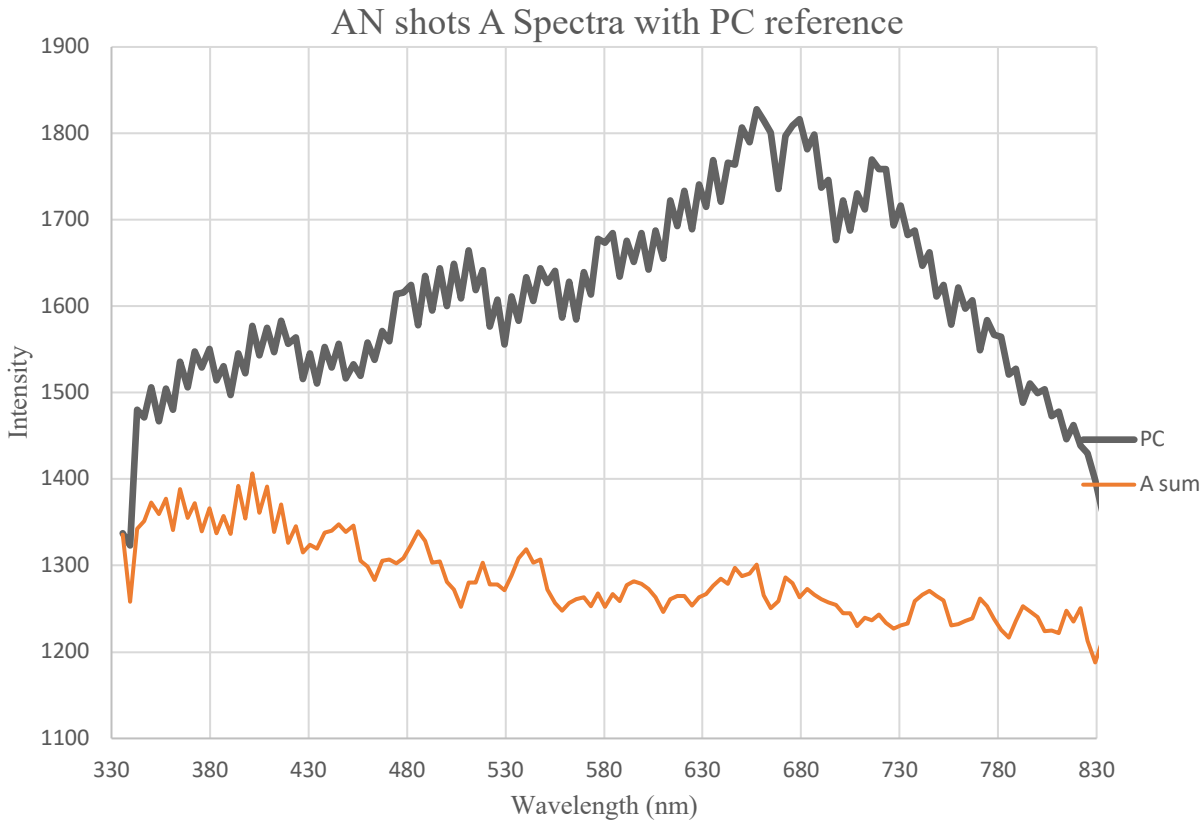

Figure 5.37: Spectra of AN and PC for reference

5.4 Conclusions

Laser ablation experiments of RDX films on PC indicate an interesting phenomena when compared to laser ablation experiments of pure PC. The laser ablation of bare PC produces bright plasma plumes, whereas the ablation of RDX films on PC does not produce bright plumes. Instead, the combination of RDX and PC results in the suppression of bright plumes. It has been proposed that this effect is due to RDX melting into the molten PC below following laser shots,

producing a “snow-pack” feature, which is responsible for the suppression of bright plasma plumes. To investigate the effect of lesser and lesser amounts of RDX (thinner films) on PC, variably sprayed films of RDX on PC were laser ablated and plume images analyzed to try and extract the magnitude of darkening or suppression of brightness at low RDX coverages. It has been observed that this darkening of plasma plumes is very noisy and inconsistent. The rate at which plumes recover brightness from dark to bright has been observed to be somewhat consistent and recovery rates were calculated for all spray times. It was found that more RDX on PC, up to a limit, results in slower recovery to brightness than thinner RDX films. This observation is consistent with more “snow-pack” formed with thicker films than thinner, which requires more laser shots to be removed.

Initially, it was hypothesized that for thin films of RDX on PC should be ablated in a single shot due to the fact that material removal via laser ablation is ten times as deep in RDX than it is in PC. This model is too simplistic, and the reality is that the “snow-pack” features formed following laser shots are not as easily removed via laser ablation as pure RDX. Removal of the “snow-pack” features takes several laser shots, as the RDX has diffused into molten PC, and ultimately the material being removed is PC with RDX diffused into it. At the longest spray times, a steady state in recovery rates is reached because RDX can only diffuse into PC to a certain depth before the PC solidifies. Following laser shots, the PC is only molten temporarily, and the RDX has a finite amount of time to diffuse into the PC. The steady state of recovery rates

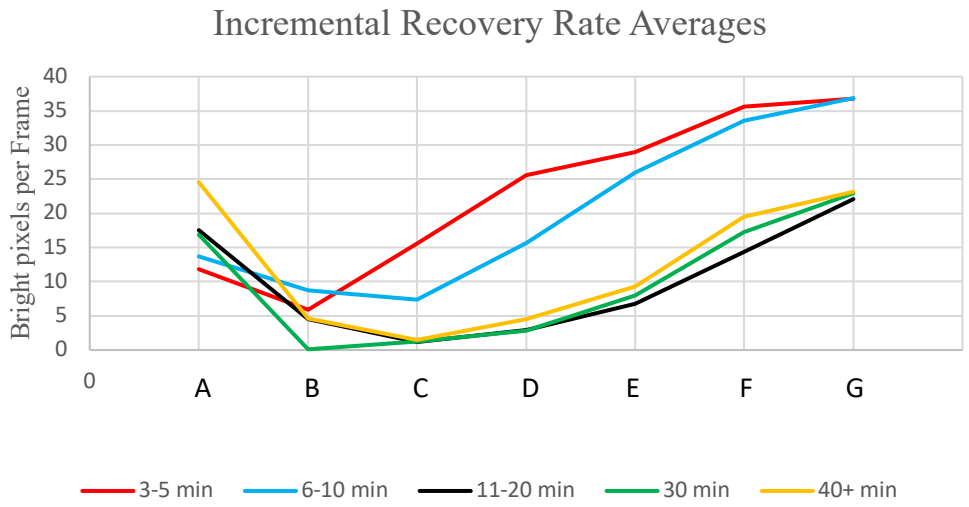

Figure 5.38 Incrementally grouped recovery rates

is reached when the amount of RDX that can diffuse into the temporarily molten PC is maximized at a particular film thickness. Beyond films of this thickness, the increasing amount of RDX does not significantly affect recovery rates, because the amount of "snow-pack" is not changing beyond this thickness. Thin RDX films recover from darkness to brightness more rapidly than thick films because there is less "snow-pack" feature to be removed, and higher degrees of brightness are recovered in fewer laser shots.

Figure 5.38 is a plot of the recovery rates from dark to bright incrementally grouped by spray times and plotted together for comparisons of rates from differently sprayed regions. It is evident that short spray times have faster recovery rates than longer sprayed regions. The 3-5 minute sprayed regions have a recovery rate of 7.42 pixels per frame. The 6-10 minute sprayed regions recover at 7.37 pixels per frame. The 11-20 minute sprayed regions recover at 5.22 pixels per frame. The 30 minute sprayed regions recover at 4.56 pixels per frame. The regions sprayed for 40 minutes and longer recover at 5.41 pixels per frame.

The collection of hundreds of images led to the observation of the snowpack and pattern of bright, dark, bright plumes when RDX films on PC are laser ablated. The ability to collect so much data by performing many experiments in the laboratory on a small scale, using only mg of material, demonstrate one of the advantages over full-scale detonations which are expensive and limited in the amount that can be performed each year.

5.5 REFERENCES

1. Orland, A.; Blumenthal, R., *Nebulizing Spray Technique for Deposition of Propellant Thin Films*, *Journal of Propulsion and Power* 2005, *21*, 571-573.
2. Casper IV, Walter F. *A microsecond time-resolved spectroscopic study of laser induced plasmas and their interactions with solid materials.* Ph.D. Dissertation, Auburn University, Auburn, AL, 2015.

Chapter 6 RDX Spectra

6.1 Introduction

It was desirable to collect spectra of RDX on PC to investigate certain puzzling observations: RDX emission is very short lived and has been very difficult to collect spectra of these plasmas. Most of the spectra are either dark, or they appear to be simply the spectra of the underlying PC. Additionally, the collection of RDX spectra were a priority to further investigate the observed pattern of bright then dark then bright plume emission of RDX on successive laser shots, and what role the previously described "snow-pack" might have on the spectra. Previous attempts to collect RDX spectra from laser ablation experiments of thin films of RDX on PC have been largely unsuccessful. The ability to collect many spectra each experiment using the high-speed camera and sum the resulting spectral images has resulted in some success in acquiring RDX spectra.

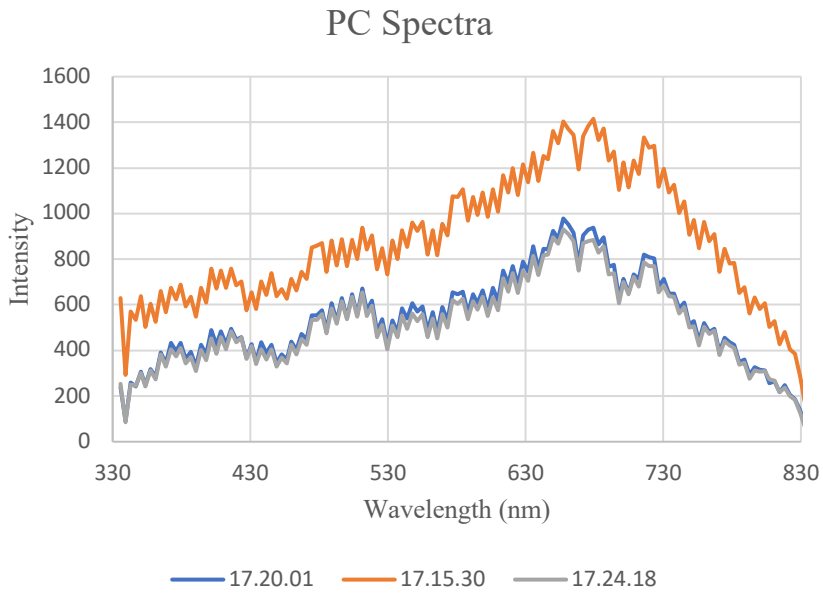

Figure 6.1: Spectra of PC plumes from the first (A) laser shot

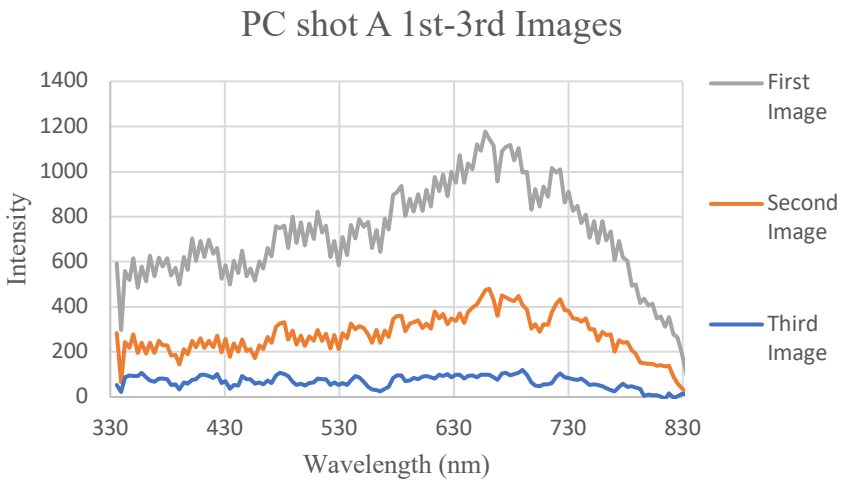

Figure 6.2: PC spectra 1st-3rd Images

6.2 PC Spectra

Spectra of plain PC were collected as a reference since it is the substrate in the RDX experiments. The summed

spectra of the first images of the A shots (first laser shots at a given position) of the plasma plumes from three separate PC laser ablation experiments are shown in Figure 6.1. The shape of PC spectra does not change as time elapses. These PC experiments are highly reproducible. Blackbody temperature fits to these PC spectra are best with a plasma temperature of 2240K +/- 15. The spectra from the A laser shot first image (0-100 μs), second image (100-200 μs), and third image (200-300 μs) of a PC laser ablation experiment are shown in figure 6.2. The intensity drops with each successive image, but there is no wavelength shift in spectral features, indicative of a constant surface temperature plasma, losing intensity as it collapses and decreases in size. This is consistent with Casper's observations. [1]

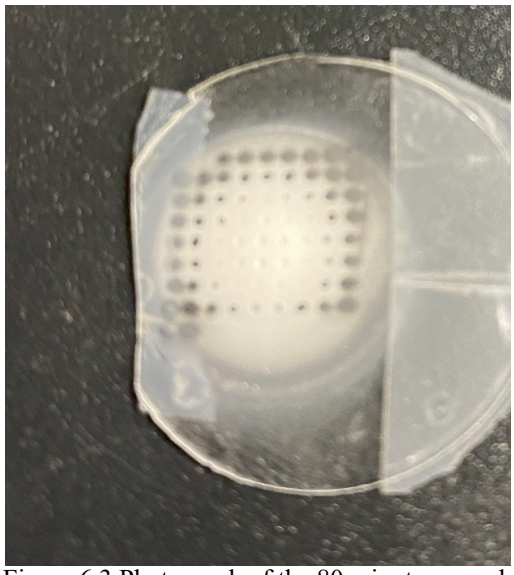
Figure 6.3 Photograph of the 80 minute spayed RDX film on PC after laser irradiation.

6.3 RDX on PC

The spectra of RDX films were collected from the laser ablation of a thick RDX film produced by an 80 minute spray. The thickness of the 80 minute sprayed RDX film in microns, ~70 μm, is estimated below using the same method as in chapter 2 equation 1.

$$80\ minutes \times \frac{1.5\ mL}{60\ minutes} \times \frac{5\ mg}{mL} \times \frac{g}{1000\ mg} \times \frac{cm^3}{1.82\ g} = 0.00549\ cm^3$$

$$Volume\ Cylinder = \pi r^2 H \tag{1}$$

$$0.00549\ cm^3 = \pi \times (0.5\ cm)^2 \times H$$

$$H = \frac{0.00549\ cm^3}{0.785\ cm^2} = 0.00699\ cm \times \frac{10{,}000\ \mu m}{cm} = 69.9\ \mu m$$

A photograph of the 80 minute sprayed RDX film on PC following laser ablation is included in Figure 6.3. Upon visual inspection of the film, it is evident that laser ablation at positions near the center of the film did not penetrate through the RDX to the underlying PC, while laser ablation at peripheral laser positions on the RDX film have exposed circles of the underlying PC much larger than the actual laser spot diameter. Laser ablation positions at

intermediate locations between the center and periphery locations have a smaller hole in the RDX, only as wide as the laser spot.

For analysis purposes, laser spots were organized into three groups: positions where the RDX was entirely removed at the periphery, positions where RDX was partially removed, and positions where the underlying RDX appeared intact even at the center of the laser spot, with no visual penetration through to the underlying PC. The differences in these three different types of spots are attributed to differences in the film thickness across the spray deposited RDX film. The large spots at the periphery are due to sublimation of the thinner RDX by the laser plume. Spectra from each of the three different types of spots were summed by laser shot A-G, and plotted in figure 6.4, with the spectra vertically offset to prevent overlap.

The shape of the spectra in which RDX was removed changes from shot A to shot G, see Figure 6.4. In shot A the spectra resemble

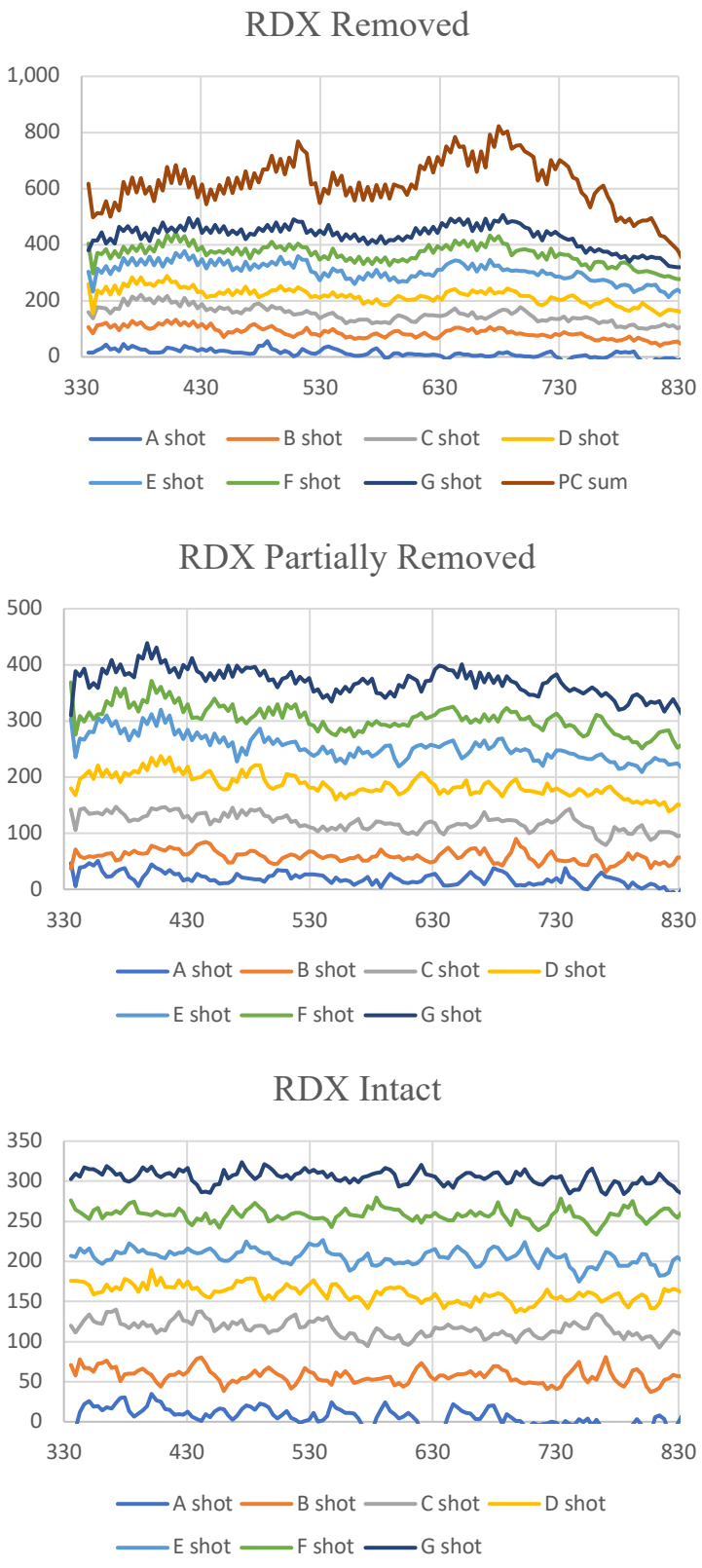

Figure 6.4 – the summed spectra of each laser shot (A-G) in each physically different region from the experiment shown in figure 6.3 (see text details)

the spectrum of intact RDX with only a slow decrease in signal from short wavelength to longer wavelength. With each laser shot, the spectra transition from the shape of intact to RDX to a shape that resembles the spectrum of pure PC. It is assumed that the spectra of shot A are representative of the pure RDX on the top of the film, and that shot G is spectra of the underlying PC following RDX removal.

For the early shots, A-C, the RDX partially removed plot (Figure 6.4) is similar in shape to the intact RDX spectra. By shot G of the partially removed RDX, spectral features around ~660 nm resemble the spectrum of pure PC, but these features in the partially removed spectrum are not as clear as in shot G of the RDX removed spectrum. The spectral shape progression from intact RDX on shot A, to a spectral profile resembling PC in shot G indicates the presence of some amount of PC in the plasma plume produced by shot G as the RDX film becomes thinned from laser shots A-F, see Figure 6.4. It is hypothesized that shot G could be the spectrum of the previously described "snow-pack" features formed when RDX diffuses into underlying molten PC.

At the intact RDX positions, the spectrum appears as nothing more than a slow decrease in signal from short wavelength to longer wavelength. The best fit to the sum of the first images of the A-G shots are shown in figure 6.5 along with the best fit corresponding to a temperature of 8725K +/- 50 . Figure 6.6 is a similarly constructed PC spectra of a sum of shots A-G fit to a blackbody curve with a best fit temperature of 2240K +/- 5for comparison. The blackbody curve was only fit to the PC spectra to the left of the peak because it was assumed that the drop off at higher wavelengths was due to loss of signal. In chapter 4, a blackbody curve was fit to a PC spectrum with a best fit

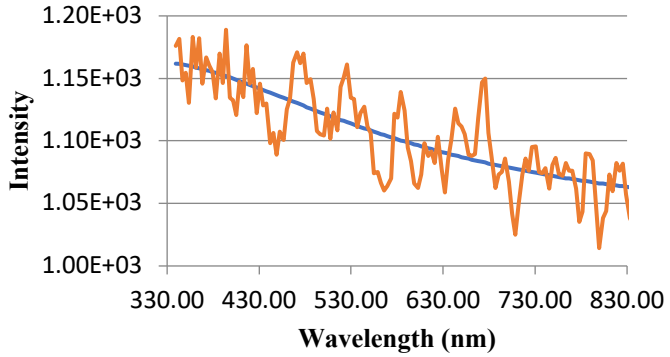

Figure 6.5: RDX on PC Shots A-G sum fit to blackbody

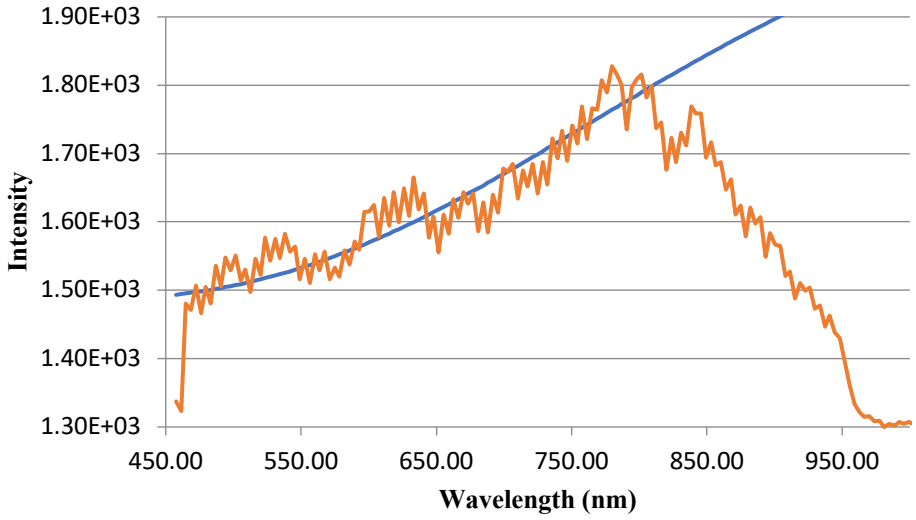

Figure 6.6: PC shots A-G sum spectra fit to blackbody curve

temperature of 4300K. It is suspected that this fit and temperature were not accurate because the entire spectrum was used for the fit, rather than excluding the region to the right of the peak in figure 6.6 which is thought to be signal loss at higher wavelengths.

Following the laser ablation experiment, during handling of the film to storage, some of the RDX flaked off, revealing the formation of a "snow-pack" in regions where RDX was not entirely removed, see Figure 6.7. This observation is consistent with the "snow-pack" formed in the laser ablation of thin films of RDX, described previously in chapter 4, and is attributed to the diffusion of RDX into the molten PC layer below. Laser irradiation of an 80 minute sprayed sample of RDX on PC resulted in these different types of features. The spectra of the completely removed spots resembled those of the intact RDX in early shots and transitioned to spectra that also have dominant feature of pure PC, and presumably represent the spectra of the "snowpack." For the early shots, A-C, in the intermediate region the spectra is similar in shape to the intact RDX spectra. By shot G of the partially removed RDX, spectral features around ~660 nm resemble the spectrum of pure PC. The spectral shape progresses from intact RDX on shot A, to a spectral profile resembling

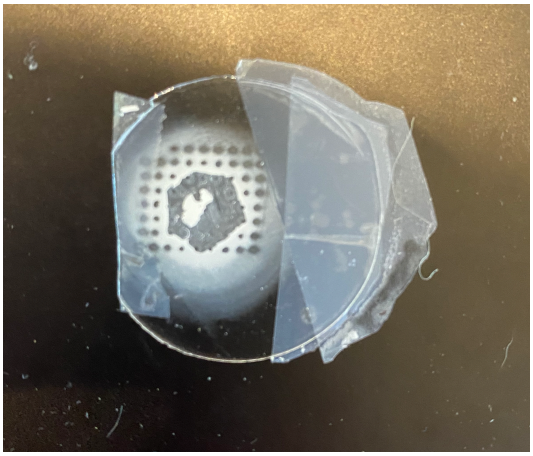

Figure 6.7: 80 minute RDX on PC following laser ablation and accidental RDX flaking, revealing "snow-pack"

PC in shot G. It is hypothesized that the shot G of the partially removed region could be the spectrum of previously described "snow-pack." At the intact RDX positions, the spectrum appears as nothing more than a slow decrease in signal from short wavelength to longer wavelength. A black body plot was fit to the spectra of intact RDX, and a plume temperature estimated from the blackbody equation. The plume temperature estimated for RDX is 8725K +/- 50, compared to that of 2240K +/- 5 for PC plumes. This change in temperature provides some explanation of why RDX plumes have been difficult to optically image or collect spectra.

Equation 2 is used to calculate the blackbody intensity as a function of temperature. Equation 3 calculates the blackbody energy emitted per meter/second as a function of wavelength. The energy emitted summed across all wavelengths was multiplied by the spherical plasma surface area to yield the initial Energy Emitted from Plume (J/s). A plume energy of 0.005 J is divided by the initial energy emitted from the plume (J/s) to estimate the Initial Lifetime (s) of a 50 mJ plume. A RDX plasma (8725K) radiates the 50 mJ in 1.21E-14 seconds, and a PC plasma (2240K) radiates the 10 mJ in 2.80E-12 seconds. The RDX plasma radiates the same amount of energy in about 1/230th the time required for PC.

$$I = \left(\frac{8\pi hc}{\lambda^5}\right)\left(\frac{1}{e^{\frac{hc}{\lambda kT}}-1}\right) \qquad (2)$$

$$E = \left(\frac{c}{4}\right)\left(\frac{8\pi hc}{\lambda^5}\right)\left(\frac{1}{e^{\frac{hc}{\lambda kT}}-1}\right) \qquad (3)$$

The ability to distinguish the spectra of RDX films on PC from those of plain PC, as well as correlate RDX spectra shapes to the thickness of the RDX film from which the laser ablated plume was imaged, demonstrate the effectiveness of this laboratory scale method for energetic materials analysis, as well as its application for standoff detection of energetic materials.

6.4 REFERENCES

1. Casper IV, Walter F. *A microsecond time-resolved spectroscopic study of laser induced plasmas and their interactions with solid materials.* Ph.D. Dissertation, Auburn University, Auburn, AL, 2015.

Chapter 7 Ammonium Nitrate Spectra

7.1 Ammonium Nitrate Pellet

Laser ablation experiments of ammonium nitrate were performed to investigate the role the three NO_2 groups might have on plume lifetimes and temperatures of RDX laser ablation plumes. Gottfried characterized ammonium nitrate (AN) as a semi-energetic material, based on velocities of laser induced shockwaves she measured. [1] Saturated Ammonium Nitrate in acetonitrile solution was sprayed on PC and no spectra were observed. It was suspected that there was not enough ammonium nitrate to generate a plume, so ammonium nitrate pellets were placed behind a PC film with a small hole cut in it.

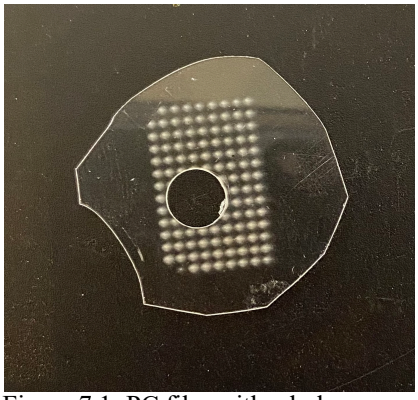

Figure 7.1: PC film with whole, through which AN pellets ablated

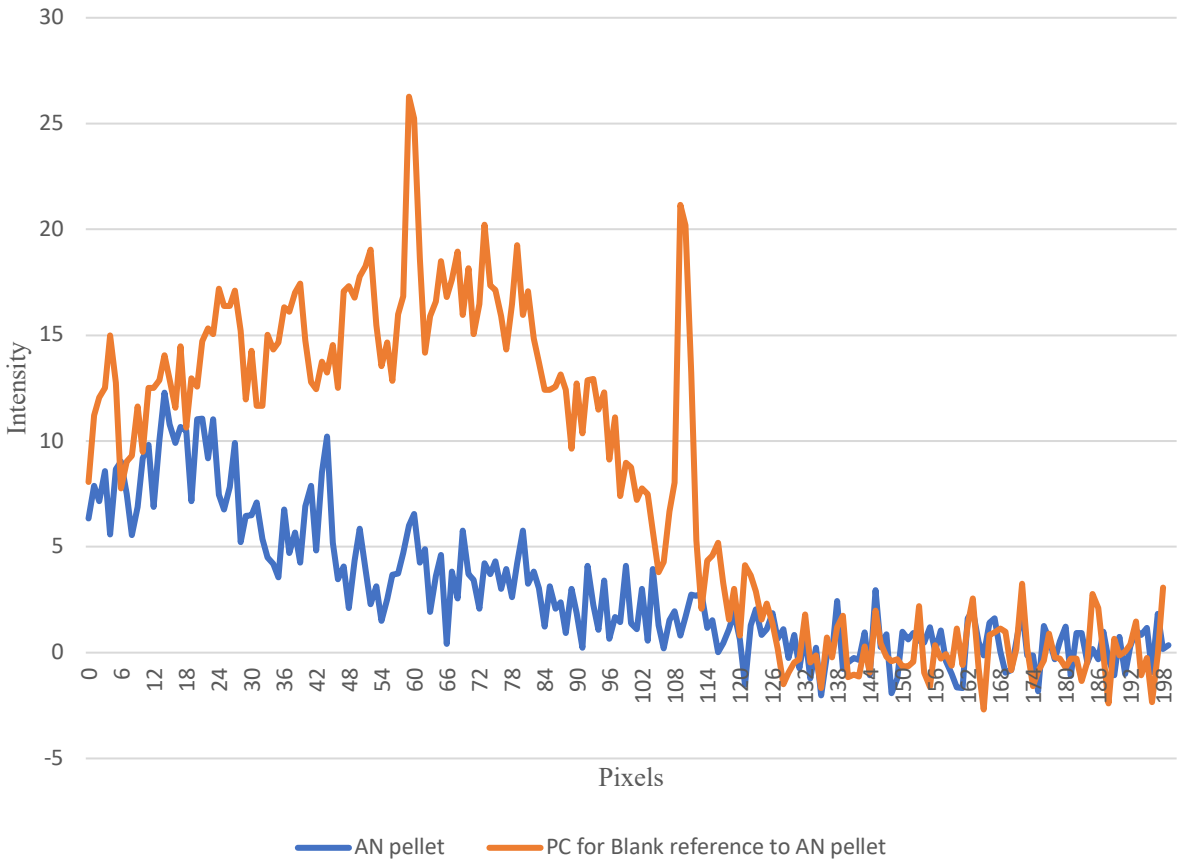

Figure 7.2 – Spectra of the A shots on AN pellets and PC.

A photo of the PC film with the hole through which ammonium nitrate pellets were exposed to laser ablation is in figure 7.1. From the image of the PC film with a hole, the positions at which ammonium nitrate pellets were exposed to the laser through the hole, were identified. Spectra from the A laser shots (first laser shots at the given position) were then summed to generate the spectra of ammonium nitrate, see figure 7.2. The A laser shots from regions clearly on the PC film were also identified and summed to generate reference spectra of PC, also see figure 7.2. The summed spectrum of AN has a clearly different shape and intensity than the surrounding PC region. The major feature of the AN spectra is a broad peak located at higher energy, shorter wavelengths than the PC spectra. This observation is in agreement with Casper's spectra of ammonium nitrate films. [2]

7.2 Ammonium Nitrate Drop-cast

Another AN experiment was performed. In this experiment AN was dissolved in water to the point of saturation, and then drop-cast on a PC film. This sample was dried overnight, before the sample was laser ablated and spectral images were collected. Figure 7.3 is the photograph of a dried, drop-cast ammonium nitrate film on PC following laser ablation. The first images of the A through G laser shots are shown in Figure 7.4. The spectra have been smoothed using a 5-2-1 signal averaging. These spectra were background corrected by subtracting ninth Images from the first images. A spectrum obtained from pure PC, obtained and processed in the same manner as the AN spectra is included for comparison. The shape of the AN spectra changes from shots A to shot G as ammonium nitrate is removed by the ablation process. The early shots A – B are considered representative of the ablation of pure ammonium nitrate, while later shots, C – G indicate an increasing fraction of PC in the plume. The A shot first image was fit to a blackbody and a best fit was obtained at a temperature of 8930K +/- 35.

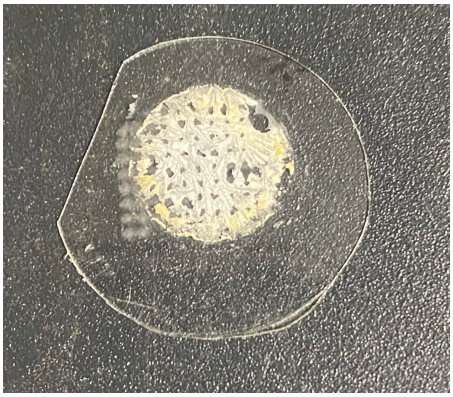

Figure 7.3: Photo of AN drop-cast on PC following laser ablation

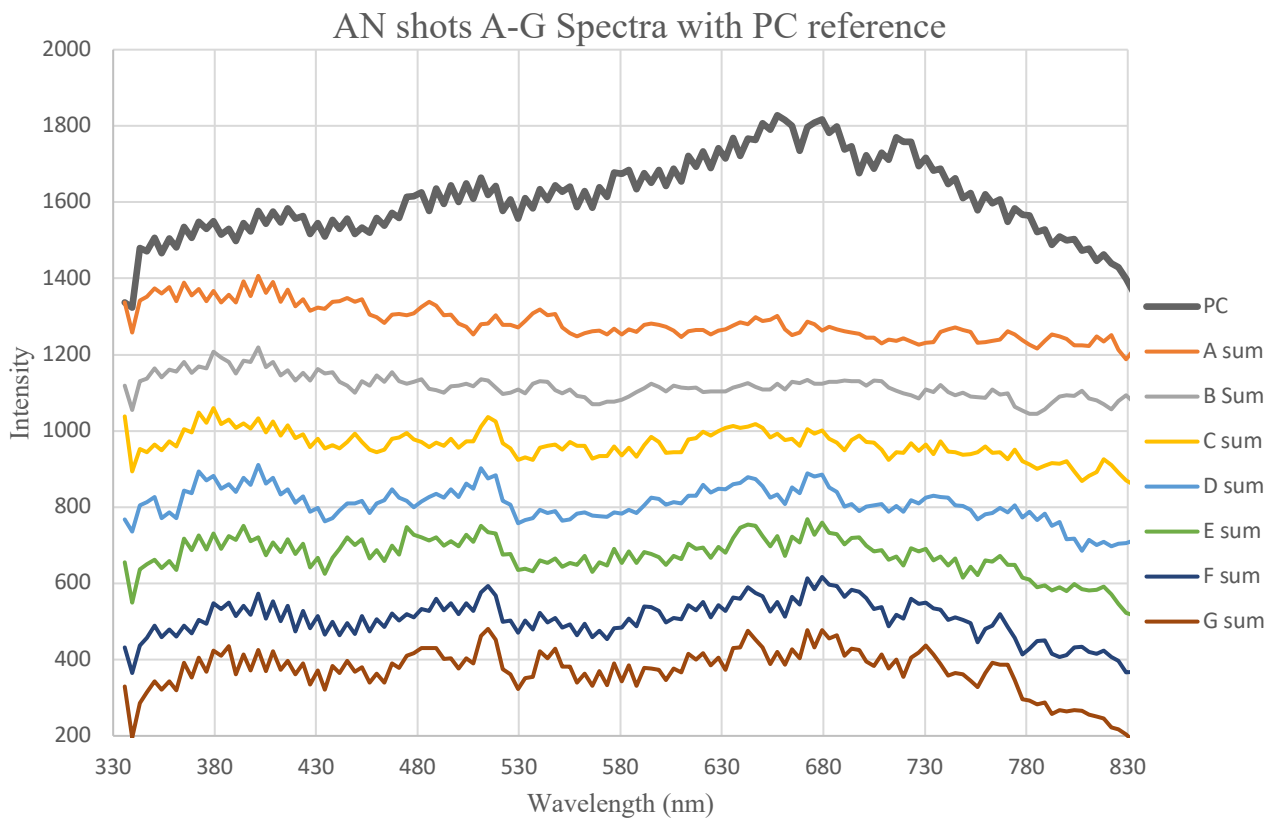

Figure 7.4: First image spectra of the A-G laser shots on AN and an A shot PC spectrum

The AN spectra from first image (0-100 µs), second image (100-200 µs) and third Image (200-300 µs) of the A shot are plotted in Figure 7.5. The estimated black body temperature of the plasma in the first image is 8930K +/- 35. By the second image, the plasma cooled to 7990K +/- 35, and in the third image it is 7740K +/- 35. Hence, from the second image on, consistent with Casper's observations, these spectra do not significantly change shape (or temperature) through time but only decrease in intensity. This observation likely indicates a plasma surface at a constant temperature, with the decay in intensity through time an effect of the collapsing plasma at a constant surface temperature. [1]

Similar to one of the conclusions stated at the end of chapter 6, the detection of ammonium nitrate and estimation of the plume temperature of laser ablated plumes of ammonium nitrate using laboratory scale experiments demonstrate the effectiveness of this technique and its potential to be used for standoff detection of energetic materials.

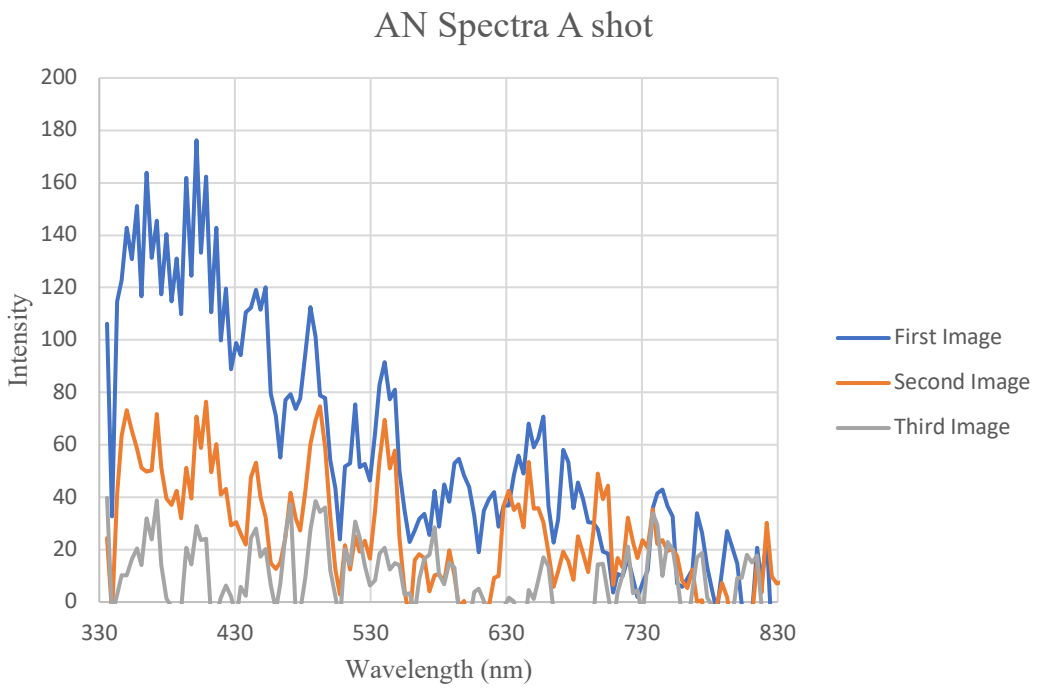

Figure 7.5: AN spectra First - Third Images

7.3 REFERENCES

1. J.L. Gottfried, *Influence of exothermic chemical reactions on laser-induced shock waves*, Phys. Chem. Chem. Phys. 16, 21452 (2014)
2. Casper IV, Walter F. *A microsecond time-resolved spectroscopic study of laser induced plasmas and their interactions with solid materials.* Ph.D. Dissertation, Auburn University, Auburn, AL, 2015.

Chapter 8 Metals on Double-Sided Tape Spectra

8.1 Double-sided Tape Spectra

Laser ablation experiments involving metals powder on double-sided Scotch tape were conducted, out of curiosity using readily available materials in lab, to investigate what affect metals have on the spectral profile of plasma plumes. For comparison, and to determine what spectral features might be a result of the underlying tape, the spectra of A-G shots first image sums of double sided tape were also collected. As with all other spectra, all spectra in this chapter have been background corrected by subtracting the ninth image sums of each shot A-G from the first image sums, and smoothed using a one-two-five-two-one signal average. As seen in Figure 8.1, bare double-sided tape has a broad spectral feature at ~420 nm, a sharper peak at ~485 nm, and another broad spectral feature at ~640 nm. The spectra of double sided tape does not change from shot to shot, as shot G looks very similar to shot A, indicating there is no shot dependence for the spectral signature of double sided tape. The spectra of PC obtained using a

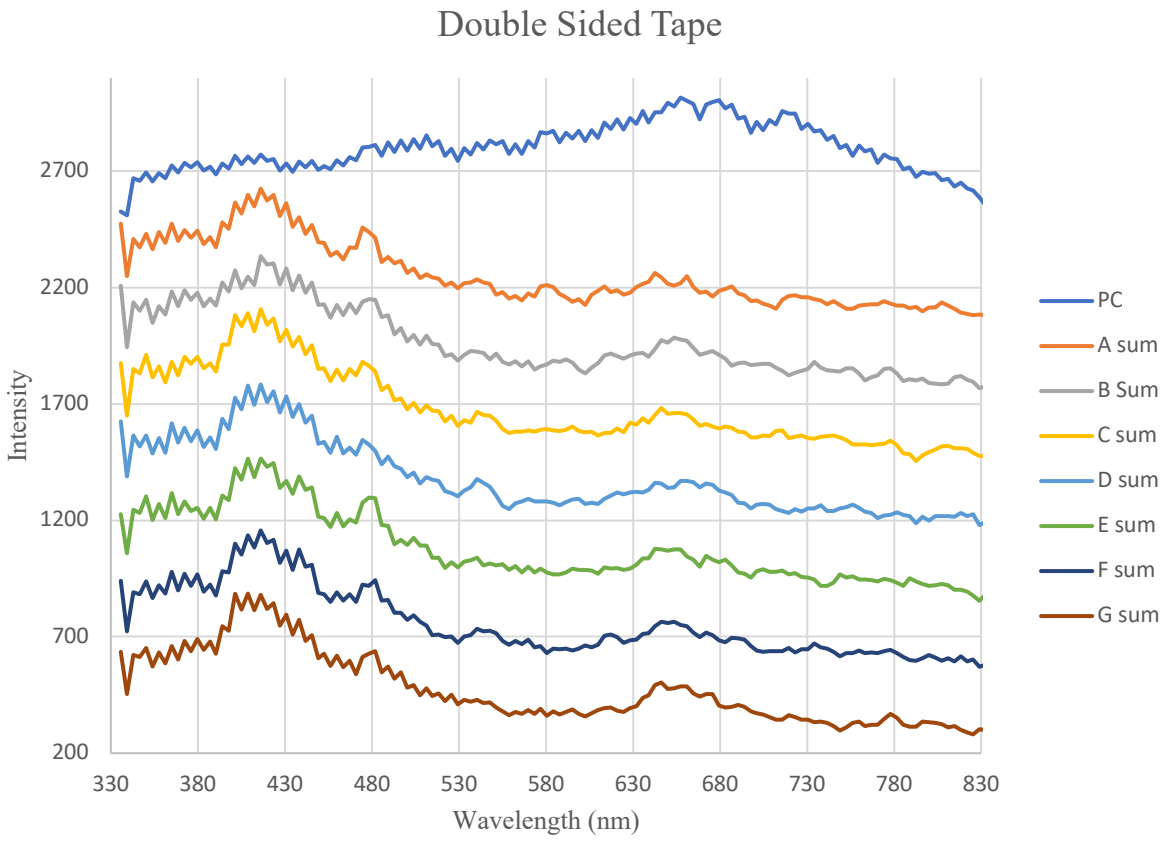

Figure 8.1: Double Sided Tape spectra A-G shots with PC for reference

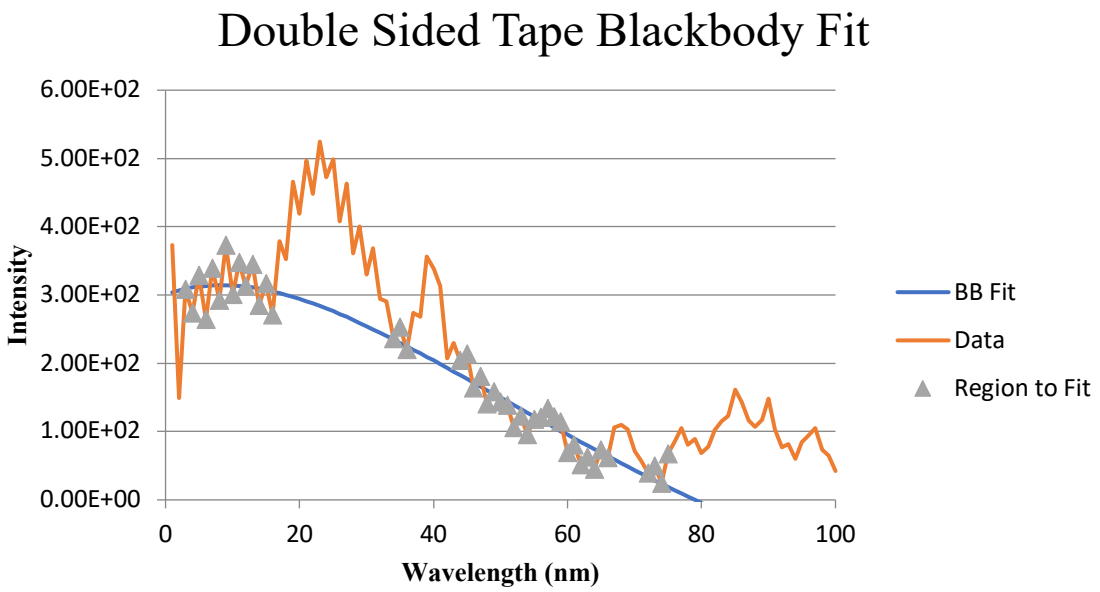

Figure 8.2: Blackbody curve fit to selected regions of Double sided tape spectra B Sum

blackbody fit to the entire spectral region is included at the top of the plot. The broad spectral feature at around 670 nm in pure PC is also present in double sided tape, and suggests that the double sided tape used in the experiment is composed in part of PC. A black body temperature curve was fit to the smooth regions of the B shot double sided tape spectra (indicated by the triangles), and a plasma temperature of 7920K +/- 15 was estimated. The blackbody fit is shown in Figure 8.2. The temperatures of best fit are only estimates, as several sharp spectral peaks and broad features are ignored in the fit.

8.2 Iron on Double-sided tape Spectra

The spectra of shots A-G first images laser ablation experiments of Iron on double sided tape were collected and processed in the same way as the plain double sided tape. For reference, the spectra of PC and double sided tape are included, see Figure 8.3. The spectral profile of Iron on double sided tape changes from shot A to shot G. The spectral shape in shot A resembles the shape of plain double sided tape, but has more of a rise at short wavelengths, likely indicative of a higher temperature plasma than that of plain double sided tape. This rise at short wavelengths with the PC features make the shape very difficult to fit to a blackbody. Only the G shot could be

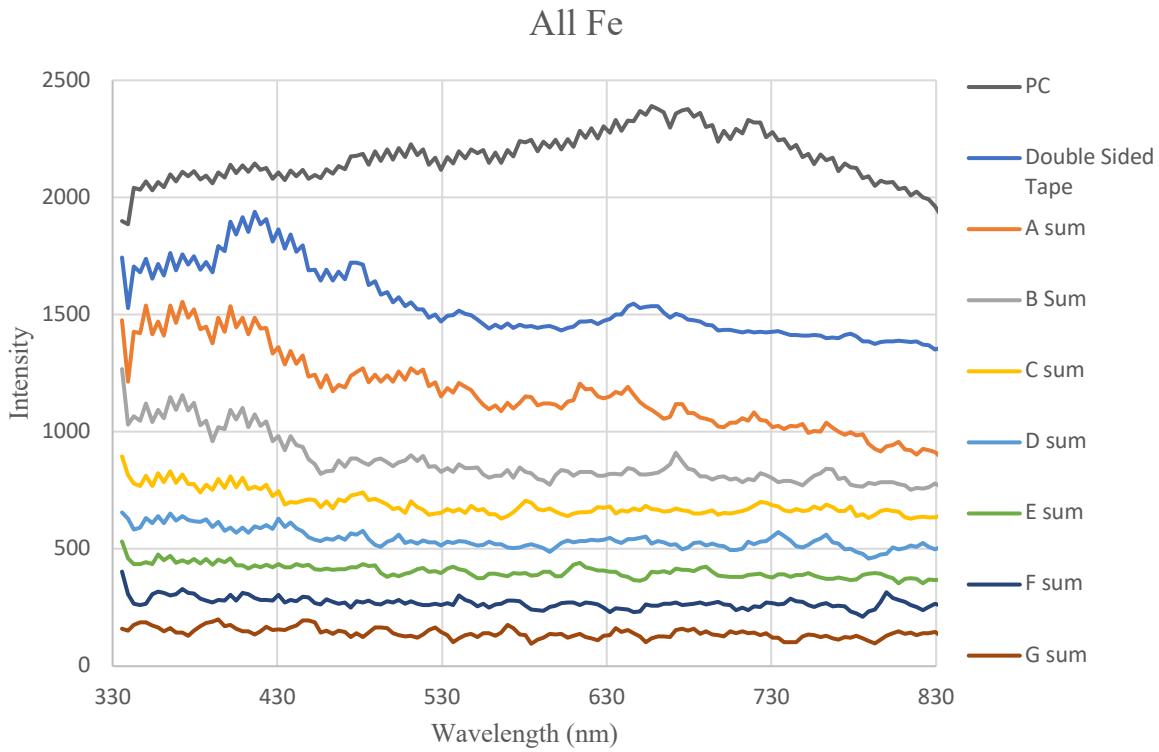

Figure 8.3: Fe on double sided tape spectra shots A-G

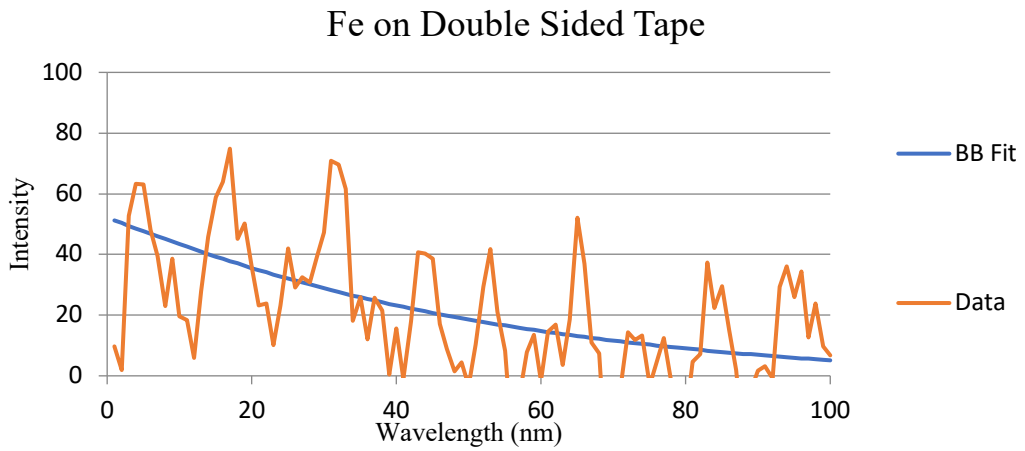

Figure 8.4: Fe G shot spectrum fit to blackbody curve.

fit to a black body, with a best fit temperature of 12,450K +/- 225, see Figure 8.4. The general shape of shot A persists but decreases in slope in shots B and C. By shot D, the spectra appear dark and flat, with very little features. Beyond shot D, the flattening of the spectral signal continues and by shot G the signal is nearly horizontal. All metals used in this experiment were

stored for over 10 years in the lab, and likely have developed an oxide layer. Naturally formed iron oxide films were determined to be 3-5 nm thick by AES and XPS.[1] It is possible that the change in shape through progression of shots A to G could be due to the removal of that oxide layer. Iron is known to oxidize readily and takes several laser shots to remove and change spectral shape to the flat profile by shots C and D. Iron oxide systems are known to melt at ~1600K [2], well below the temperature of the plasma produced in shot G.

8.3 Nickel on double-sided tape Spectra

The spectra of shots A-G first images laser ablation experiments of Nickel on double sided tape were collected and processed in the same way as the plain double sided tape, see figure 8.5. Nickel has a strong spectral signature in shot A, with some sign of the double sided tape spectral features at ~420 nm and the broad feature at 670 nm that is also common to PC. The nickel spectra of shot A also has a broad feature at ~500 nm that is not present in double sided tape or pure PC. Blackbody curves were not able to be fit to the Ni spectra. Nickel is a noble metal, not likely that there is a thick oxide. Naturally forming nickel oxide films were

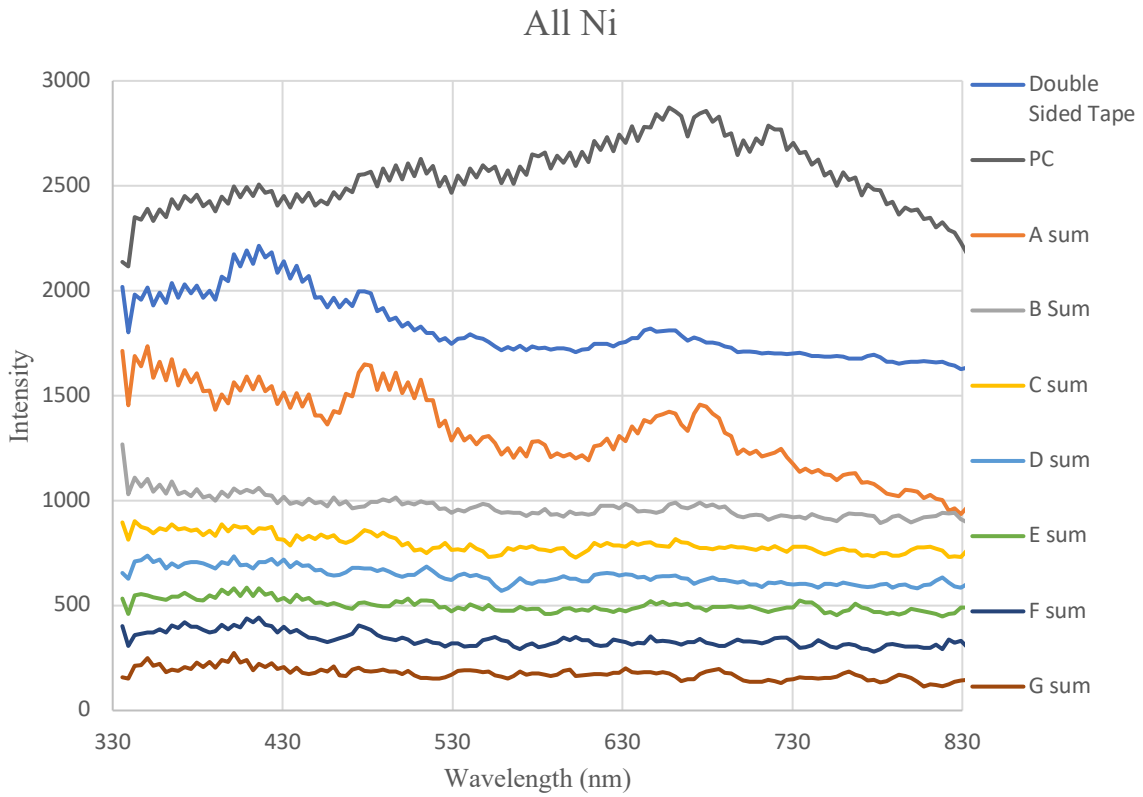

Figure 8.5: Ni on double sided tape spectra shots A-G

determined to be 0.5-1.0 nm thick by AES and XPS.[1] It only takes one shot for the spectra to go flat, perhaps this is because any metal oxide is very thin and is ablated in only one laser shot, causing shots B-G to appear flat after the oxide is ablated by shot A.

8.4 Cobalt on double-sided tape spectra

The spectra of shots A-G first images of laser ablation experiments of Cobalt on double sided tape were collected and processed in the same way as all of the others, see figure 8.6. In contrast to the other metals that have spectral signal in shot A and then go dark, Cobalt is dark in shot A and then begins to show spectral signal in shots B and beyond. Blackbody curves could not be fit to the Co spectra. Beyond shot A the spectra have a rise at short wavelengths, likely indicative of a higher temperature plasma. The rising slope at short wavelengths does not occur until after shot A. It is hypothesized that in shot A, cobalt or cobalt oxide is removed. It is possible that in the first shot Cobalt is partially removed and diffuses into the melted double

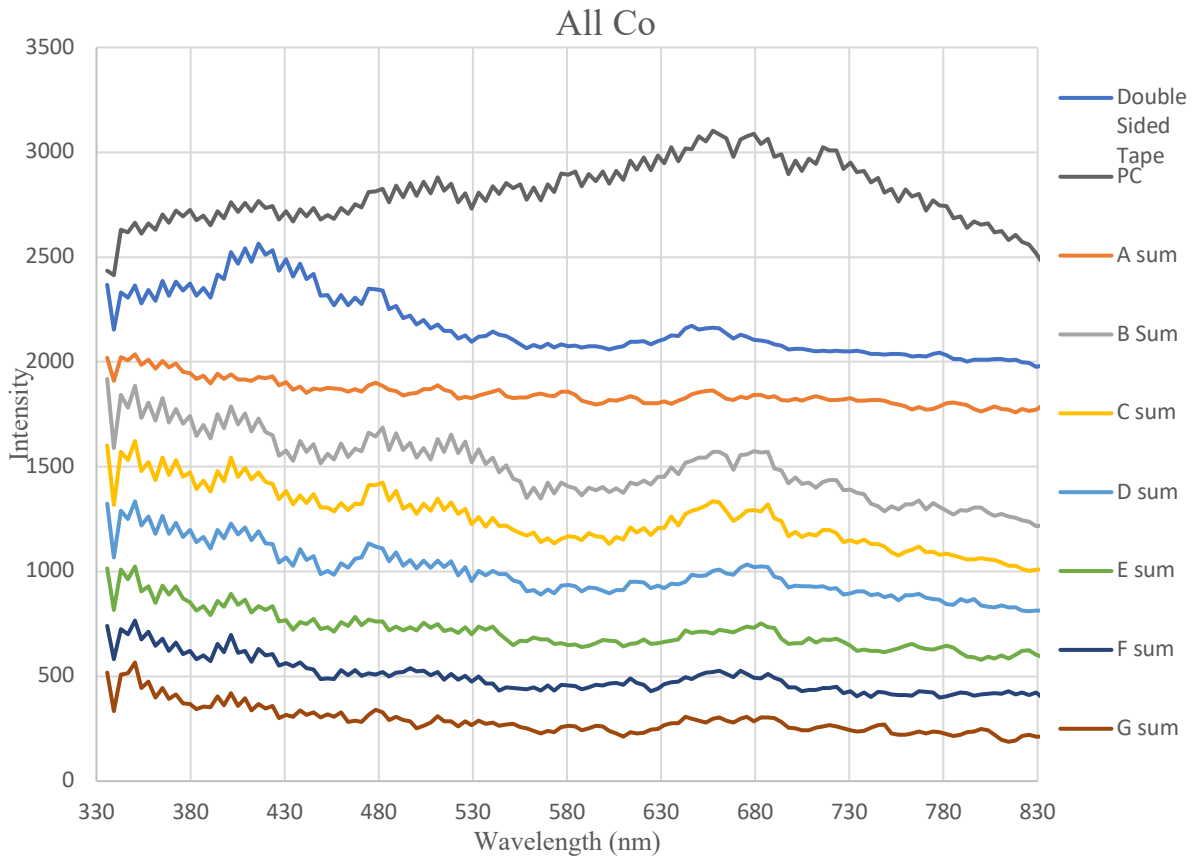

Figure 8.6: Co on double sided tape spectra shots A-G

sided tape below, leaving a Co/tape "snow-pack." The drop in double sided tape signal in shots B-G is interpreted as the removal of this Co/tape "snow-pack." Cobalt oxide films have been observed to be 1-3 nm. [3]

8.5 Metal Oxides

Iron oxide forms the thickest metal oxides, with nickel and cobalt oxides being similarly thin. If metal oxides are being ablate they might behave like a thermite. The very high temperature of the G shot of the Fe sample might indicate that iron oxide could possibly be a mildly energetic material as Fe_2O_3 is oxidizer, the tape is oxidizable, and a reaction akin to that of Al in thermite might be taking place. More shots remove oxide layer, could be a reason for Fe signal for several shots as opposed to only one for Ni and Co. The metals could act as mild energetics.

The feasibility of utilizing laser induced breakdown spectroscopy as a laboratory-scale technique to assess the performance of composite energetic materials with metal additives is addressed with this brief study on the effects of metals on the spectra of double sided tape laser induced plasmas.

8.6 References

1. Mathieu, H.J.; Datta, M.; Landolt, D. Thickness of natural oxide films determined by AES and XPS with/without sputtering. Landolt Materials Department, Swiss Federal Institute of Technology (EPFL), CH-lOO7 Lausanne, Switzerland
2. Keiichiro KASHIMURA1); Kazuhiro NAGATA2).. Removal of Fe3O4 Film Using Atmospheric Transferred Plasma at Low Temperature. 1) Formerly Department of Chemistry and Materials Science, Tokyo Institute of Technology. Now at National Institute for Fusion Science, Toki 509-5292 Japan. 2) Department of Chemistry and Materials Science, Tokyo Institute of Technology, 2-12-1 Ookayama, Meguro-ku, Tokyo 152-8552 Japan. (Received on December 17, 2008; accepted on October 15, 2009).
3. Tracy, Joseph B.; Weiss, Dirk N.; Dinega, Dmitry P.; Bawendi, Moungi G. Exchange biasing and magnetic properties of partially and fully oxidized colloidal cobalt nanoparticles. Phys. Rev. B 72, 064404 – Published 2 August 2005

Chapter 9 Conclusions

Laser ablation experiments of the energetic material RDX on PC indicated four interesting phenomena when compared to laser ablation experiments of pure PC. First, the broad, blackbody emission of laser induced PC plasmas decreases in intensity but does not shift in wavelength through the majority of the emission process.[1] Second, the emission of PC lasts for hundreds of microseconds, but the emission of RDX under the same experimental conditions lasts only nanoseconds. Third, the laser induced ablation pits on RDX are ten times as deep as they are with PC. [1,2] Fourth, the previously unknown, nature of the power density threshold for laser ignition of RDX has been observed. The

To address the latter two phenomena, a model study was carried out to investigate whether the laser ignition of RDX at high laser fluence is simply the result of thermal ignition resulting from heating by a blackbody plasma raising the temperature of the RDX above the thermal threshold for reaction. Using only a few reasonable assumptions, the model produces laser ablation pits in RDX that are approximately ten times deeper than those observed on PC, resulting from a black body plasma re-radiating onto the RDX surface, and subliming molecular RDX. Increasing the laser power in the model to a value comparable to those at the reported threshold for laser ignition, results in temperatures of over 900K at the surface which would result in thermal ignition.

The lack of a wavelength shift as the signal level drops seems to indicate that the plasma is emitting at a constant temperature, however this is puzzling sense the plasma is losing energy through emission of light, so it would be expected to cool. Casper rationalized this strange observation by hypothesizing that the plasma in laser ablation is optically dense. Only the surface of an optically dense plasma is visible to the external observer, and the emission at a constant wavelength, or temperature, is the result of a phase transition from a strongly emitting plasma to a much less emissive neutral gas at the surface. Within this model, the decrease in intensity is due to the decrease in surface area of the plasma as the interface recedes radially inward, as the plasma radiatively loses energy. Casper's experimental setup was modified with the addition of a fast camera to image plumes spectrally using a diffraction grating spectrometer. Where Casper could only collect one spectrum per laser pulse, the fast camera enabled the collection of 20 images, each 100 μs apart in time, each of seven laser pulses at a given spot on the sample. With the collection of many more spectra, it was possible to construct an average

RDX spectrum. When fit to blackbody curves it was discovered that RDX plasmas are much hotter than PC plasmas, with a surface temperature estimated at 8725K +/- 50 compared to 2240K +/- 15 for PC. As a result of this observation, the rapid disappearance of the visible RDX emission is proposed to be an effect of the hotter surface of the RDX plasma compared to PC. Hotter bodies radiate heat away at a faster rate than cooler bodies. The hotter RDX plasma radiates away its energy 230 times faster than the lower temperature PC plasma. The results of this work are strong evidence in support of the proposition that these phenomena are the result of a plasma/gas phase transition by studying the laser ablation and resulting plasma plumes of RDX films on PC.

The ability to collect hundreds of images of laser ablation plumes using seven laser spots at the same sample position revealed a new anomaly. When the same region of RDX coated PC is exposed to a series of consecutive laser shots, the visible emission from the first shot is bright, then goes dark for the second and third shots, and returns to bright again for the subsequent shots. There is some variability to this pattern, sometimes the visible emission is dark for only one shot, sometimes it lasts for 3 or more shots, and sometimes the first shot is bright, and other times it is dark. It is proposed that the pure RDX which is cleanly ablated results in the bright image of the first images of the first and often second shots. Using microscopy, it was found that white layers that cannot be removed with solvent are present on the PC around and on the laser irradiation pit following ablation from seven laser shots. These white layers have been described as “snow-pack” in this work, and are attributed to the subsurface melting of the PC, into which RDX can diffuse. By the second or third laser shot, the top layer of RDX has been removed, and the RDX+PC mixture is being ablated and the resulting plasma appears dark. This theory is consistent with previous reports that RDX needs PC to initiate via laser irradiation under the conditions used in these experiments, and that without the PC component, the pure RDX plasma does not ignite. After both the RDX and “snow-pack” have been fully ablated, the images of the plasmas return to bright. As previously mentioned, the RDX and underlying “snow-pack” removal can take several laser shots for plasmas to return to bright, depending on the thickness of the RDX film, and how much RDX is able to diffuse into the molten PC to create the “snow-pack.” In other words, once dissolved into the PC the RDX no longer sublimes. To investigate the effect of lesser and lesser amounts of RDX (thinner films) on PC, variably sprayed films of RDX on PC were laser ablated and plume images analyzed to try and extract the magnitude of

darkening or suppression of brightness at low RDX coverages. It has been observed that this darkening of plasma plumes is very noisy and inconsistent. The rate at which plumes recover brightness from dark to bright has been observed to be somewhat consistent and recovery rates were calculated for all spray times over numerous experiments.

Initially, it was hypothesized that RDX on PC should be ablated in a single shot due to the fact that material removal via laser ablation is ten times as deep in RDX than it is in PC. This model is too simplistic, and the reality is that the "snow-pack" features formed following laser shots are not as easily removed via laser ablation as pure RDX. Removal of the "snow-pack" features takes several laser shots, as the RDX has diffused into molten PC, and ultimately the material being removed is PC with RDX diffused into it. At the longest spray times, a steady state in recovery rates is reached because RDX can only diffuse into PC to a certain depth. Following laser shots, the PC is only molten temporarily, and the RDX has a finite amount of time to diffuse into the PC before it solidifies. The steady state of recovery rates is reached when the amount of RDX that can diffuse into the temporarily molten PC is maximized at a particular film thickness. Beyond films of this thickness, the increasing amount of RDX does not significantly affect recovery rates, because the amount of "snow-pack" is not changing beyond this thickness. Thin RDX films recover from darkness to brightness more rapidly than thick films because there is less "snow-pack" feature to be removed, and higher degrees of brightness are recovered in fewer laser shots.

The recovery rates from dark to bright were incrementally grouped by spray times and plotted together for comparisons of rates from differently sprayed regions in Figure 9.1. It is evident that short spray times have faster recovery rates than longer sprayed regions. The 3-5 minute sprayed regions have a recovery rate of 7.42 pixels per frame. The 6-10 minute sprayed regions recover at 7.37 pixels per frame. The 11-20 minute sprayed regions recover at 5.22 pixels per frame. The 30 minute sprayed regions recover at 4.56 pixels per frame. The regions sprayed for 40 minutes and longer recover at 5.41 pixels per frame.

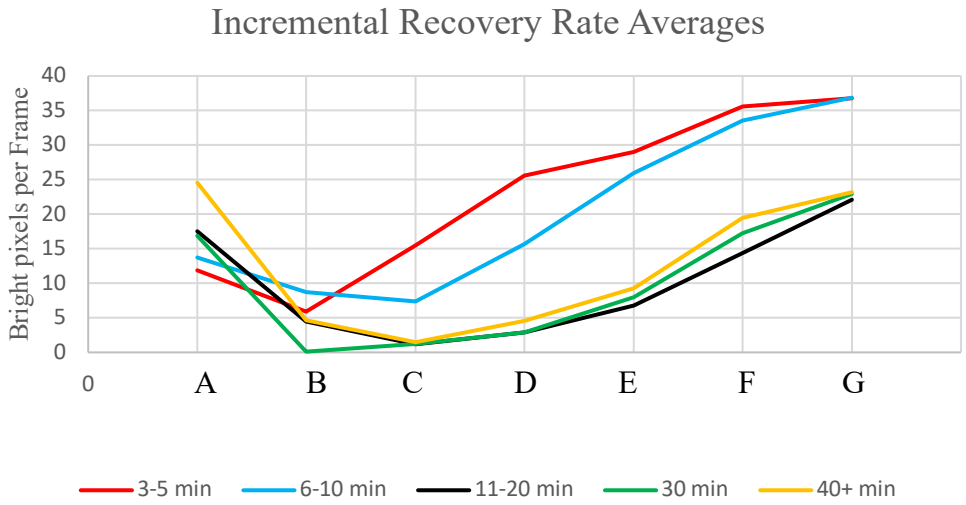

Figure 9.1: Incrementally grouped brightness recovery rates. 1-7 are the shot numbers A-G.

	Depth (Micrometers)	Laser shots to recover brightness	Estimated "snow-pack" thickness (Micrometers)
RDX removal rate	6	4	24
PC removal rate	0.6	4	2.4

Table 9.1 – estimated "snow-pack" thickness from recovery rates

RDX/"snow-pack" film thicknesses can be estimated from the depth of RDX removed in a single laser shot, and the number of laser shots required to recover brightness. A single laser shot on RDX forms a 6 µm deep ablation pit, and on PC a 0.6 µm ablation pit. [1,2] Across the majority of film thicknesses/RDX spray times in this work, plume brightness is recovered in four laser shots following the suppression of brightness on the second laser shot. With this in mind, it is estimated that the "snow-pack" thickness must be about 2.4 µm, assuming material is removed at a rate more akin to PC than that of RDX, under the assumption that the "snow-pack" is RDX which has diffused into molten PC. For reference, it was estimated in chapter 2 that a 5 minute sprayed RDX film is ~12 µm thick, and in chapter 6 that an 80 minute sprayed film is ~70 µm thick.

It was also found that audio recordings on a smart phone indicate louder pops associated with the dark plasmas (energetic), which could provide an inexpensive way to investigate laser ignition further. Analysis of a histogram of plume images indicates a distribution of pixel intensities that does not change in intensity or shift through time but just decreases in population.

This observation is further confirmation that the plasma emits at a constant temperature, and that cooling is evident as just a fewer number of hot pixels, rather than a drop in intensity. Finally, out of curiosity, fast spectra were collected for the laser ablation of a few metals on double sided tape. Spectra of the metals on tape show signs of the plain tape, PC, and features not common to either, making blackbody fitting difficult. Only Iron could be fit to a blackbody, with a best fit temperature of 12,450K +/- 225, compared to an estimated 7920K +/-15 temperature for plain double sided tape. Spectra of successive laser shots on the metals indicated shape change from shots A to G. This change in shape was attributed to the possibility that an oxide layer formed on the metals, as they had been stored in lab for over ten years. It is proposed that in the first shots the oxide layer could be being ablated, and that on later shots the spectral shape appears different as a result of the removal of this oxide layer.

Iron oxide forms the thickest metal oxides, with nickel and cobalt oxides being similarly thin. If metal oxides are being ablated on plastic tape, it is possible they might behave like a thermite. The very high temperature of the G shot of the Fe sample might indicate that iron oxide could possibly be a mildly energetic material as Fe_2O_3 is an oxidizer, the tape is oxidizable, and a reaction akin to that of Al in thermite might be taking place. As more shots remove the oxide layer, it could be a reason for Fe signal to persist for several shots as opposed to only one for Ni and Co. As a result, the metals could act as mild energetics.

9.1 REFERENCES

1. Casper IV, Walter F. *A microsecond time-resolved spectroscopic study of laser induced plasmas and their interactions with solid materials.* Ph.D. Dissertation, Auburn University, Auburn, AL, 2015.
2. J.L. Gottfried, *Influence of exothermic chemical reactions on laser-induced shock waves*, Phys. Chem. Chem. Phys. 16, 21452 (2014)

Appendix

10.1 Routine for sample translation using DMC motion control [1]

```
#WAFER2

SPY=3750;
SPZ=7500;
#AI+5;

#MOVE1
#LOOP1;
PRY=-500;
AI+5;
WT 1201;
BG Y;
AM Y;
PRY=-500;
AI+5;
WT 1201;
BG Y;
AM Y;
PRY=-500;
AI+5;
WT 1201;
BG Y;
AM Y;
PRY=-500;
AI+5;
WT 1201;
BG Y;
AM Y;
PRY=-500;
AI+5;
WT 1201;
BG Y;
AM Y;
PRY=-500;
AI+5;
WT 1201;
BG Y;
AM Y;
PRY=-500;
AI+5;
WT 1201;
BG Y;
AM Y;
PRY=-500;
AI+5;
WT 1201;
BG Y;
```

```
AM Y;
PRY=-500;
AI+5;
WT 1201;
BG Y;
AM Y;
PRZ=-1000;
AI+5;
WT 1201;
BGZ;
AM Z;
MG "Line 1 complete";

#MOVE2
#LOOP2;
AMY;
AMZ;
PRY=500;
AI+5;
WT 1201;
BG Y;
AM Y;
PRY=500;
AI+5;
WT 1201;
BG Y;
AM Y;
PRY=500;
AI+5;
WT 1201;
BG Y;
AM Y;
PRY=500;
AI+5;
WT 1201;
BG Y;
AM Y;
PRY=500;
AI+5;
WT 1201;
BG Y;
AM Y;
PRY=500;
AI+5;
WT 1201;
BG Y;
```

```
AM Y;
PRY=500;
AI+5;
WT 1201;
BG Y;
AM Y;
PRY=500;
AI+5;
WT 1201;
BG Y;
AM Y;
PRZ=-1000;
AI+5;
WT 1201;
BGZ;
AM Z;
MG "Line 2 complete";

#MOVE3
#LOOP3;
AMY;
AMZ;
PRY=-500;
AI+5;
WT 1201;
BG Y;
AM Y;
PRY=-500;
AI+5;
WT 1201;
BG Y;
AM Y;
PRY=-500;
AI+5;
WT 1201;
BG Y;
AM Y;
PRY=-500;
AI+5;
WT 1201;
BG Y;
AM Y;
PRY=-500;
AI+5;
WT 1201;
BG Y;
```

```
AM Y;
PRY=-500;
AI+5;
WT 1201;
BG Y;
AM Y;
PRY=-500;
AI+5;
WT 1201;
BG Y;
AM Y;
PRY=-500;
AI+5;
WT 1201;
BG Y;
AM Y;
PRZ=-1000;
AI+5;
WT 1201;
BGZ;
AM Z;
MG "Line 3 complete";

#MOVE4
#LOOP4;
AMY;
AMZ;
PRY=500;
AI+5;
WT 1201;
BG Y;
AM Y;
PRY=500;
AI+5;
WT 1201;
BG Y;
AM Y;
PRY=500;
AI+5;
WT 1201;
BG Y;
AM Y;
PRY=500;
AI+5;
WT 1201;
BG Y;
```

```
AM Y;
PRY=500;
AI+5;
WT 1201;
BG Y;
AM Y;
PRY=500;
AI+5;
WT 1201;
BG Y;
AM Y;
PRY=500;
AI+5;
WT 1201;
BG Y;
AM Y;
PRY=500;
AI+5;
WT 1201;
BG Y;
AM Y;
PRZ=-1000;
AI+5;
WT 1201;
BGZ;
AM Z;
MG "Line 4 complete";

#MOVE5
#LOOP5;
AMY;
AMZ;
PRY=-500;
AI+5;
WT 1201;
BG Y;
AM Y;
PRY=-500;
AI+5;
WT 1201;
BG Y;
AM Y;
PRY=-500;
AI+5;
WT 1201;
BG Y;
```

```
AM Y;
PRY=-500;
AI+5;
WT 1201;
BG Y;
AM Y;
PRY=-500;
AI+5;
WT 1201;
BG Y;
AM Y;
PRY=-500;
AI+5;
WT 1201;
BG Y;
AM Y;
PRY=-500;
AI+5;
WT 1201;
BG Y;
AM Y;
PRY=-500;
AI+5;
WT 1201;
BG Y;
AM Y;
PRZ=-1000;
AI+5;
WT 1201;
BGZ;
AM Z;
MG "Line 5 complete";

#MOVE6
#LOOP6;
AMY;
AMZ;
PRY=500;
AI+5;
WT 1201;
BG Y;
AM Y;
PRY=500;
AI+5;
WT 1201;
BG Y;
```

```
AM Y;
PRY=500;
AI+5;
WT 1201;
BG Y;
AM Y;
PRY=500;
AI+5;
WT 1201;
BG Y;
AM Y;
PRY=500;
AI+5;
WT 1201;
BG Y;
AM Y;
PRY=500;
AI+5;
WT 1201;
BG Y;
AM Y;
PRY=500;
AI+5;
WT 1201;
BG Y;
AM Y;
PRY=500;
AI+5;
WT 1201;
BG Y;
AM Y;
PRZ=-1000;
AI+5;
WT 1201;
BGZ;
AM Z;
MG "Line 6 complete";

#MOVE7
#LOOP7;
AMY;
AMZ;
PRY=-500;
AI+5;
WT 1201;
BG Y;
```

```
AM Y;
PRY=-500;
AI+5;
WT 1201;
BG Y;
AM Y;
PRY=-500;
AI+5;
WT 1201;
BG Y;
AM Y;
PRY=-500;
AI+5;
WT 1201;
BG Y;
AM Y;
PRY=-500;
AI+5;
WT 1201;
BG Y;
AM Y;
PRY=-500;
AI+5;
WT 1201;
BG Y;
AM Y;
PRY=-500;
AI+5;
WT 1201;
BG Y;
AM Y;
PRY=-500;
AI+5;
WT 1201;
BG Y;
AM Y;
PRZ=-1000;
AI+5;
WT 1201;
BGZ;
AM Z;
MG "Line 7 complete";

#MOVE8
#LOOP8;
AMY;
```

```
AMZ;
PRY=500;
AI+5;
WT 1201;
BG Y;
AM Y;
PRY=500;
AI+5;
WT 1201;
BG Y;
AM Y;
PRY=500;
AI+5;
WT 1201;
BG Y;
AM Y;
PRY=500;
AI+5;
WT 1201;
BG Y;
AM Y;
PRY=500;
AI+5;
WT 1201;
BG Y;
AM Y;
PRY=500;
AI+5;
WT 1201;
BG Y;
AM Y;
PRY=500;
AI+5;
WT 1201;
BG Y;
AM Y;
PRY=500;
AI+5;
WT 1201;
BG Y;
AM Y;
PRZ=-1000;
AI+5;
WT 1201;
BGZ;
AM Z;
```

```
MG "Line 8 complete";

#MOVE9
#LOOP9;
AMY;
AMZ;
PRY=-500;
AI+5;
WT 1201;
BG Y;
AM Y;
PRY=-500;
AI+5;
WT 1201;
BG Y;
AM Y;
PRY=-500;
AI+5;
WT 1201;
BG Y;
AM Y;
PRY=-500;
AI+5;
WT 1201;
BG Y;
AM Y;
PRY=-500;
AI+5;
WT 1201;
BG Y;
AM Y;
PRY=-500;
AI+5;
WT 1201;
BG Y;
AM Y;
PRY=-500;
AI+5;
WT 1201;
BG Y;
AM Y;
PRY=-500;
AI+5;
WT 1201;
BG Y;
AM Y;
```

```
PRZ=-1000;
AI+5;
WT 1201;
BGZ;
AM Z;
MG "Line 9 complete";

#MOVE10
#LOOP10;
AMY;
AMZ;
PRY=500;
AI+5;
WT 1201;
BG Y;
AM Y;
PRY=500;
AI+5;
WT 1201;
BG Y;
AM Y;
PRY=500;
AI+5;
WT 1201;
BG Y;
AM Y;
PRY=500;
AI+5;
WT 1201;
BG Y;
AM Y;
PRY=500;
AI+5;
WT 1201;
BG Y;
AM Y;
PRY=500;
AI+5;
WT 1201;
BG Y;
AM Y;
PRY=500;
AI+5;
WT 1201;
BG Y;
AM Y;
```

```
PRY=500;
AI+5;
WT 1201;
BG Y;
AM Y;
PRZ=-1000;
AI+5;
WT 1201;
BGZ;
AM Z;
MG "Line 10 complete";

#MOVE11
#LOOP11;
AMY;
AMZ;
PRY=-500;
AI+5;
WT 1201;
BG Y;
AM Y;
PRY=-500;
AI+5;
WT 1201;
BG Y;
AM Y;
PRY=-500;
AI+5;
WT 1201;
BG Y;
AM Y;
PRY=-500;
AI+5;
WT 1201;
BG Y;
AM Y;
PRY=-500;
AI+5;
WT 1201;
BG Y;
AM Y;
PRY=-500;
AI+5;
WT 1201;
BG Y;
AM Y;
```

```
PRY=-500;
AI+5;
WT 1201;
BG Y;
AM Y;
PRY=-500;
AI+5;
WT 1201;
BG Y;
AM Y;
PRZ=-1000;
AI+5;
WT 1201;
BGZ;
AM Z;
MG "Line 11 complete";


#MOVE12
#LOOP12;
AMY;
AMZ;
PRY=500;
AI+5;
WT 1201;
BG Y;
AM Y;
PRY=500;
AI+5;
WT 1201;
BG Y;
AM Y;
PRY=500;
AI+5;
WT 1201;
BG Y;
AM Y;
PRY=500;
AI+5;
WT 1201;
BG Y;
AM Y;
PRY=500;
AI+5;
WT 1201;
BG Y;
```

```
AM Y;
PRY=500;
AI+5;
WT 1201;
BG Y;
AM Y;
PRY=500;
AI+5;
WT 1201;
BG Y;
AM Y;
PRY=500;
AI+5;
WT 1201;
BG Y;
AM Y;
PRZ=-1000;
AI+5;
WT 1201;
BGZ;
AM Z;
MG "Line 12 complete";

#MOVE13
#LOOP13;
AMY;
AMZ;
PRY=-500;
AI+5;
WT 1201;
BG Y;
AM Y;
PRY=-500;
AI+5;
WT 1201;
BG Y;
AM Y;
PRY=-500;
AI+5;
WT 1201;
BG Y;
AM Y;
PRY=-500;
AI+5;
WT 1201;
BG Y;
```

```
AM Y;
PRY=-500;
AI+5;
WT 1201;
BG Y;
AM Y;
PRY=-500;
AI+5;
WT 1201;
BG Y;
AM Y;
PRY=-500;
AI+5;
WT 1201;
BG Y;
AM Y;
PRY=-500;
AI+5;
WT 1201;
BG Y;
AM Y;
PRZ=-1000;
AI+5;
WT 1201;
BGZ;
AM Z;
MG "Line 13 complete";

#MOVE14
#LOOP14;
AMY;
AMZ;
PRY=500;
AI+5;
WT 1201;
BG Y;
AM Y;
PRY=500;
AI+5;
WT 1201;
BG Y;
AM Y;
PRY=500;
AI+5;
WT 1201;
BG Y;
```

```
AM Y;
PRY=500;
AI+5;
WT 1201;
BG Y;
AM Y;
PRY=500;
AI+5;
WT 1201;
BG Y;
AM Y;
PRY=500;
AI+5;
WT 1201;
BG Y;
AM Y;
PRY=500;
AI+5;
WT 1201;
BG Y;
AM Y;
PRY=500;
AI+5;
WT 1201;
BG Y;
AM Y;
PRZ=-1000;
AI+5;
WT 1201;
BGZ;
AM Z;
MG "Line 14 complete";



MG "Wafer Complete";

EN;
```

10.2 Open specific images/files Macro (using Visual Basic) [2]

```
        Dummy = Open_Selected_Images() ;

        function Open_Selected_Images() {

//      Select the Directory of the spots to be opened
```

```
	dir_root = getDirectory("Choose an Experiment (XX-YY-ZZ) Directory ");
//	print(dir_root);
	temp_string = substring(dir_root, lengthOf(dir_root)-4,lengthOf(dir_root)-3);
//	print(temp_string);
	if(temp_string != "-"){
		Dialog.create("Warning");
		Dialog.addMessage("Select an Experiment (XX-YY-ZZ) Directory ");
		Dialog.show();
		dir_root = getDirectory("Choose an Experiment (XX-YY-ZZ) Directory ");
		}

//	Get the files/directories to determine the number of shots of the experiment
	list_root = getFileList(dir_root);
	NShots = 0;

	Dialog.create("Select Image Number");
	Image_label = newArray(9);
	Image_label[0] = "1st Images";
	Image_label[1] = "2nd Images";
	Image_label[2] = "3rd Images";
	Image_label[3] = "4th Images";
	Image_label[4] = "5th Images";
	Image_label[5] = "6th Images";
	Image_label[6] = "7th Images";
	Image_label[7] = "8th Images";
	Image_label[8] = "9th Images";
	Dialog.addChoice("Type", Image_label);
	Dialog.show();
	Image_Select = Dialog.getChoice();
	print(Image_Select);
	if(Image_Select == "1st Images") Image_Number = "00";
	if(Image_Select == "2nd Images") Image_Number = "01";
	if(Image_Select == "3rd Images") Image_Number = "02";
	if(Image_Select == "4th Images") Image_Number = "03";
	if(Image_Select == "5th Images") Image_Number = "04";
	if(Image_Select == "6th Images") Image_Number = "05";
	if(Image_Select == "7th Images") Image_Number = "06";
	if(Image_Select == "8th Images") Image_Number = "07";
	if(Image_Select == "9th Images") Image_Number = "08";


	for (i=0; i<list_root.length; i++) {
		if(endsWith(list_root[i],"/")){
			NShots = NShots+1;
		}
	}
```

```
	if(NShots > 0){
		A_File_Names = getFileList(dir_root + "/A/1st Images/");
		File_Name_Base = A_File_Names[0];
		Shot = getString("Enter Shot", "" )+ " ";
		if(lengthOf(Shot) != 0 ){
			Parse_Input_Open_Images (Shot, Image_Number, File_Name_Base );
			}
	}

	function Prepare_Image_File_Name (Shot, Image_Number, File_Name_Base ) {
		if(lengthOf(Shot) == 1 ) Shot = "00" + Shot;
		if(lengthOf(Shot) == 2 ) Shot = "0" + Shot;
		Image_Name = substring(File_Name_Base ,0,20) + Shot + ")_"+
Image_Number+".bmp" ;
//		print(Image_Name);
		return Image_Name;
		}

	function Parse_Input_Open_Images (Shot, Image_Number, File_Name_Base ) {
			ii_last = 0;
			for(ii=0; ii<lengthOf(Shot); ii++){
				if(substring(Shot,ii,ii+1) == " " || substring(Shot,ii,ii+1) == "," || ii
== lengthOf(Shot)) {
					temp_string = substring(Shot,ii_last,ii);
					if(substring(temp_string,0,1) == " ") temp_string =
substring(temp_string,1,lengthOf(temp_string));
					if(substring(temp_string,lengthOf(temp_string)-
1,lengthOf(temp_string)) == " ") temp_string = substring(temp_string,0,lengthOf(temp_string)-
1);
					if(lengthOf(temp_string) > 1) {
						print(temp_string);
						Image_Name = "";
						Image_Name = Prepare_Image_File_Name
(temp_string, Image_Number, File_Name_Base );
//						print(dir_root + Image_Name);
						open(dir_root + Image_Name);
						}
					if(lengthOf(temp_string) == 1 && temp_string != " " &&
temp_string != ","  ) {
						print(temp_string);
						Image_Name = "";
						Image_Name = Prepare_Image_File_Name
(temp_string, Image_Number, File_Name_Base );
//						print(dir_root + Image_Name);
						open(dir_root + Image_Name);
						}
```

```
                                        ii_last = ii;
                                        }
                                }


        }
```

10.3 X-Shot Sort Macro

```
// This macro processes all the files in a folder.

        extension = ".bmp";
        dir1 = getDirectory("Choose Source Directory ");
        Directory_Images = File.directory ;
        list = getFileList(dir1);
        Spots_per_Row = 9;
        Number_Rows = 14;
        nshots = floor((list.length-1)/(Spots_per_Row*Number_Rows*20));
        nshots = getNumber("Number of Shots", nshots);
        setBatchMode(true);
        MakeDirectories(nshots, dir1);
        max = 20*nshots*(floor((list.length)/(nshots*20)));
        for (i=0; i<max; i++) {
                        if (endsWith(list[i], extension)) processImage(dir1, list[i], nshots);
                }


        function MakeDirectories(nshots, dir1) {
                SubDirLetter = "A";
                ASCII_code_Letter = charCodeAt(SubDirLetter,0);
                for( i = 0; i<(nshots); i++) {
                        Letter = ASCII_code_Letter + i ;
                        ASCII_Letter = fromCharCode(Letter);
                        File.makeDirectory(dir1 + "//" + ASCII_Letter + "/");
                        File.makeDirectory(dir1 + "//" + ASCII_Letter + "/1st Images/" );
                        File.makeDirectory(dir1 + "//" + ASCII_Letter + "/2nd Images/" );
                        File.makeDirectory(dir1 + "//" + ASCII_Letter + "/3rd Images/" );
                        File.makeDirectory(dir1 + "//" + ASCII_Letter + "/4th Images/" );
                        File.makeDirectory(dir1 + "//" + ASCII_Letter + "/5th Images/" );
                        File.makeDirectory(dir1 + "//" + ASCII_Letter + "/6th Images/" );
                        File.makeDirectory(dir1 + "//" + ASCII_Letter + "/7th Images/" );
                        File.makeDirectory(dir1 + "//" + ASCII_Letter + "/8th Images/" );
                        File.makeDirectory(dir1 + "//" + ASCII_Letter + "/9th Images/" );
                        File.makeDirectory(dir1 + "//" + ASCII_Letter + "/10th+ Images/" );
                }
        }
```

```
function processImage(dir1, name, nshots) {
n_ms_wait = 50;
open(dir1+name);
//wait(n_ms_wait);
len =lengthOf(name);
Image_Number = substring(name, len-6, len-4 );
Exp_Number = substring(name, len-13, len-8 );
ITest = (parseInt(Exp_Number) - nshots*(floor(parseInt(Exp_Number)/nshots)));
SubDirLetter = "A";
ASCII_code_Letter = charCodeAt(SubDirLetter,0);
Letter = ASCII_code_Letter + ITest;
ASCII_Letter = fromCharCode(Letter);
if (Image_Number == "00"){
        filename_save= dir1+"//" + ASCII_Letter + "/1st Images/"+name;
        saveAs("BMP", filename_save);
        }
if (Image_Number == "01"){
        filename_save= dir1+"//" + ASCII_Letter + "/2nd Images/"+name;
        saveAs("BMP", filename_save);
        }
if (Image_Number == "02"){
        filename_save= dir1+"//" + ASCII_Letter + "/3rd Images/"+name;
        saveAs("BMP", filename_save);
        }
if (Image_Number == "03"){
        filename_save= dir1+"//" + ASCII_Letter + "/4th Images/"+name;
        saveAs("BMP", filename_save);
        }
if (Image_Number == "04"){
        filename_save= dir1+"//" + ASCII_Letter + "/5th Images/"+name;
        saveAs("BMP", filename_save);
        }
if (Image_Number == "05"){
        filename_save= dir1+"//" + ASCII_Letter + "/6th Images/"+name;
        saveAs("BMP", filename_save);
        }
if (Image_Number == "06"){
        filename_save= dir1+"//" + ASCII_Letter + "/7th Images/"+name;
        saveAs("BMP", filename_save);
        }
if (Image_Number == "07"){
        filename_save= dir1+"//" + ASCII_Letter + "/8th Images/"+name;
        saveAs("BMP", filename_save);
        }
if (Image_Number == "08"){
```

```
                filename_save= dir1+"//" + ASCII_Letter + "/9th Images/"+name;
                saveAs("BMP", filename_save);
                }
        if (Image_Number == "09" || Image_Number == "10" || Image_Number == "11" ||
Image_Number == "11" || Image_Number == "12" || Image_Number == "13" || Image_Number
== "14" || Image_Number == "15" || Image_Number == "16" || Image_Number == "17" ||
Image_Number == "18" || Image_Number == "19"  ){
                filename_save= dir1+"//" + ASCII_Letter + "/10th+ Images/"+name;
                saveAs("BMP", filename_save);
                }
        }
        close();
```

10.4 Make Pattern Montage Macro

```
// This macro processes all the files in a folder.

        extension = ".bmp";
        n_ms_wait = 50;
        dir_root = getDirectory("Choose Source Directory ");
//      Directory_Images = File.directory ;
        list_root = getFileList(dir_root);
        lendirroot =lengthOf(dir_root);
        lenlistroot =lengthOf(list_root[1]);
        setBatchMode(true);
        if(File.isDirectory(dir_root + "//even/" )){
                        dir1 = dir_root + "//even/" ;
                        Generate_xth_Shot_Image_Montages( dir1);
                        dir1 = dir_root + "//odd/" ;
                        Generate_xth_Shot_Image_Montages( dir1);
                        run("Image Sequence...", "open=[" + dir_root + "//even/Even 1st Images
Pattern Montage.bmp] sort");
                        run("Make Montage...", "columns=9 rows=1 scale=1 font=36 border=10
label");
                        saveAs("BMP", dir_root + "//even/Even All Shots Montage");
                        close();
                        close();
                        run("Image Sequence...", "open=[" + dir_root + "//odd/Odd 1st Images
Pattern Montage.bmp] sort");
                        run("Make Montage...", "columns=9 rows=1 scale=1 font=36 border=10
label");
                        saveAs("BMP", dir_root + "//odd/Odd All Shots Montage");
                        close();
                        close();
                        open(dir_root + "//even/Even All Shots Montage.bmp");
                        open(dir_root +"//odd/Odd All Shots Montage.bmp");
```

```
                    run("Images to Stack", "method=[Copy (top-left)] name=Stack title=[]");
                    run("Make Montage...", "columns=1 rows=2 border=10 scale=1");
                    saveAs("BMP", dir_root +"//Even(top)Odd(bottom Montage.bmp");
                    close();
                    close();
                }
        if(File.isDirectory(dir_root + "//A/")){
                    dir1 = dir_root + "//A/" ;
                    Generate_xth_Shot_Image_Montages( dir1);
                    dir1 = dir_root + "//B/" ;
                    Generate_xth_Shot_Image_Montages( dir1);
                    dir1 = dir_root + "//C/" ;
                    Generate_xth_Shot_Image_Montages( dir1);
                    run("Image Sequence...", "open=[" + dir_root + "//A/A 1st Images Pattern
Montage.bmp] sort");
                    run("Make Montage...", "columns=9 rows=1 scale=1 font=36 border=10
label");
                    saveAs("BMP", dir_root + "//A/A All Shots Montage");
                    run("Image Sequence...", "open=[" + dir_root + "//B/B 1st Images Pattern
Montage.bmp] sort");
                    run("Make Montage...", "columns=9 rows=1 scale=1 font=36 border=10
label");
                    saveAs("BMP", dir_root + "//B/B All Shots Montage");
                    run("Image Sequence...", "open=[" + dir_root + "//C/C 1st Images Pattern
Montage.bmp] sort");
                    run("Make Montage...", "columns=9 rows=1 scale=1 font=36 border=10
label");
                    saveAs("BMP", dir_root + "//C/C All Shots Montage");
                    open(dir_root + "//A/A All Shots Montage.bmp");
                    open(dir_root + "//B/B All Shots Montage.bmp");
                    open(dir_root + "//C/C All Shots Montage.bmp");
                    run("Images to Stack", "method=[Copy (top-left)] name=Stack title=[]");
                    run("Make Montage...", "columns=1 rows=3 border=10 scale=1");
                    saveAs("BMP", dir_root +"//A(top)B(middle)C(bottom) Montage.bmp");
                    close();
                    close();
                    }
        if(!(File.isDirectory(dir_root + "//A/")) && !(File.isDirectory(dir_root + "//even/" )) ){
                Generate_xth_Shot_Image_Montages( dir_root);
                run("Image Sequence...", "open=[" + dir_root + "//1st Images Pattern
Montage.bmp] sort");
                run("Make Montage...", "columns=9 rows=1 scale=1 font=36 border=10 label");
                saveAs("BMP", dir_root  + "//All Shots Montage");
        }
        close();
        close();
```

```
 function Generate_xth_Shot_Image_Montages(dir1) {
        // Run for 1st Images
   list = getFileList(dir1 + "//1st Images/");
        run("Image Sequence...", "open=[" + dir1 + "//1st Images/"+list[1]+"] number=153
sort");
        if (nSlices>2) {
                                makeMontage();
                                saveAs("BMP", dir1 +"//1st Images Pattern Montage.bmp" );
                                }
        close();
        // Run for 2nd Images
   list = getFileList(dir1 + "//2nd Images/");
        run("Image Sequence...", "open=[" + dir1 + "//2nd Images/"+list[1]+"] number=153
sort");
        if (nSlices>2) {
                                makeMontage();
                                saveAs("BMP", dir1 +"//2nd Images Pattern Montage.bmp" );
                                }
        close();
        // Run for 3rd Images
   list = getFileList(dir1 + "//3rd Images/");
        run("Image Sequence...", "open=[" + dir1 + "//3rd Images/"+list[1]+"] number=153
sort");
        if (nSlices>2) {
                                makeMontage();
                                saveAs("BMP", dir1 +"//3rd Images Pattern Montage.bmp" );
                                }
        close();
        // Run for 4th Images
   list = getFileList(dir1 + "//4th Images/");
        run("Image Sequence...", "open=[" + dir1 + "//4th Images/"+list[1]+"] number=153
sort");
        if (nSlices>2) {
                                makeMontage();
                                saveAs("BMP", dir1 +"//4th Images Pattern Montage.bmp" );
                                }
        close();
        // Run for 5th Images
   list = getFileList(dir1 + "//5th Images/");
        run("Image Sequence...", "open=[" + dir1 + "//5th Images/"+list[1]+"] number=153
sort");
        if (nSlices>2) {
                                makeMontage();
                                saveAs("BMP", dir1 +"//5th Images Pattern Montage.bmp" );
                                }
```

```
	close();
	// Run for 6th Images
   list = getFileList(dir1 + "//6th Images/");
	run("Image Sequence...", "open=[" + dir1 + "//6th Images/"+list[1]+"] number=153
sort");
	if (nSlices>2) {
				makeMontage();
				saveAs("BMP", dir1 +"//6th Images Pattern Montage.bmp" );
				}
	close();
	// Run for 7th Images
   list = getFileList(dir1 + "//7th Images/");
	run("Image Sequence...", "open=[" + dir1 + "//7th Images/"+list[1]+"] number=153
sort");
	if (nSlices>2) {
				makeMontage();
				saveAs("BMP", dir1 +"//7th Images Pattern Montage.bmp" );
				}
	close();
	// Run for 8th Images
   list = getFileList(dir1 + "//8th Images/");
	run("Image Sequence...", "open=[" + dir1 + "//8th Images/"+list[1]+"] number=153
sort");
	if (nSlices>2) {
				makeMontage();
				saveAs("BMP", dir1 + "//8th Images Pattern Montage.bmp" );
				}
	close();
	// Run for 9th Images
   list = getFileList(dir1 + "//9th Images/");
	run("Image Sequence...", "open=[" + dir1 + "//9th Images/"+list[1]+"] number=153
sort");
	if (nSlices>2) {
				makeMontage();
				saveAs("BMP", dir1 +"//9th Images Pattern Montage.bmp" );
				}
	close();
	close();
	close();
	close();
	close();
	close();
	close();
	close();
	close();
	}
```

```
 function makeMontage() {
    setBatchMode(true);
    id=getImageID;
    n= nSlices;
          columns=9;
    rows = nSlices/9;
    sw=getWidth; sh=getHeight;
    type = ""+bitDepth;
    if (type=="24") type = "RGB";
    newImage("test", type+" black", columns*getWidth, rows*getWidth, 1);
    iw=getWidth/9; ih=getHeight/17;
    montage=getImageID;
    selectImage(id);
    for (irow=0; irow<16; irow++) {
                for (icol=0; icol<9; icol++){
                selectImage(id);
                setSlice(irow*9+icol+1);
                run("Select All");
                run("Copy");
                selectImage(montage);
//                      If irow is even
                if (irow == 2*(floor(irow/2))) makeRectangle((icol)*iw,(floor(irow)+0.5)*iw, sw,
sh);
//                      If irow is odd
                if (irow != 2*(floor(irow/2))) makeRectangle(sw*9-
(icol+1)*iw,(floor(irow)+0.5)*iw, sw, sh);
                run("Paste");
                      if (irow*9+icol >= (n -1))icol =9;
                      if (irow*9+icol >= (n -1))irow =17;
                }
    }
    resetMinAndMax();
    setBatchMode(false); // display the montage
 }
```

10.5 Create Circle Overlay for Variable Spray Time Experiments

```
//setTool("oval");
makeOval(222, 214, 606, 720);
makeOval(142, 340, 606, 720);
makeOval(142, 340, 606, 716);
makeOval(-6, 340, 754, 716);
makeOval(-6, 340, 754, 724);
makeOval(-6, 322, 754, 742);
makeOval(-6, 322, 746, 742);
```

```
run("Add Selection...");
//setTool("line");
makeLine(304, 216, 308, 1170);
run("Add Selection...");
makeLine(218, 818, 796, 808);
```

10.6 Collect 20 Image Frames following each laser shot

```
/*****************************************************************************
***/
/*
 * File name: Grab_20_Frames_Triggered.cpp
 *
 * Synopsis:  This routine collects 20 frames into buffers then writes them out to image files
 *
 * NOTE:      This example assumes that the hard disk is sufficiently fast
 *            to keep up with the grab. Also, removing the sequence display or
 *            the text annotation while grabbing will reduce the CPU usage and
 *            might help if some frames are missed during acquisition.
 *            If the disk or system are not fast enough, set GRAB_SCALE to 0.5,
 *            FRAME_NUMBER_ANNOTATION to M_NO or SAVE_SEQUENCE_TO_DISK to
M_NO.
 */
#include <Windows.h>
#include <direct.h>
#include <mil.h>
#include <stdio.h>
#include <stdlib.h>
#include <conio.h>
#include <iostream>
#include <string>
#include <ctime>

#define STRING_LENGTH_MAX  100

/* Sequence file name.*/
#define SEQUENCE_FILE M_TEMP_DIR MIL_TEXT("MilSequence.avi")

/* Image acquisition scale. */
#define GRAB_SCALE   1.0

/* Quantization factor to use during the compression.
   Valid values are 1 to 99 (higher to lower quality).
*/
#define COMPRESSION_Q_FACTOR   50

/* Annotation flag. Set to M_YES to draw the frame number in the saved image. */
```

```
#define FRAME_NUMBER_ANNOTATION  M_NO

/* Archive flag. Set to M_NO to disable AVI Import/Export to disk. */
#if (!M_MIL_USE_CE)
#define SAVE_SEQUENCE_TO_DISK  M_YES
#else
#define SAVE_SEQUENCE_TO_DISK  M_NO
#endif

/* Maximum number of images for the multiple buffering grab. */
#define NB_GRAB_IMAGE_MAX  22

/* User's archive hook function prototype (called for every grabbed frame). */
MIL_INT MFTYPE ArchiveFunction(MIL_INT HookType, MIL_ID HookId, void MPTYPE
*HookDataPtr);

/* User's archive function hook data structure. */
typedef struct
  {
  MIL_ID MilSystem;
  MIL_ID MilDisplay;
  MIL_ID MilImageDisp;
  MIL_ID *MilCompressedImage;
  MIL_INT NbGrabbedFrames;
  MIL_INT NbArchivedFrames;
  MIL_INT SaveSequenceToDisk;
  MIL_INT OnBoardAttribute;
  MIL_ID   MilImage[22]   ;

  } HookDataStruct;


/* Main function. */
/* -------------- */
int MosMain(void)
{
  MIL_ID     MilApplication, MilSystem, MilDigitizer, MilDisplay, MilImageDisp;
  MIL_ID     MilGrabImages[NB_GRAB_IMAGE_MAX];
  MIL_ID     MilCompressedImage[2] = {0, 0};
  MIL_INT    CompressAttribute=0, OnBoardAttribute=0;
  MIL_INT    NbFrames=0,   Selection=1,   LicenseModules=0,   n=0, i=0;
  MIL_INT    FrameCount=0, FrameMissed=0, NbFramesReplayed=0, Exit=0;
  MIL_DOUBLE FrameRate=0,  TimeWait=0,    TotalReplay=0;
  MIL_DOUBLE GrabScale=GRAB_SCALE;
  MIL_INT    SaveSequenceToDisk = SAVE_SEQUENCE_TO_DISK;
  MIL_INT       M_COUNT=20, N_LOOP=0, NExpNumber = 1;
```

```
  HookDataStruct UserHookData;
  MIL_TEXT_CHAR Text[STRING_LENGTH_MAX]= {MT('\0'),};
  time_t ttNow = time(0);
  tm * ptmNow;
  ptmNow =localtime(&ttNow);
        time_t rawtime;
        struct tm * timeinfo;
        char timebuffer[80], datebuffer[80];

        time (&rawtime);
        timeinfo = localtime(&rawtime);
        strftime(timebuffer,sizeof(timebuffer),"C:/FastCameraData/%m-%d-%Y/%H-%M-
%S/",timeinfo);
        strftime(datebuffer,sizeof(datebuffer),"C:/FastCameraData/%m-%d-%Y/",timeinfo);
        char * TimeDir = timebuffer;
        char * DateDir = datebuffer;
        char * RootDir = "C:/FastCameraData/";
        char * CurrDir = _getcwd( NULL, 0 );
        //cout << CurrDir;



        int root_err = _mkdir(RootDir);
        if(root_err)
        /* This part of the routine is used in the case that the root directory already exists */
        {
                int date_err = _mkdir(DateDir);
                if(date_err)
                /* This part of the routine is used in the case that the date directory already exists
*/
                {
                        int full_err = _mkdir(TimeDir);
                        //if(full_err)
                        ///* This part of the routine is used in the case that the time directory
already exists */
                        //{
                        //      cout << "\n\n Directory Aleady Exists";
                        //}
                        //else
                        ///* This part of the routine is used in the case that the time directory was
just created */
                        //{
                        //      cout << "\n\n Directory Created";
                        //}

                }
```

```
                else
                /* This part of the routine is used in the case that the date directory was just
created */
                {
                        _mkdir(TimeDir);
                        //cout << "\n\n Directory Created";
                }
        }
        else
        /* This part of the routine is used in the case that the root directory does not exist */
        {
                _mkdir(RootDir);
                _mkdir(DateDir);
                _mkdir(TimeDir);
                //cout << "\n\n Directory Created";
        }

  MIL_TEXT_CHAR Text2[STRING_LENGTH_MAX]= {MT('\0'),};
                MosSprintf(Text2, STRING_LENGTH_MAX,
MIL_TEXT("C:/FastCameraData/%02ld-%02ld-20%ld/%02ld-%02ld-%02ld/"), 1+ptmNow-
>tm_mon, ptmNow->tm_mday,
                                        (ptmNow->tm_year)-100, ptmNow->tm_hour, ptmNow-
>tm_min,ptmNow->tm_sec);

        /* Allocate defaults. */
  MappAllocDefault(M_SETUP, &MilApplication, &MilSystem, &MilDisplay,
                                &MilDigitizer, M_NULL);


  /* Print a message */
  MosPrintf(MIL_TEXT("\nSEQUENCE AQUISITION:\n"));
  MosPrintf(MIL_TEXT("--------------------\n\n"));
  //MosPrintf(MIL_TEXT(" %ld-%ld \n\n"), 1+ptmNow->tm_mon, ptmNow->tm_mday);

  /* Rik Bypass Ask and Use Option Sections */
  MosPrintf(MIL_TEXT("\nRecording uncompressed images on each trigger...\n"));
  MosPrintf(MIL_TEXT("\nTo Stop hit any key...\n\n"));
  CompressAttribute = M_NULL;
  //MosPrintf(MIL_TEXT("Enter Experiment number 1-9 only.\n"));
  //MosPrintf(MIL_TEXT("Images collection will begin on next laser shot.\n"));
  //NExpNumber= MosGetch();

        /*Code to turn off Error Messaging*/
        MappControl(M_ERROR, M_PRINT_DISABLE);

        /*Code to turn Error Messaging back on*/
```

```
        //MappControl(M_ERROR, M_PRINT_ENABLE);


  do {

                /* Allocate the grab buffers to hold the sequence buffering. */
                //MappControl(M_ERROR, M_PRINT_DISABLE);

                    //for (NbFrames=0, n=0; n<NB_GRAB_IMAGE_MAX; n++)
                for (NbFrames=0, n=0; n<NB_GRAB_IMAGE_MAX; n++)
                        {
                        MbufAllocColor(MilSystem,
                                                MdigInquire(MilDigitizer,
M_SIZE_BAND, M_NULL),
                                                (MIL_INT)(MdigInquire(MilDigitizer,
M_SIZE_X, M_NULL)*GrabScale),
                                                (MIL_INT)(MdigInquire(MilDigitizer,
M_SIZE_Y, M_NULL)*GrabScale),
                                                8L+M_UNSIGNED,
M_IMAGE+M_GRAB+OnBoardAttribute, &MilGrabImages[n]);
                        if (MilGrabImages[n])
                                {
                                NbFrames++;
                                MbufClear(MilGrabImages[n], 0xFF);
                                }
                        else
                                break;
                        }
                //MappControl(M_ERROR, M_PRINT_ENABLE);



              /* Free buffers to leave space for possible temporary buffers. */
                for (n=0; n<2 && NbFrames; n++)
                        {
                        NbFrames--;
                        MbufFree(MilGrabImages[NbFrames]);
                        }

                /* Halt continuous grab. */
                MdigHalt(MilDigitizer);

                /* Initialize User's archiving function hook data structure. */
                UserHookData.MilSystem          = MilSystem;
                UserHookData.MilDisplay         = MilDisplay;
                UserHookData.MilImageDisp       = MilImageDisp;
```

```
                UserHookData.MilCompressedImage  = MilCompressedImage;
                UserHookData.SaveSequenceToDisk  = SaveSequenceToDisk;
                UserHookData.OnBoardAttribute    = OnBoardAttribute;
                UserHookData.NbGrabbedFrames     = 0;
                UserHookData.NbArchivedFrames = 0;



                /* Acquire the sequence. The processing hook function will
                        be called for each image grabbed to NbFrames.
                */
                //MdigProcess(MilDigitizer, MilGrabImages, NbFrames, M_SEQUENCE,
                //          M_DEFAULT, ArchiveFunction, &UserHookData);
                MdigProcess(MilDigitizer, MilGrabImages, NbFrames,
M_SEQUENCE+M_FRAMES_PER_TRIGGER(20) ,
                                                M_TRIGGER_FOR_FIRST_GRAB,
ArchiveFunction, &UserHookData);



                /* Read and print final statistics. */
                MdigInquire(MilDigitizer, M_PROCESS_FRAME_COUNT,  &FrameCount);
                MdigInquire(MilDigitizer, M_PROCESS_FRAME_RATE,   &FrameRate);
                MdigInquire(MilDigitizer, M_PROCESS_FRAME_MISSED, &FrameMissed);
                MosPrintf(MIL_TEXT("\n\n%ld frames archived (%ld missed), at %.1f
frames/sec ")
                                                MIL_TEXT("(%.1f
ms/frame).\n"),UserHookData.NbGrabbedFrames,

FrameMissed, FrameRate, 1000.0/FrameRate);

                for (n=0; n<UserHookData.NbGrabbedFrames; n++)
                        {
                                MosSprintf(Text, STRING_LENGTH_MAX,
MIL_TEXT("%sImg_%02ld_%02ld_%ld_(%03ld-%05ld)_%02ld.bmp"), Text2, 1+ptmNow-
>tm_mon, ptmNow->tm_mday,
                                                (ptmNow->tm_year)-100, NExpNumber, N_LOOP,
n);
                                MbufExport(Text,M_BMP,MilGrabImages[n]);
                        }
                        N_LOOP++;
  }
  while (!MosKbhit());

  /* print finished. */
        MosPrintf(MIL_TEXT("Experiment ended.\n"));
        MosPrintf(MIL_TEXT("Press <Enter> to end.\n"));
```

```
        MosGetch();
  /* Free all allocated buffers. */
  MbufFree(MilImageDisp);
  for (n=0; n<NbFrames; n++)
     MbufFree(MilGrabImages[n]);
  for (n=0; n<2; n++)
     if (MilCompressedImage[n])
       MbufFree(MilCompressedImage[n]);

  /* Free defaults. */
  MappFreeDefault(MilApplication, MilSystem, MilDisplay, MilDigitizer, M_NULL);

  return 0;
}


//* User's archive function called each time a new buffer is grabbed. */
//* ------------------------------------------------------------------*/
//
//* Local defines for the annotations. */
//#define STRING_LENGTH_MAX  30
#define STRING_POS_X       20
#define STRING_POS_Y       20

MIL_INT MFTYPE ArchiveFunction(MIL_INT HookType, MIL_ID HookId, void MPTYPE
*HookDataPtr)
  {
  HookDataStruct *UserHookDataPtr = (HookDataStruct *)HookDataPtr;
  MIL_ID ModifiedImage = 0;
  MIL_INT n = 0;
  MIL_TEXT_CHAR Text[STRING_LENGTH_MAX]= {MT('\0'),};

  /* Retrieve the MIL_ID of the grabbed buffer. */
  MdigGetHookInfo(HookId, M_MODIFIED_BUFFER+M_BUFFER_ID, &ModifiedImage);

  /* Increment the frame count. */
  UserHookDataPtr->NbGrabbedFrames++;

  ///* Draw the frame count in the image if enabled and if the buffer is not on-board. */
  if((FRAME_NUMBER_ANNOTATION == M_YES) && (!UserHookDataPtr-
>OnBoardAttribute))
    {
    MosSprintf(Text, STRING_LENGTH_MAX, MIL_TEXT(" %ld "), UserHookDataPtr-
>NbGrabbedFrames);
    MgraText(M_DEFAULT, ModifiedImage,   STRING_POS_X, STRING_POS_Y, Text);
    }
```

```
/* Copy the new grabbed image to the display. */
MbufCopy(ModifiedImage, UserHookDataPtr->MilImageDisp);

return 0;
}
```

References

1. http://www.galilmc.com/download/comref/com_optima.pdf
2. https://docs.microsoft.com/en-us/dotnet/visual-basic/